ASSESSMENT OF CLIMATE CHANGE IMPACTS ON STREAMFLOW TRENDS USING A WATER BALANCE MODEL

by

Kevin Matthews

A Thesis Submitted to the Faculty of the

College of Engineering and Computer Science

in Partial Fulfillment of the Requirements for the Degree of

Master of Science

Florida Atlantic University

Boca Raton, Florida

December 2012

ASSESSMENT OF CLIMATE CHANGE IMPACTS ON STREAMFLOW TRENDS USING A WATER BALANCE MODEL

by

Kevin Matthews

This thesis was prepared under the direction of the candidate's thesis advisor, Dr. Ramesh S. V. Teegavarapu, Department of Civil, Environmental and Geomatics Engineering, and has been approved by the members of his supervisory committee. It was submitted to the faculty of the College of Engineering and Computer Science and was accepted in partial fulfillment of the requirements for the degree of Master of Science.

SUPERVISORY COMMITTEE:

Ramesh S. V. Teegavarapu, Ph.D., P.E.
Thesis Advisor

Evangelos I. Kaisar, Ph.D.

Panagiotis D. Scarlatos, Ph.D.
Chair, Department of Civil, Environmental and Geomatics Engineering

Panagiotis D. Scarlatos, Ph.D.

Mohammad Ilyas, Ph.D.
Interim Dean, College of Engineering and Computer Science

Barry T. Rosson, Ph.D.
Dean, Graduate College

November 19, 2012
Date

ACKNOWLEDGMENTS

I would like to specially thank Dr. Ramesh Teegavarapu for his advice, input and encouragement throughout the program and with this research. Thanks to fellow/former students Aneesh Goly and Andre` McBarnette for their guidance and advice as well as my friend Lola Burford. Finally I would like to thank my other friend(s) and family for their encouragement and support.

ABSTRACT

Author:	Kevin Matthews
Title:	Assessment of Climate Change Impacts on Streamflow Trends Using A Water Balance Model
Institution:	Florida Atlantic University
Thesis Advisor:	Dr. Ramesh Teegavarapu
Degree:	Master of Science
Year:	2012

Significant changes in climate and their impacts are now visible in various places around the globe and are expected to become more evident in the coming decades. For each increase in temperature, there are environmental and societal consequences. It has important implications for existing water resources systems as well as for future water resources planning and management. Water accounting (identifying, quantifying and reporting information of water flow in a system) is the first step towards formulating productive and sustainable water management strategies in a region. Thus, water balance models could be an empowering tool for water resource managers to prepare for and mitigate the effects of climate change on their local hydrologic resources. This thesis offers an insight into how such a tool can be used to assess and predict future streamflow trends in an effort to mitigate or manage any potential effects.

ASSESSMENT OF CLIMATE CHANGE IMPACTS ON STREAMFLOW TRENDS USING A WATER BALANCE MODEL

LIST OF FIGURES

LIST OF TABLES

CHAPTER 1. INTRODUCTION

Climate change constitutes one of earth's most fundamental challenges and will remain so for a long time in the future. Significant changes in climate and their impacts are now visible in various places around the globe and are expected to become more evident in the coming decades. As global climate change has become a cause for concern, it has been shown that globally, temperatures are increasing and climate change is taking place more rapidly than originally forecasted and subsequently, for each increase in temperature there are environmental and societal consequences.

Climate change "refers to any significant change in the measures of climate lasting for an extended period of time. In other words, climate change includes major changes in temperature, precipitation… among other effects that occur over several decades or longer" (epa.gov). That is, regions of the world and within the United States that have lower temperatures (cold) will see temperature changes such as warmer winters because of climate change (Caldwell, 2002).

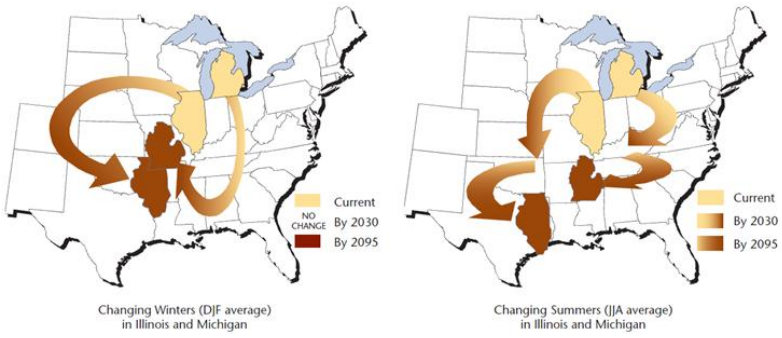

Figure 1-1: Figure showing effects of climate change for states: Illinois & Michigan

Figure 1-1 (above) shows what future temperatures will feel like for residents of the Great Lakes region. Within three decades, for example, a summer in Illinois may feel like a summer in Oklahoma does today (above right panel). By the end of the century, an Illinois summer may well feel like one in east Texas today, while a Michigan summer will probably feel like an Arkansas summer. Average winter climates will similarly shift (above left panel), and other states and provinces in the region will experience comparable changes.

The impacts and the importance of understanding the effects of global climate is so important that an international body that focuses solely on climate change was formed by the United Nations, this is the Intergovernmental Panel on Climate Change (IPCC). The IPCC is a scientific body which reviews scientific, economic, and other data related to climate change. As such, data collected by IPCC shows that, "changes in climate and their impacts are visible regionally, and are expected to become more pronounced in the next decades. [It] has a real impact on ecosystems, biodiversity, human life and many economic activities (Report: Waterborne transport, p.7). The resulting climate change globally, has been attributed to human development(s), such as population growth, the industrial revolution, and technological advancements of which some examples being the burning of fossil fuels like coal and oil that increase the concentration of atmospheric carbon dioxide (CO2) and the clearing of land for agriculture, industry, and other human activities that increase concentrations of greenhouse gases. Naturally occurring greenhouse gases are essential components of the climate process. These gases effectively prevent part of the heat radiated by the Earth's surface from otherwise

escaping to space (TRB Special Report 290, 2008). In the absence of these greenhouse gases, the Earth's temperature would be too cold to support life as we know it today. However, direct atmospheric measurements made over the past 50 years have documented the steady growth in greenhouse gas concentrations.

The increase concentrations of greenhouse gases affects the atmosphere as follows- As sunlight passes through the atmosphere and warms the Earth's surface, the heat is radiated back towards space. Most of the outgoing heat in absorbed by higher concentrated greenhouse gas molecules and re-emitted in all directions, warming the surface of the Earth and the lower atmosphere.

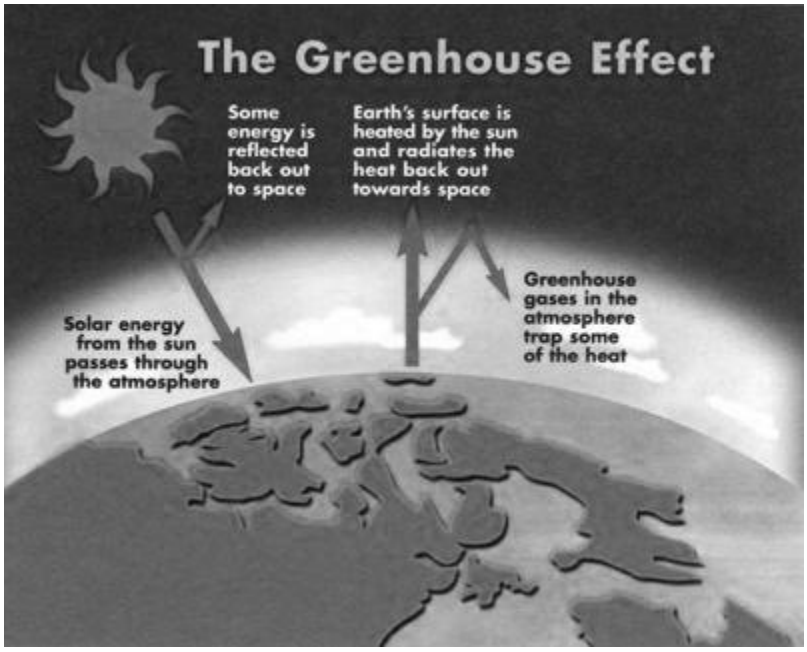

Figure 1-2 – Illustration of greenhouse gas effects (Image Source: http://globalprep.wikispaces.com/Global+Warming)

1.1 Changing Temperature

Over the last decades, temperatures have been rising, with more rapid increases

since 1970 than earlier. IPCC reported that average global temperatures increased 0.74°C during the past 100 years, with most of that increase experienced in the last 50 years. Although some attributes of climate change may be due to natural variability, it has been determined that human activities have also contributed to this change. According to IPCC, global average warming is expected to rise by about 0.4°C during the next 20 years. The IPCC climatologic models project average global temperature increases ranging from 1.1°C to 6.4°C by the end of the 21st century. Figure 1-3 shows a graphical illustration of various model temperature rise projections for 2100. The graph shows that temperature would have risen by between 0.6 to 4° C above 1900 levels.

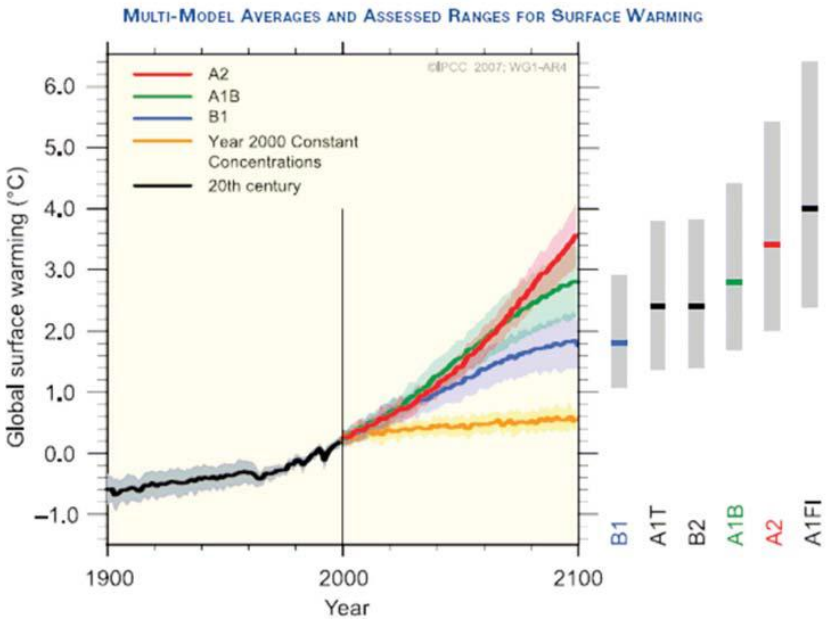

Figure 1-3: Change in Temperature due to Climate Change (IPCC, 2007)

An increase in average temperature may cause extreme climatological events that could have significant implications. In the last 50 years, the frequency of cold days and nights has declined, while hot days, hot nights, and heat waves have become more

frequent. The number of days with temperature above average temperatures has been increasing since the 1970s, as well as the intensity and length of periods of drought. IPCC report that it is virtually certain that the next century will witness warmer and more frequent hot days and nights over most land areas (IPCC Report, 2007).

1.2 Changing Precipitation Patterns and Climate Change

Further, another impact of climate change is the changing precipitation patterns. Any changes in precipitation patterns will have an impact streamflow as they are directly proportional. Over the past century precipitation amounts have increased in several regions, while drying has been observed in others. The IPCC predicts that it is virtually certain that the frequency of heat waves and heavy precipitation will increase over most areas; and likely that drought and intense tropical cyclone activity will increase. The IPCC also report the paradoxical situation that warming climate increases the incidence of both floods and drought, but at different times and places. The change in the flow regime of rivers caused by the decreasing buffering of water in snow cover is expected to enhance extreme hydrological events with more floods in winter and more droughts in summer (PIANC Report, 2006).

For instance, for the Great Lakes Region, it is projected that because of warmer temperatures there will be an increase in the amount of precipitation during the winter and a decrease in precipitation during the summer. Changes in the seasonal precipitation cycle are likely to be higher, with winter and spring rain increasing and summer rain decreasing by up to 50 percent (Kling et al., 2003). Consequently water levels in the north may have higher levels than those in the south and this in turn will affect how this

resource is managed and how changing precipitation impacts infrastructure and soil conditions (Hyman et al., 2007). Changing precipitation patterns also affect sea levels and the intensity of storms. With climate change, sea levels are increasing and storms are more intense. Strong storms tend to have longer periods of intense precipitation, and wind damage increases exponentially with wind speed (Hyman et al., 2007).

Climate change has important implications for existing water resources systems as well as for future water resources planning and management. Water resources are essential renewable resources that are the basis for existence and development of a society. Proper utilization of these resources requires assessment and management of the quantity and quality of the water resources both spatially and temporally (Moreda, 1999).

Water shortages, diminishing water quality, and others including flooding, are problems that are increasing in all areas around the world. The growth of population demands for increased domestic water supplies and expansion in agriculture and industry at the same time is putting enormous pressure on the limited fresh water resources, and is forcing various agencies and governmental organization to revisit and assess how water resources are managed in a region.

Water accounting (identifying, quantifying and reporting information of water flow in a system) is the first step towards formulating productive and sustainable water management strategies in a region (Singh et al, 2009). In some regions, there is limited recorded hydro-meteorological data available and there are often gaps in records to construct complete water budget for a watershed. Also, it is difficult to measure actual evapotranspiration and groundwater recharge. Therefore the available datasets are

generally augmented with water balance modeling to estimate monthly and yearly water balance. Water balance modeling is an attempt to conceptualize and aggregate relatively complex hydrological processes and their heterogeneity into mathematical equations (Singh et al., 2009). Which are then used to simulate different water fluxes over time and space of a system. This offers a time efficient and cost effective approach for reasonable estimation of surface water balance components of a watershed. Most existing catchment water balance models do not account for potable water supply, wastewater discharges and surface and groundwater extractions. These components of surface water cycle can significantly impact streamflow in various regions (Singh et al., 2009).

Water balance models have been used to accurately simulate historical basin discharges (e.g., Xu and Singh 1998), forecast changes in discharges based on climate changes (e.g., Gleick 1987; Arnell 1992; Jiang et al. 2007), and are relatively straightforward to apply. Thus, water balance models could be an empowering tool for water resource managers to prepare for and mitigate the effects of regional climate change on their local hydrologic resources (Fish, 2011).

This thesis offers insight into how such a tool can be used to assess and predict future trends in an effort to mitigate or manage any potential effects. The overall goal is evaluating the adequacy, suitability and robustness of the proposed rainfall-runoff model. The objective of this thesis is to investigate the effects of climate change on streamflows in various watersheds in Florida by the application of a developed water balance model known as the Thomas Model (aka “abcd” model).

1.3 Thesis Outline

This thesis is subdivided into eight (8) chapters including introduction and the last chapter, which present the results and conclusion. Following the introduction in Chapter 2 is a brief description of climate change in Florida, various climate change models, and water balance modeling. The methodology is presented in Chapter 3, followed by the case study areas, data source information, and an analysis of the historical/projected meteorological data for detecting any trends in Chapters 4 and 5. Chapter 6 will focus on the model development and application process which includes the calibration and validation. Chapter 7 will provide the results and discussion which is followed by the concluding remarks in Chapter 8.

CHAPTER 2. LITERATURE REVIEW

Assessing the hydrological impacts basically relies on water budget modeling and analysis of the interaction among precipitation, evapotranspiration, soil moisture, and runoff under the influences of changing climate, using climate models, downscaling techniques, and hydrological models (Chen, 2011**)**. This review provides a brief description of the components of climate change and various water balance models.

2.1 Climate Change in Florida

Florida is home to over 18 million people and its population is projected to increase over the coming decades. Implications of climate change impacts on the vulnerable ecosystem of Florida have been the focus of many studies, including this research. Because of the low topography of Florida, coastal regions are highly vulnerable to sea level rise and elevated storm surges (sfwmd.gov). Understanding the vulnerabilities and assessment of projections associated with climate change at the regional and local scales are extremely important to the success of future infrastructure investments to meet the needs of both the built and natural environments of the state. The southern portion of the state is quite unique in that is has the largest marsh in the United States (Greater Everglades ecosystem) that is situated among large tracts of agricultural lands and heavily populated urban areas (Obeysekera, et al., 2011).Various authorities at all levels of government in partnerships with private entities, are committed to restoring some of

these natural marsh system to their natural free flowing state. In recent times, the emphasis placed on climate change due to human-induced impacts has generated new questions on the sustainability of coastal environments with a heightened concern for the success of large-scale environmental projects throughout Florida (Obeysekera, et al 2011). A pre-requisite of any climate change investigation is to examine the historical trends in climatic and other associated environmental data. A review of this historical data indicates a general decrease in wet season precipitation and an increase in temperature.

2.2 Global Circulation Models

To evaluate trends in temperature and precipitation, Global Circulation Models (GCMs) combined with statistical or dynamic downscaling techniques are generally used. GCMs are numerical models representing physical processes in the atmosphere, ocean, cryosphere and land surface, currently they are the most advanced tools available for simulating the response of the global climate system to increasing greenhouse gas concentrations. There are other models that can be used to provide globally-or regionally-averaged estimates of the climate response, however GCMs, in conjunction with nested regional models, have the potential to provide geographically and physically consistent estimates of regional climate change which are required in impact analysis. (www.ipcc-data.org)

GCMs portray the climate using a three dimensional grid over the globe, typically having a horizontal resolution of between 250 and 600 km, 10 to 20 vertical layers in the atmosphere and sometimes as many as 30 layers in the oceans. Their

resolution is very coarse relative to the scale of exposure units in most impact assessments, therefore many physical processes, such as those related to clouds, that occur at smaller scales cannot be properly modeled. Due to the fact that the GCM scale outputs were not designed to provide results at the finer scales required for some watershed and basin-scale impact studies and related decisions, a number of varied types of techniques to 'downscale' the model scales to finer temporal and spatial scales were developed that are more closely relevant to some watershed decisions (IPCC, 2007).

2.3 Global Projections Downscaling

The use of global climate-projection information for assessing projected regional or local conditions usually requires two fundamental steps. (1) How to spatially downscale this information. (2) How to compensate for the source GCM simulation biases when developing the projected climate information (bias-correct climate model output). There are two primary approaches to downscaling the information are statistical (non-dynamical) and dynamical downscaling, where the latter is performed using a regional climate model. Both class types and available sources of downscaled CMIP3 (Coupled Model Inter-comparison Project, phase -3) information within these class types are described below.

2.3.1 Statistical Downscaling

Statistical downscaling uses equations to transform global-scale output to regional-scale conditions (Lenart, 2008). This downscaling approach applies the information from GCMs to the region by using a series of equations to relate variations in global climate to variations in local climate. Due to the fact that the statistical approach

requires less computational effort than dynamic downscaling, it offers the opportunity for testing scenarios for longer timeframes such as, many decades or even centuries, rather than the brief "time slices" of the dynamical downscaling approach (Lenart, 2008). Statistical downscaling often involves the correction of factors inaccurately modeled by GCMs (bias removal). Many models may overestimate precipitation in the various regions, for instance, on the order of a millimeter a day, or roughly an inch a month (Bader et al. 2008). So, for instance, a downscaling effort would typically correct that bias before modeling future rainfall (Lenart, 2008).

2.3.2 Dynamical Downscaling

Dynamical downscaling modifies output from GCMs into regional meteorological models (Lenart, 2008). Rather than using equations to bring global-scale projections down to a regional level, dynamic downscaling involves using numerical meteorological modeling to reflect how global patterns affect local weather conditions (Lenart, 2008). The amount of calculations involved in dynamical downscaling makes it difficult if not impossible to produce decades-long simulations with different GCMs or multiple emissions scenarios (Maurer, and Hidalgo, 2007). As a result, most research aimed at producing regional projections involves statistical downscaling to consider potential impacts on specific regions or sectors (Lenart, 2008).

2.4 Downscaled Data Used for Analysis

For this study, the data used for analysis was statistically downscaled GCM data derived using a methodology known as Bias Correction Spatial Disaggregation (BCSD). This method was originally developed by Wood et al. (2004) and used extensively for

water resources investigations in the recent years (Maurer, 2007). In this method, bias-correction is achieved by using a quantile-based mapping technique at 2◦, common to all GCMs, followed by a spatial downscaling step to interpolate data to the 1/8◦ scale.

2.5 Climate Change Scenarios

The IPCC developed a set of scenarios to represent the range of driving forces and emissions in the scenario literature so as to reflect current understanding and knowledge about underlying uncertainties. Four different narrative storylines were developed to describe consistently the relationships between emission driving forces and their evolution and add context for the scenario quantification. Each storyline represents different demographic, social, economic, technological, and environmental developments. Each scenario represents a specific quantitative interpretation of one of four storylines. These scenarios are labeled as A1, A2, B2 and B1 in order of decreasing emissions (Liu et al., 2009). The set of scenarios consists of six scenario groups drawn from the four families: one group each in A2, B1, B2, and three groups within the A1 family, characterizing alternative developments of energy technologies: A1FI (fossil fuel intensive), A1B (balanced), and A1T (predominantly non-fossil fuel). These current set of emissions scenarios was an update to and replacement for the IS92 scenarios (IPCC). These set of scenarios is outlined in the IPCC Special Report on Emission Scenarios (SRES).

2.6 Special Report on Emissions Scenarios (SRES)

2.6.1 Scenario A1

A1. According to the IPCC, the A1 storyline and scenario family describes a

future with very rapid economic growth, global population that peaks in mid-century and declines thereafter. They also state that there will also be the rapid introduction of new and more efficient technologies. The major underlying themes are convergence among regions, capacity building and increased cultural and social interactions, with a substantial reduction in regional differences in per capita income. As previously mentioned, the A1 scenario family branches off into three other groups that describe alternative directions of technological change in the energy system (IPCC, 2007).

2.6.2 Scenario A2

For the A2 storyline and scenario family the IPCC states that they (it) describe a very heterogeneous world with an underlying theme of self-reliance and preservation of local identities. Fertility patterns across regions converge very slowly, which results in continuously increasing population. Economic development is primarily regionally oriented and per capita economic growth and technological change more fragmented and slower than other storylines (IPCC, 2007).

2.6.3 Scenario B1

With the B1 storyline and scenario family, a convergent world with the same global population, that peaks in mid-century and declines thereafter is described, as in the A1 storyline, but with rapid change in economic structures toward a service and information economy, with reductions in material intensity and the introduction of clean and resource-efficient technologies. The focus is on global solutions to economic, social and environmental sustainability, including improved equity, but without additional climate initiatives (IPCC, 2007).

2.6.4 Scenario B2

The B2 storyline and scenario family describes a world in which the focus is on local solutions to economic, social and environmental sustainability. It is a world with continuously increasing global population, at a rate lower than that of storyline and scenario family A2, and less rapid and more diverse technological change than in the A1 and B1 storylines. While the scenario is also oriented towards environmental protection and social equity, it focuses on local and regional levels (IPCC, 2007).

2.7 Climate Change Models

A coordinated set of global coupled climate model experiments for twentieth- and twenty-first-century climate was run by 16 modeling groups from 11 countries for assessment in the Intergovernmental Panel on Climate Change (IPCC) Fourth Assessment Report (AR4). This effort was organized by the World Climate Research Programme (WCRP) Climate Variability and Predictability (CLIVAR) Working Group on Coupled Models (WGCM) Climate Simulation Panel, and constitutes the third phase of the Coupled Model Intercomparison Project (CMIP3). The dataset is called the WCRP CMIP3 multimodel dataset. The multimodel data were made openly available for analysis and academic applications (Meehl et al. 2007).

From the SRES family of emission scenarios, only three were used in the CMIP3 climate change simulation runs for the IPCC Fourth Assessment report: SRES-B1, SRES-A1B and SRES-A2. This report will use only SRES-A1B climate change simulation run for analyzing the potential impact on streamflow trends. The various models are listed in Table 2-1 below.

Table 2-1: Description of the CMIP3 Models (Maurer et al., 2007)

Modeling Group, Country	WCRP CMIP3 I.D.	SRES A2 runs	SRES A1b runs	SRES B1 runs	Primary Reference
Bjerknes Centre for Climate Research	BCCR-BCM2.0	1	1	1	Furevik et al.,2003
Canadian Centre for Climate Modeling & Analysis	CGCM3.1 (T47)	1...5	1...5	1...5	Flato andBoer, 2001
Meteo-France / Centre National de Recherches Meteorologiques, France	CNRM-CM3	1	1	1	Salas-Melia etal., 2005
CSIRO Atmospheric Research, Australia	CSIRO-Mk3.0	1	1	1	Gordon et al.,2002
US Dept. of Commerce / NOAA / Geophysical Fluid Dynamics Laboratory, USA	GFDL-CM2.0	1	1	1	Delworth etal., 2006
NASA / Goddard Institute for Space Studies, USA	GISS-ER	1	2, 4	1	Russell et al.,2000
Institute for Numerical Mathematics, Russia	INM-CM3.0	1	1	1	Diansky andVolodin, 2002
Institut Pierre Simon Laplace, France	IPSL-CM4	1	1	1	IPSL, 2005
Center for Climate System Research (The University of Tokyo), National Institute for Environmental Studies, and Frontier Research Center for Global Change (JAMSTEC), Japan	MIROC3.2 (medres)	1...3	1...3	1...3	K-1 modeldevelopers, 2004
Meteorological Institute of the University of Bonn, Meteorological Research Institute of KMA	ECHO-G	1...3	1...3	1...3	Legutke andVoss, 1999
Max Planck Institute for Meteorology, Germany	ECHAM5/ MPI-OM	1...3	1...3	1...3	Jungclaus etal., 2006
Meteorological Research Institute, Japan	MRI-CGCM2.3.2	1...5	1...5	1...5	Yukimoto etal., 2001
National Center for Atmospheric Research, USA	CCSM3	1...4	1...3, 5...7	1...7	Collins et al.,2006
National Center for Atmospheric Research, USA	PCM	1...4	1...4	2...3	Washington etal., 2000
Hadley Centre for Climate Prediction and Research / Met Office, UK	UKMO-HadCM3	1	1	1	Gordon et al.,2000

2.8 Water Balance Models

In order to fully understand and develop any hydrologic model, a fundamental understanding of the natural hydrologic cycle itself will be required. The earth's water is always in continuous motion, it has no beginning or end. The natural water cycle, also known as the hydrologic cycle, describes the continuous movement of water above, on, and below the surface of the Earth and always changing states between liquid, vapor, and ice at various places in the water cycle (usgs.gov). To further explain the cycle, water evaporates from land and ocean surface and become part of atmosphere in the form of water vapor; the water vapor then rises until it condenses (clouds) and then precipitates on the earth's surface (rain). The precipitated water may then interact (intercept) with vegetation, becomes overland flow, infiltrate into the soil, flow through the soil (subsurface flow) and discharges into streams as surface runoff. The infiltrated water may percolate deeper to recharge groundwater, later emerging as spring and seeping into streams to form surface runoff and finally flowing into the sea or evaporating into the atmosphere as the hydrological cycle continues (Moreda, 1999). Figure 2-1 below shows a simple illustration of said cycle.

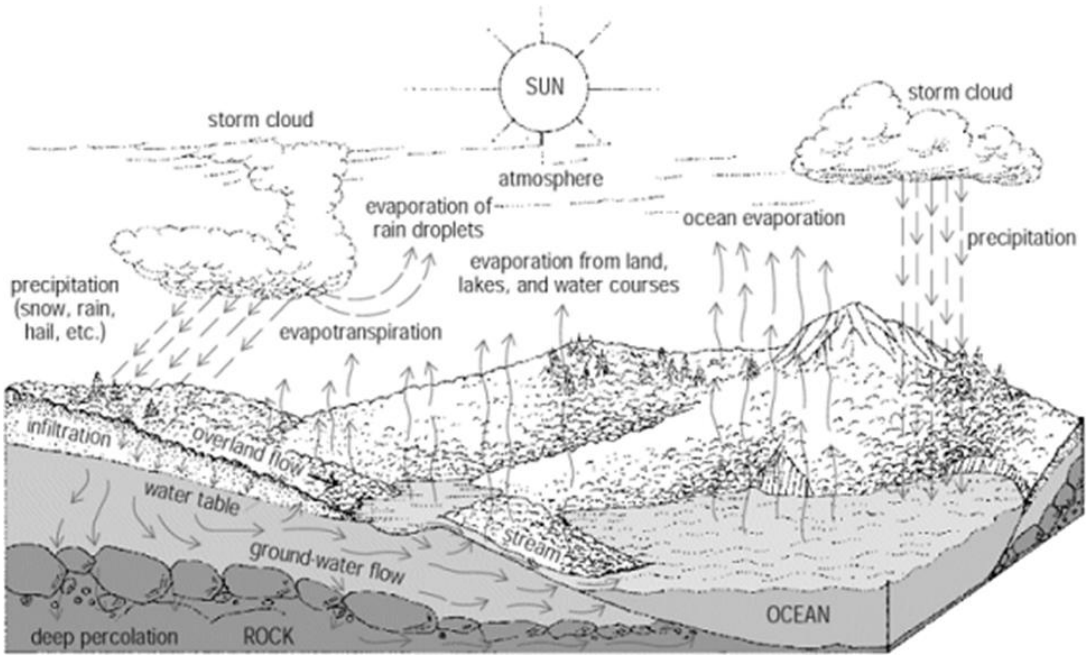

Figure 2-1 - Hydrologic Cycle (Image Source:

http://accessscience.com/content/Hydrology/329800)

The fundamental structure of any monthly water balance model attempts to mimic the hydrological processes by conceptualizing the catchment as interconnected storages, through which the water passes from input as rainfall to output as stream flow. The development of these models began in the 1940s by Thornthwaite (1948) and later revised by Thornthwaite and Mather (1955, 1957). They have since been adopted, modified, and applied to a wide range of hydrological problems (e.g. Gabos and Gasparri, 1983; Alley, 1984, 1985; Vandewiele *et al*., 1992; Xu and Vandewiele, 1995) (Xu, and Singh, 1998) .A thorough review of water balance model was done by Xu and Singh, (1998) which can be referenced for additional in-depth information. This section provides a brief outline of various water balance approaches for characterizing catchment hydrology.

Water balance models have been developed at various time scales (e.g. hourly, daily, monthly and yearly) and to varying degrees of complexity (Fish, 2011). A number of varying models and parameter estimation techniques have been considered, ranging from relatively complex conceptual models with 10 to 15 parameters for arid regions in Africa (e.g. Pitman, 1973) to very simple models with 2 to 5 parameters for humid regions in temperate zones (e.g. Vandewiele *et al*., 1992; Makhlouf and Michel, 1994; and Xu *et al*., 1996a) (Xu and Singh, 1998).

Precipitation constitutes the largest component in a water balance equation, a number of monthly water balance models have been developed using only precipitation (rainfall) as input. An example of this kind of model is the Tennessee Valley Authority (TVA) model for prediction of monthly water yield developed by Snyder (1963). The model partitions runoff into three components: (1) immediate runoff, (2) delayed runoff, and (3) time function, assumed to have no interaction with other components (Xu, and Singh, 1998). Other models, such as the Thomas (1981) abcd model uses rainfall and temperature as input. A key feature of these models is that the temperature is used to estimate potential evapotranspiration by the Thornthwaite approach, which together with monthly precipitation is used as input data for the models (Xu and Singh, 1998).

Another set of developed monthly models uses monthly precipitation and potential evapotranspiration as the sole inputs. These models have been developed in a wide range of climatic regions for an extensive range of applications and vary considerably in their complexity (Xu and Singh, 1998). An example of these models was developed by Pitman (1973, 1978) for generating monthly river flows for the South African catchments. It uses 12 parameters to compute actual evapotranspiration,

interception, surface runoff, soil moisture and runoff from upper and lower zones.

There are even monthly models that uses daily time step as input. Haan (1972) developed a model for simulating monthly streamflow by using this approach. The estimated average potential evapotranspiration and daily rainfall are used as input. The model uses four parameters and has two storages. It is believed that the use of daily rainfall as input improves the estimation of such processes, however the use of daily data increases the amount of work and may limit research to fewer catchments instead of water balance computations over large geographical units (Xu and Singh, 1998).

Whichever the model, two key component are use as inputs, precipitation and evapotranspiration. As previously mentioned, precipitation is a major contributor to any water balance model which may enter the system in different forms, such as rainfall, storms, dew or any form of water landing from atmosphere. It is a key forcing variable in hydrological models and hence spatially and temporally correct rainfall measurement is critical in hydrologic modeling processes and the management of water resources. The accuracy of measurement and analysis of precipitation data from a network of stations can significantly impact reliability of water balance computations. The amount of precipitation can be defined as an accumulated total volume for any selected time period. No reliable water balance computation is possible with insufficient knowledge of the spatial rainfall patterns (Xu & Singh, 1996). Evapotranspiration also plays an important role in water balance calculations. It is the second largest quantity in a hydrological water balance. Accurate spatial and temporal predictions of ET are required for water balance models (Xu & Singh, 1996).

The Thomas (1981) abcd model was chosen for this research because it has been

proven in the past to provide accurate estimations of rainfall surface runoff using precipitation and temperature (used to obtain potential evapotranspiration) data. It is a simple model with only four, easily calibrated parameters, and it can be used an effective tool for estimating the hydrological effects of various climate change scenarios. The Thomas Model is a nonlinear water balance model which accepts precipitation and potential evapotranspiration as input, producing stream flow as output. The model has four parameters *a, b, c* and *d*, each having a physical interpretation. The parameter *a* reflects the propensity of runoff to occur before the soil is fully saturated. The parameter *b* is an upper limit on the sum of evapotranspiration and soil moisture storage. The parameter *c* is equal to the fraction of streamflow, which arises from groundwater, so that it is equivalent to the base flow index. The reciprocal of the parameter *d* is equal to the groundwater residence time, so that *d* is proportional to the base flow recession constant (Sankarasubramanian and Vogel, 2002).

CHAPTER 3. METHODOLOGY

3.1 Thomas model

This study employs the 'abcd' model introduced by Thomas (1981) and Thomas et al. (1983) because it is comparable with other water balance models and each of its parameters has a physical interpretation. It requires time series of monthly precipitation, potential evapotranspiration and streamflow data to enable calibration. The following equations and steps were used to develop the models: The initial groundwater storage ($S_{G(O)}$), initial soil storage ($S_{W(O)}$), and the *a, b, c , d* parameters were specified along with the obtained precipitation (P_t) and estimated potential evapotranspiration data (PE_t). Given P_t and $S_{W(O)}$, the available water (W_t) was determined

$$W_t = P_t + S_{W(O)} \qquad \forall t \tag{3.1}$$

Given W_t, the evapotranspiration opportunity (Y_t) was determined

$$Y_t = \frac{W_t + b}{2a} - \left\{ \frac{(W_t + b)^2}{(2a)^2} - \frac{W_t b}{a} \right\}^{0.5} \qquad \forall t \tag{3.2}$$

Given W_t and Y_t, the overland runoff ($R_{O(t)}$) and groundwater recharge ($R_{G(t)}$)was determined

$$R_{O(t)} = (1-c)(W_t - Y_t) \qquad \forall t \tag{3.3}$$

$$R_{G(t)} = c(W_t - Y_t) \qquad \forall t \tag{3.4}$$

Given $R_{G(t)}$ and $S_{G(O)}$, the groundwater storage ($S_{G(t)}$) was determined

$$S_{G(t)} = \frac{R_{G(t)} + S_{G(O)}}{d+1} \qquad \forall t \tag{3.5}$$

Given $S_{G(t)}$, determine base flow or ground water contributing to stream($Q_{G(t)}$)

$$Q_{G(t)} = d \times S_{G(t)} \qquad \forall t \tag{3.6}$$

Given $R_{O(t)}$ and $Q_{G(t)}$, the total flow was determined

$$Q_{T(t)} = R_{O(t)} + Q_{G(t)} \qquad \forall t \tag{3.7}$$

The soil moisture storage at the end of the period t ($S_{W(t)}$) was determined and the process repeated for each interval.

$$S_{W(t)} = Y_t e^{-PE/b} \qquad \forall t \tag{3.8}$$

3.2 PE Estimation

Evaporation data input is necessary component of the abcd model; however, evaporation data are seldomly collected. The potential evapotranspiration (PE, (φ_t)) required for the "abcd" water balance model was estimated using a widely used method

developed by Thornthwaite and Wilm (1994). The PE value for a given month is based on the mean monthly air temperature efficiency index, which is defined as the sum of 12 monthly values of heat index given by:

$$\varphi_t = k_t k_1 \left(\frac{10 T_{am}}{j} \right)^{k_2 J^3 + k_4 J + k_4 J + k_5} \quad \forall t \tag{3.9}$$

$$J = k_6 \sum_{t=1}^{12} T_{am}^{1.514} \tag{3.10}$$

Where:

$\varphi_t =$ The potential evapotranspiration of month, t

$T_{am} =$ The mean monthly air temperature of month, t

$J =$ The annual heat index (°C)

$k_t =$ The monthly correction constant function of latitude (Grey, 1973)

$k_1 = 16.0$ mm/month

$k_2 = 6.75 \text{x} 10^{-7}$ °C^{-3}

$k_3 = -7.71 \text{x} 10^{-5}$ °C^{-2}

$k_4 = 1792 \text{x} 10^{-2}$ °C^{-1}

$k_5 = 0.49239$

$k_6 = 0.08745$

3.3 Model Calibration - Objective function

Conventional approaches to model calibration assume that the primary objective is to obtain a "best fit" to the observed stream-flows at a particular location. The main idea behind the parameter estimation procedure is to select parameter values that minimize the differences between the simulated and recorded stream-flows. An objective function is a method that is employed to compute a numerical measure of the deviation between the model calculated output and the observed catchment output. Four (4) different objective functions, root mean squared error (RMSE), squared error (SE) absolute error (AE) and mean absolute error (MAE) were used to optimize each catchment. To ensure that the optimization procedures produced hydrologically reasonable parameters, searches were constrained to operate within pre-specified limits. Refer to Table 3-1 below for parameter limits.

Table 3-1: Parameter Calibration Range

Range	Initial Soil Storage (mm)	Initial Groundwater Storage (mm)	a	b	c	d
Upper Limit	5	310	1	15	0.8	0.5
Lower Limit	3	200	0.5	0	0	0

Below are the formulations of each of these objective functions.

Objective Functions:

$$\text{Minimize} \quad \sum_{t=1}^{T} \left| \theta'_{B,t} - \theta^{o}_{B,t} \right| \tag{3.11}$$

$$\text{Minimize} \quad \sum_{t=1}^{T}(\theta'_{B,t} - \theta^{o}_{B,t})^2 \tag{3.12}$$

$$\text{Mimimize} \quad \sqrt{\frac{1}{T}\sum_{t=1}^{T}(\theta'_{B,t} - \theta^{o}_{B,t})^2} \tag{3.13}$$

$$\text{Minimize} \quad \frac{1}{T}\sum_{t=1}^{T}\left|\theta'_{B,t} - \theta^{o}_{B,t}\right| \tag{3.14}$$

Where:

$\theta'_{B,t}$ = Estimated discharge value, time interval *i*

$\theta^{o}_{B,t}$ = Observed discharge value

t = Index for time interval (month)

T = Number of Time intervals

3.4 Optimization Software

In this research, Microsoft Excel Generalized Reduced Gradient (GRG) solver was initially used. These solvers analyze the solution space for a given objective function by analyzing the gradient of the objective function. The search of the solution space is initiated at a "user-defined" starting point and variables are modified within specified constraints until the solver converges to a local or global optimum solution. GRG Solver is considered robust in optimizing relatively simple non-linear problems; however, it is possible for the solver to become "trapped" in local optimum solutions (Sharif, 2012). To overcome this limitation, Microsoft Evolutionary solver was used. This solver is based on genetic algorithm (GA). It is a search technique used in computing, to find true or

approximate solutions to optimization and search problems and are categorized as global search heuristics. GA is a particular class of evolutionary algorithms that use techniques inspired by evolutionary biology such as inheritance, mutation, selection, and crossover. If properly initialized, GA is known to converge at global optimum solutions.

3.5 Model Validation - Performance Measures

Selection of an acceptable model requires both subjective and objective judgments. The results may be influenced by a variety of causes such as problems in calibration. These problems could be related to errors in the data used in calibration and/or problems related to use of a period of record that does not contain enough of the physical processes needed to calibrate key parameters (Moreda, F., 1999). After the model has been calibrated and the parameters estimated, it then has to be tested to see how well it will perform on a different data set. This testing or validation can is an important stage of the model analysis. If the model produces acceptable results, then the model can be put into use. For this study, five performance measures will be used to validate the model. The performance of each calibration methods are compared using widely recognized and commonly used error measures, root mean squared error (RMSE), squared error (SE), mean absolute error (MAE) , absolute error (AE), and coefficient of correlation (ρ), based on actual and estimated rainfall values at the station.

3.5.1 Root Mean Square Error (RMSE)

The RMSE is the difference between forecast and corresponding observed values are each squared and then averaged over the sample. The square root of the average is then taken. Since the errors are squared before they are averaged, the RMSE gives a relatively high

weight to large errors. This means the RMSE is most useful when large errors are particularly undesirable. The inverse values of RMSE are proportionately used as weights.

3.5.2 Squared Error (SE)

The error is the difference between the measured values of the data point minus the predicted value of said data point. Each error is squared and the summed.

3.5.3 Absolute Error (AE)

AE is the total sum of the absolute value of each individual error. Absolute errors do not always give an indication of how important the error may be, the measurement only shows how large the error actually is between each point.

3.5.4 Mean Absolute Error (MAE)

The MAE measure is the average over the verification sample of the absolute values of the differences between forecast and the corresponding observation. The MAE is a linear score which means that all the individual differences are weighted equally in the average.

3.5.5 Correlation Coefficient (ρ)

Correlation Coefficient measures the strength and the direction of a linear relationship between two variables. It is a concept from statistics that measure how well trends in the predicted values follow trends in past actual values. The correlation coefficient is a number between 0 and 1. If there is no relationship between the predicted values and the actual values the correlation coefficient is 0. As the strength of the relationship between the predicted values and actual values increases so does the correlation coefficient. A perfect fit gives a coefficient of 1.0. Therefore, in general the higher the correlation coefficient the better the model is doing.

The error measures, RMSE, MAE, AE, SE, and ρ are given by, respectively:

$$RMSE = \sqrt{\frac{1}{T}\sum_{t=1}^{T}(\theta_t' - \theta_t^o)^2} \tag{3.15}$$

$$MAE = \frac{1}{T}\sum_{t=1}^{T}\left|\theta_t' - \theta_t^o\right| \tag{3.16}$$

$$AE = \sum_{t=1}^{T}\left|\theta_t' - \theta_t^o\right| \tag{3.17}$$

$$SE = \sum_{t=1}^{T}(\theta_t' - \theta_t^o)^2 \tag{3.18}$$

$$\rho = \frac{\sum_{t=1}^{T}(\theta_t' - \mu_B)(\theta_t^o - \mu_j)}{(n-1)\sigma_B\sigma_j} \tag{3.19}$$

Where:

θ_t' = Estimated discharge value, time interval *i*

θ_t = Observed discharge value

B = Index for base station

j = Index for station

T = Number of time intervals

t = Index for time interval (month)

3.6 Model Ranking

A scoring system was developed in order to compare the various methods used.

To score each method, the five (5) performance measures were normalized by dividing each value with the largest value in the same group. The values were then added to 1-correlation coefficient value. The methods was ranked based on the assessed score from lowest to high, with the one with the lowest score being the best method.

3.7 Model Application

After the models were developed and ranked, each of the three models was applied to three catchments using all fifteen (15) WCRP CMIP3 Climate Model Projections (temperature and precipitation).

CHAPTER 4. CASE STUDY

4.1 Case Study Areas for Model Application

The Thomas Model discussed in this paper was applied to three (3) catchment areas in Florida to predict future stream-flows in order to assess and mitigate against any potential negative impacts. These sites were selected based on two main criteria. One criterion is the amount of streamflow data that was available to conduct the analysis. It was determined that to develop a reliable/realistic model, a long time period of continuous uninterrupted streamflow data would be required. The time period determined was 50 years of streamflow data for all the various model inputs. The other selection criterion for the catchment areas was their proximity to the weather station where the temperature and precipitation data was available that will also be used in the model. The three USGS gaging stations (hydraulic units) selected were (1) USGS 02297100 Joshua Creek at Nocatee, FL, (2) USGS 02245500 South Fork Black Creek near Penney Farms, FL, (3) USGS 02310000 Anclote River near Elfers, FL. The respective associated weather station for each unit was located in (1) Arcadia, (2) Federal Point, and (3) Tarpon Spring. Throughout this paper these areas will be referred to by the weather station location names and or the hydraulic unit location. Figure 4-1 below shows the location of the case study areas within the State of Florida.

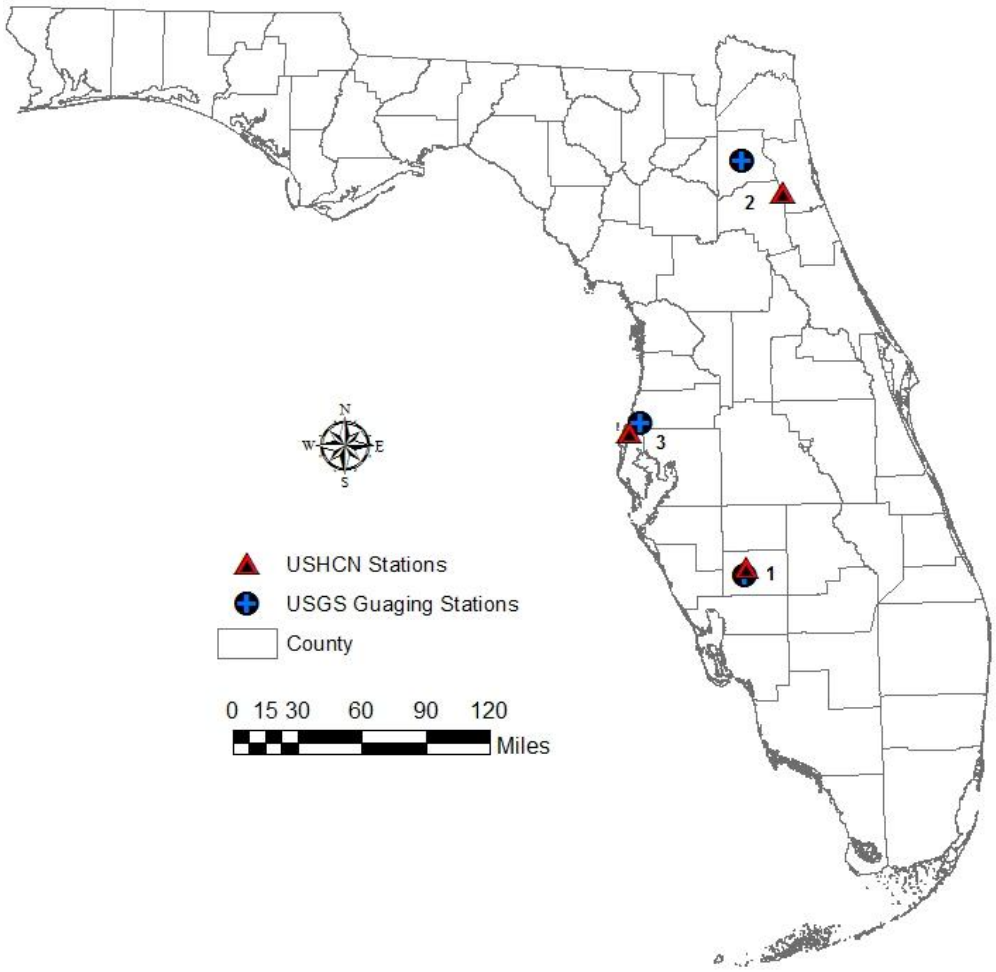

Figure 4-1: Map of Florida showing locations of case study areas -(1) Arcadia, (2) Federal Point, and (3) Tarpon Spring

4.1.1 South Fork Black Creek near Penney Farms, FL (USGS 02245500)

The South Fork black Creek catchment area hydraulic unit has the coordinate's latitude 29°58′45″ and longitude 81°51′08″. It is located on right bank at upstream side of bridge on State Highway 16, 0.7 mi downstream from Greens Creek, 2.5 mi west of Penney Farms, 9.5 mi west of Green Cove Springs, and 24 mi upstream from mouth of Black Creek (USGS, 2012).

The catchment area is approximately 134 square miles in area and is irregularly shaped (Figure 4-2) that is falls within the St. Johns Basin and the Lower St. Johns Sub-basin. The main drainage features of the basin are South Fork which drains into Black Creek. South Fork begins at Varnes Lake in the Camp Blanding State Wildlife Management Area. The South Fork flows north-northeast through Penny Farms and continues to its confluence with the North Fork. The average gradient of the South Fork channel is approximately 4.8 feet per mile with bank elevation ranging from 120 ft. The average channel gradient of Black Creek from Middleburg to the St. Johns River is approximately 0.5 feet per mile with bank elevations ranging from 10 ft. NGVD at Middleburg to less than 5 ft. NGVD at the outfall to the St. Johns River (U. S. Army Corps of Engineers - Special Publication SJ98-SP10, 1997).

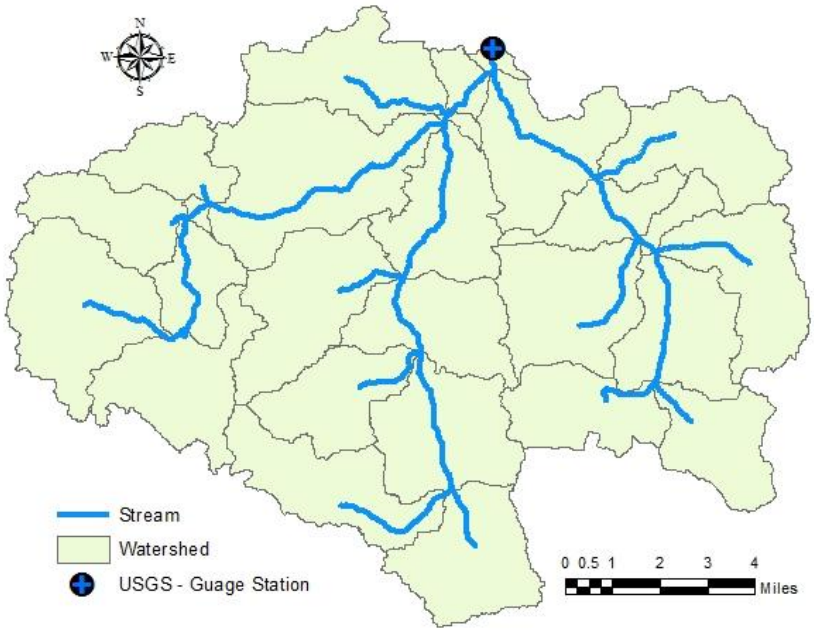

Figure 4-2: South Fork Black Creek Catchment

Table 4-1: South Fork Black Creek Guaging Station Information

USGS 02245500 South Fork Black Creek near Penney Farms, FL
Clay County, Florida
Hydrologic Unit Code 03080103
Latitude 29°58'45", Longitude 81°51'08" NAD27
Drainage area 134 square miles
Gage datum 9.82 feet above NGVD29

4.1.1.1 Land Use

The land uses of the South Fork Black Creek catchment areas were obtained from the Florida Geographic Data Library. Eight individual Florida Land Use Classification Code (FLUCC) (Level 1) land uses were identified within the catchment. Land use may alter the timing and volume of runoff, this may or may not be a desired effect depending on surface and sub-surface interactions, and other driving factors of the water balance. The drainage area is mostly underdeveloped with a urban/built-up makeup of approximately 6 percent. The largest land use classification within the catchment is upland forest, comprising approximately 64.22 percent of the basin. Wetlands account for approximately 20.46 percent of the catchment. Table 4-2 presents the distribution of land uses in the South Fork Black Creek catchment. Figure 4-3 is a map of the land uses within the catchment.

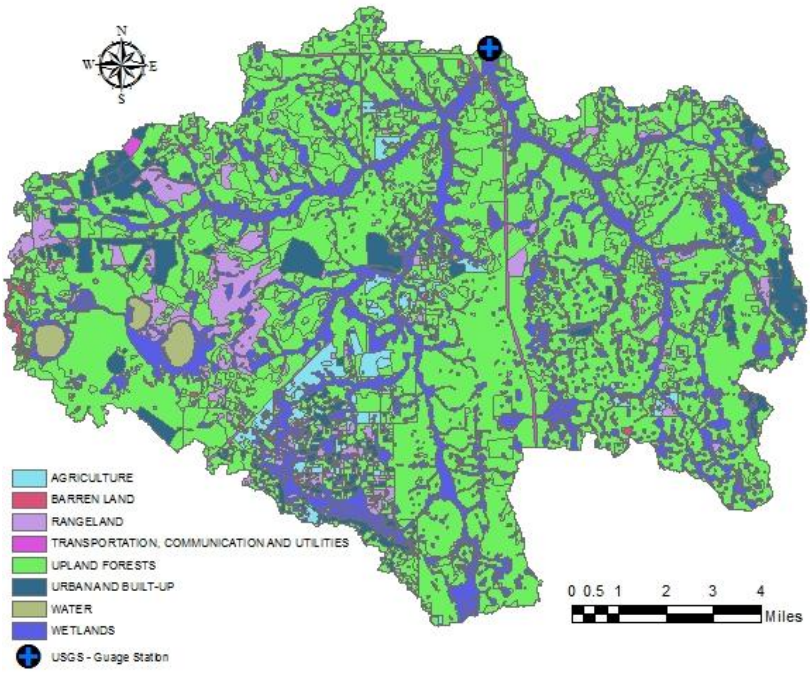

Figure 4-3: South Fork Black Creek - Land Use Map

Table 4-2: South Fork Black Creek - Level 1 Land Use Classification

Land Use Classification	Percentage
Upland Forests	64.22%
Wetlands	20.46%
Urban And Built-Up	6.15%
Rangeland	5.10%
Agriculture	2.35%
Water	0.92%
Transportation, Communication And Utilities	0.51%
Barren Land	0.29%

4.1.1.2 Soils

The soils of the South Fork Black Creek Catchment were identified by the U.S. Natural Resource Conservation Service (NRCS). Each soil type has been assigned to one of the four hydrologic soil groups (HSG) based on its runoff potential.

- A = Very well drained,
- B = Moderately well drained,
- C = Somewhat poorly drained,
- D = Very poorly drained.

Many soils have been assigned to two hydrologic soil groups in various areas, while others are unclassified. Table 4-3 presents the percentages of the HSG's within the catchment. HSG A/D is the soil group which covers the greatest portion of the basin, approximately 46.5 percent. HSG A, account for almost the same with 45.4 percent, followed by B/D, C/D, Unknown and B respectively. Figure 4-4 is a map of the HSG coverage within the South Fork Black Creek Catchment

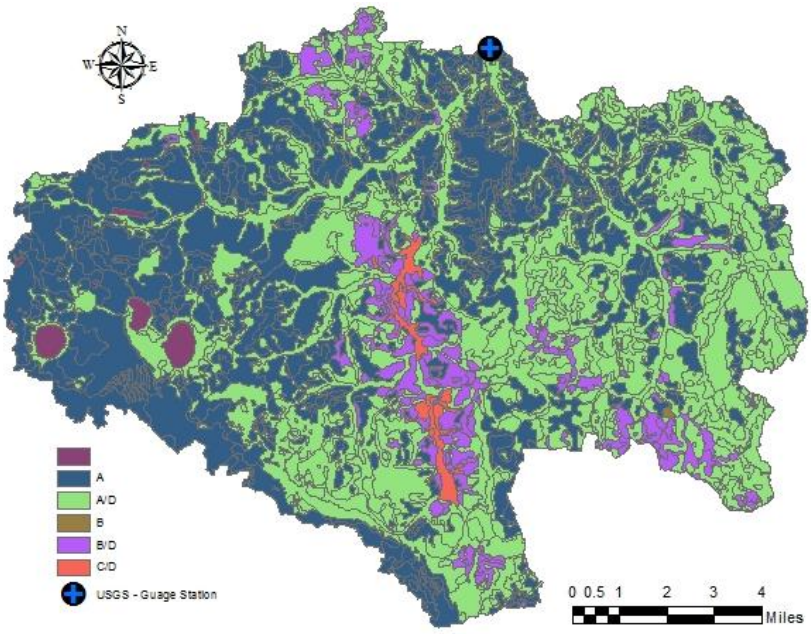

Figure 4-4: South Fork Black Creek - Soils Map

Table 4-3: South Fork Black Creek - Soils Category

Soil Type	Percentage
A/D	46.50%
A	45.39%
B/D	6.52%
C/D	0.84%
Unknown	0.73%
B	0.02%

4.1.2 Anclote River near Elfers FL (USGS 02310000)

The Anclote River Catchment area hydraulic unit has the coordinate's latitude 28°12′50″, longitude 82°40′00″ within Pasco County, FL. The hydrologic Unit 03100207 is located on left bank, 500 ft upstream from bridge on State Highway 54, 3.5 mi east of Elfers, and 16 mi upstream from mouth. The catchment area is approximately 72.5 square miles in area and is irregularly shaped (Figure 4-5); it falls within the Tampa Bay Basin and the Crystal-Pithlachascotee Subbasin. The Anclote River, rises in the karst-dominated area of the southwest central Florida ground water basin. It covers portions of two counties, northwest Hillsborough, and Pasco County.

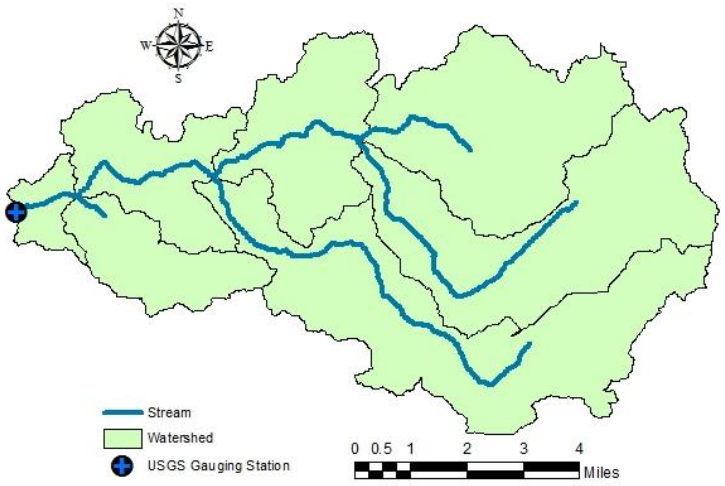

Figure 4-5: Anclote River Catchment

Table 4-4: Anclote River Gauging Station Information

USGS 02310000 Anclote River near Elfers, FL
Pasco County, Florida
Hydrologic Unit Code 03100207
Latitude 28°12'50", Longitude 82°40'00" NAD27
Drainage area 72.5 square miles
Contributing drainage area 72.50 square miles
Gage datum 0.00 feet above NGVD29

4.1.2.1 Soils

The soils of the Anclote River Catchment were identified by the U.S. Natural Resource Conservation Service (NRCS). HSG A/D is the soil group which covers the greatest portion of the basin, approximately 65.8 percent. HSG A, account for 10.4 percent, followed by B/D, B/D, B and Unknown respectively. Figure 4-6 is a map of the HSG coverage within the Anclote River Catchment

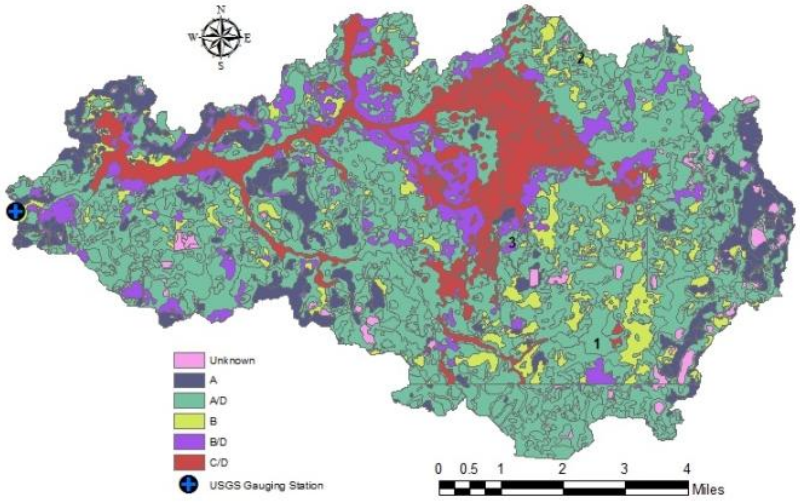

Figure 4-6: Anclote River Catchment - Soils Map

Table 4-5: Anclote River – Soil

Soil Type	Percentage
A/D	65.82%
A	10.42%
C/D	9.56%
B/D	7.46%
B	4.82%
Unknown	1.92%

4.1.2.2 Land Use

The largest land use classification within the catchment is agriculture, comprising approximately 28.43 percent of the basin. Wetlands followed closely with 27.19 percent. Other land uses within the catchment are listed in Table 4-6. Figure 4-7 is a map of the land uses within the catchment.

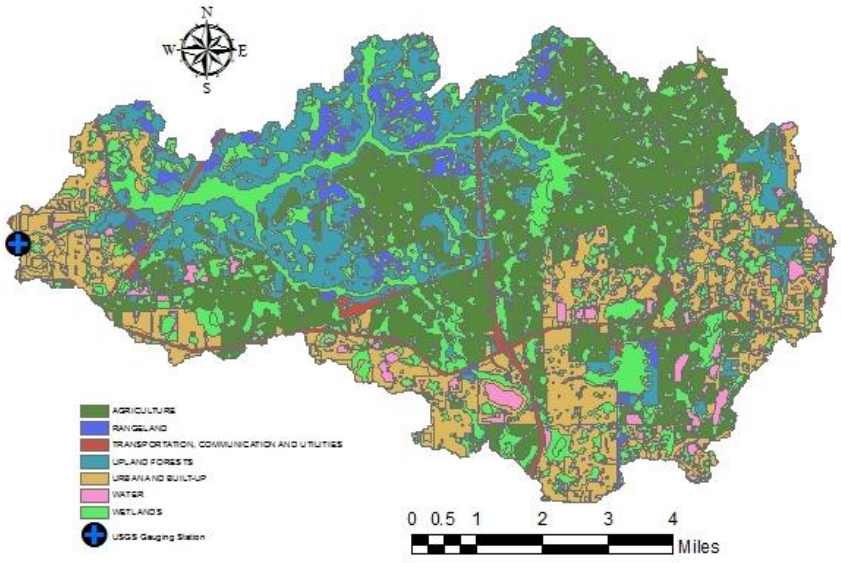

Figure 4-7: Anclote River Catchment - Land Use Map

Table 4-6: Anclote River Catchment – Level 1Land Use Classification (%)

Land Use Classification	Percentages
Agriculture	28.43%
Wetlands	27.19%
Urban And Built-Up	18.89%
Upland Forests	16.26%
Water	3.61%
Rangeland	3.19%
Transportation, Communication And Utilities	2.42%

4.1.3 Joshua Creek at Nocatee Fl (USGS 02297100)

The Joshua Creek Catchment area hydraulic unit has the coordinate's Lat 27°09′59″, long 81°52′47″ located in DeSoto County, FL. The hydrologic Unit 03100101, is near center of span on downstream side of bridge on U. S. Highway 17, 0.5 mi north of Nocatee, and 2.2 mi upstream from mouth. The catchment area is

approximately 132 square miles in area and is elongated in shape (Figure) within the Peace Basin and the Peace Sub-Basin.

Figure 4-8: Joshua Creek Catchment

Table 4-7: Joshua Creek Catchment – Gauging Station Information

USGS 02297100 Joshua Creek At Nocatee FL
De Soto County, Florida
Hydrologic Unit Code 03100101
Latitude 27°09'59", Longitude 81°52'47" NAD27
Drainage area 132 square miles
Contributing drainage area 132 square miles
Gage datum 3.94 feet above NGVD29

4.1.3.1 Land Use

The largest and most predominant land use classification within the catchment is agriculture, comprising approximately 69.66 percent of the basin. Wetlands are next with a mere 12.95 percent. Other land uses within the catchment are almost negligible and are listed in. Figure 4-9 is a map of the land uses within the catchment.

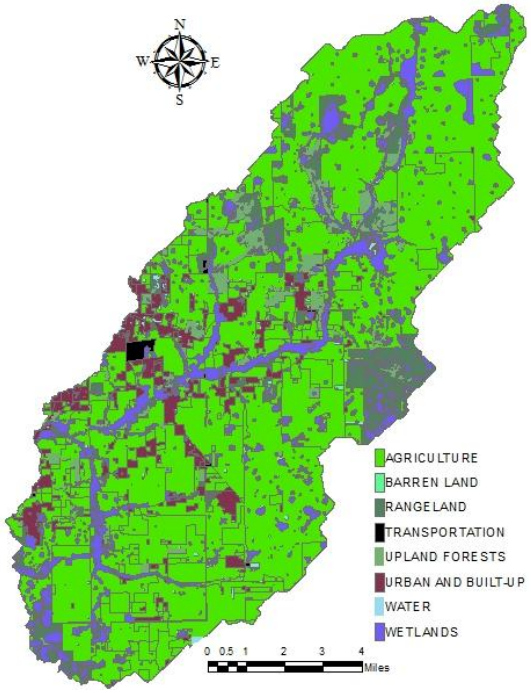

Figure 4-9: Joshua Creek Catchment - Land Use Map

Table 4-8: Joshua Creek Catchment – Level 1 Land Use Classification

Land Use Classification	Percentage
Agriculture	69.66%
Wetlands	12.95%
Urban And Built-Up	6.48%
Rangeland	6.01%
Upland Forests	3.94%
Transportation, Communication And Utilities	0.52%
Water	0.40%
Barren Land	0.04%

4.1.3.2 Soils

The soils of the Joshua Creek Catchment were identified by the U.S. Natural Resource Conservation Service (NRCS). HSG A/D is the soil group which covers the greatest portion of the basin, approximately 74.66 percent. HSG B/D, account for 15.73 percent, followed by C/D, A, Unknown and B respectively. Figure 4-10 is a map of the HSG coverage within the Anclote River Catchment.

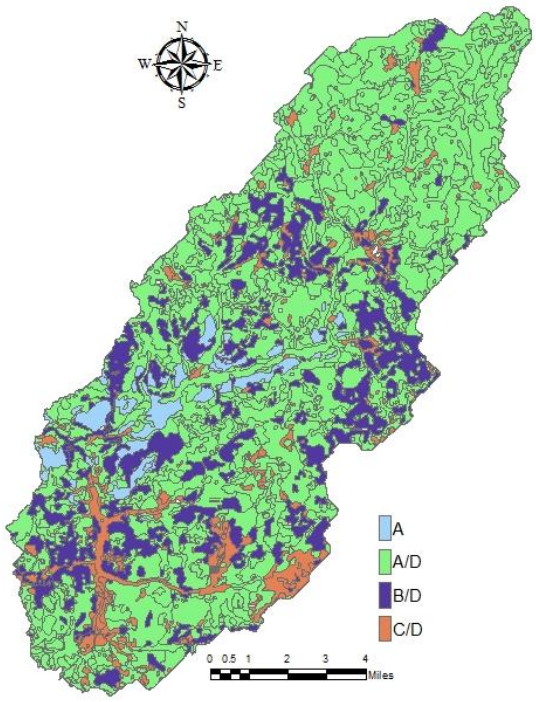

Figure 4-10: Joshua Creek Catchment - Soils Map

Table 4-9: Joshua Creek Catchment – Soil Category (%)

Soil Type	Percentage
A/D	74.66%
B/D	15.73%
C/D	6.47%
A	2.92%
Unknown	0.22%
B	0.00%

CHAPTER 5. DATA SOURCES AND ANALYSIS

5.1 Data Source

The average monthly observed streamflow data was obtained from the U.S. Geological Survey's website, the average monthly temperature and precipitation observed data were obtained from the United States Historical Climatology Network (USHCN), and the projected temperature and precipitation data was obtained from the "Bias Corrected and Downscaled WCRP CMIP3 Climate Projections" archive's website.

The United States Geological Survey (USGS) has collected water-resources data at approximately 1.5 million sites throughout the United States. Different types of data are collected; however they generally fit into the broad categories of surface water and groundwater. Surface-water data, such as gage height (stage) and streamflow (discharge), are collected at major rivers, lakes, and reservoirs. Groundwater data, such as water level, are collected at wells and springs. Water-quality data are also available for both surface water and groundwater (water.usgs.gov).

The U.S. Historical Climatology Network (USHCN) is a data set of average monthly data such as mean temperature and total monthly precipitation, used to assist in the detection of regional climate change. The USHCN is comprised of 1218 stations from the U.S. Cooperative Observing Network within the 48 contiguous United States with additional stations in other US territories. The stations used for this study were located in the Cities of Arcadia, Federal Point and Tarpon Springs.

The Bias Corrected and Downscaled WCRP CMIP3 Climate Projections" archive's focuses on developing downscaled translations of a large ensemble of CMIP3 projections over the contiguous U.S., in an effort to support risk-based adaptation planning and assessment. The archive was originally designed to serve monthly downscaled CMIP3 climate projection information developed using the Bias-Correction Spatial Disaggregation (BCSD) technique from Wood et al. (2002) (Brekke, L., et al 2011)

5.2 Model Acronyms

Throughout the rest of this paper, all the various 15 models used will be referred to by their assigned acronyms (M1 thru M15). Please refer to Table 5-1 below for description.

Table 5-1: Description of the CMIP3 Models Used in this Study

Model #	WCRP CMIP3 I.D.	Modeling Group, Country
M1	BCCR-BCM2.0	Bjerknes Centre for Climate Research
M2	CGCM3.1 (T47)	Canadian Centre for Climate Modeling & Analysis
M3	CNRM-CM3	Meteo-France / Centre National de Recherches Meteorologiques, France
M4	CSIRO-Mk3.0	CSIRO Atmospheric Research, Australia
M5	GFDL-CM2.0	US Dept. of Commerce / NOAA / Geophysical Fluid Dynamics Laboratory, USA
M6	GISS-ER	NASA / Goddard Institute for Space Studies, USA
M7	INM-CM3.0	Institute for Numerical Mathematics, Russia
M8	IPSL-CM4	Institut Pierre Simon Laplace, France
M9	MIROC3.2 (medres)	Center for Climate System Research (The University of Tokyo), National Institute for Environmental Studies, and Frontier Research Center for Global Change (JAMSTEC), Japan
M10	ECHO-G	Meteorological Institute of the University of Bonn, Meteorological Research Institute of KMA
M11	ECHAM5/ MPI-OM	Max Planck Institute for Meteorology, Germany

M12	MRI-CGCM2.3.2	Meteorological Research Institute, Japan
M13	CCSM3	National Center for Atmospheric Research, USA
M14	PCM	National Center for Atmospheric Research, USA
M15	UKMO-HadCM3	Hadley Centre for Climate Prediction and Research / Met Office, UK

5.3 Data Analysis

5.3.1 Statistical Numerical Measures

The obtained data were analyzed based on the various statistical numerical measures and graphs. Below are brief descriptions of these statistical tools.

5.3.1.1 Skewness

Skewness is a measure of symmetry or the lack of symmetry. A distribution, or data set, is symmetric if it looks the same to the left and right of the center point. If the majority of the data is at the left and the right tail is longer, the distribution is skewed right or positively skewed; if the peak is toward the right and the left tail is longer, the distribution is skewed left or negatively skewed.

5.3.1.2 Kurtosis

Kurtosis is a measure of whether the data are peaked or flat relative to a normal distribution. Higher values indicate a higher, sharper peak; lower values indicate a lower, less distinct peak. A normal distribution has kurtosis exactly 3. A distribution with kurtosis less than 3 has a central peak that is lower and broader, and its tails are shorter and thinner when compared to a normal distribution. A distribution with kurtosis greater that 3 when compared to a normal distribution, has its central peak that is higher and sharper, and its tails are longer and fatter.

5.3.1.3 Mean

The mean, sometimes referred to as the average, sum of all the data values divided by the sum of the total number of the data set. Although data points fall above, below, or at the mean, sometimes it can be used to estimate subsequent data points

5.3.1.4 Standard Deviation (STD)

The standard deviation (STD) gives an indication of how close the entire set of data is to the mean. Data sets with a small standard deviation are tightly grouped. Data sets with large standard deviations have data spread out over a wide range of values.

5.3.1.5 Range

The range is simple the distance or difference between the lowest and the highest values of a data set.

5.3.1.6 Maximum and Minimum

Maximum value is simply the highest value in the data set; minimum value is basically the reverse which is the lowest value.

5.3.1.7 Histograms

Histograms are graphs showing the summary count of data points falling in various ranges. Histograms are very useful for depicting large differences in shape or symmetry, such as whether a data set appears symmetric or skewed. They cannot be used for more precise judgments such as depicting individual values (Helsel, D., and Hirsch, R., 2002).

5.3.1.8 CDF Plots

Cumulative distribution function (CDF) is the cumulative sum of the probabilities up to the current point, which is the same as the probability that x is less than the current point. CDF plots display similar information as histograms of a data set. The CDF graph is useful to actually determine how well the distributions fit to data:

5.3.2 Arcadia Precipitation Data

Table 5-2 below provides a statistical summary (stats) of the precipitation data collected for use in the model development. The table contains both the observed (1951-2010) and the projected precipitation values (2011-2099). A quick glance of the statistical measures shows that the projected values more or less follows those of the observed values. The mean of the observed values is 4.332. The closest model to the observed mean was M4. The stats shows that all the models and the observed data sets are positively skewed, which indicates that the majority of the data points fall in the lower range. The histogram in Figure 5-1 provides a graphical illustration of this. The kurtosis values for the observed and all the 15 models were all above 3 which is an indication that its central peak is higher and sharper than that of a normal distribution, and its tails are longer and fatter.

Table 5-2: Arcadia Observed (1951-2010) - Projected Precipitation Data (2011-2099)

Models	Mean	STD	Skewness	Kurtosis	Max	Min	Range
Observed	4.332	3.724	1.342	5.077	23.700	0.000	23.700
M1	3.915	3.199	1.523	6.853	24.957	0.000	24.957
M2	4.350	2.988	0.943	3.858	16.273	0.090	16.183
M3	4.304	3.056	0.784	3.214	20.269	0.022	20.248
M4	4.337	2.941	1.013	4.696	22.062	0.151	21.910
M5	4.247	3.261	1.039	4.128	19.168	0.019	19.150
M6	3.986	2.916	0.821	3.016	14.866	0.089	14.776
M7	4.320	2.824	0.866	3.899	17.176	0.202	16.974
M8	4.362	3.285	1.056	4.147	18.541	0.092	18.449
M9	3.209	2.539	1.166	4.981	19.100	0.044	19.056
M10	4.458	3.561	0.995	3.687	18.933	0.077	18.856
M11	4.708	3.272	0.678	2.904	16.976	0.089	16.887
M12	4.481	2.964	0.745	3.730	21.807	0.092	21.716
M13	4.191	2.902	0.970	3.957	16.352	0.111	16.242
M14	4.257	3.205	0.865	3.184	17.917	0.064	17.853
M15	4.345	3.166	0.884	3.506	17.246	0.112	17.134

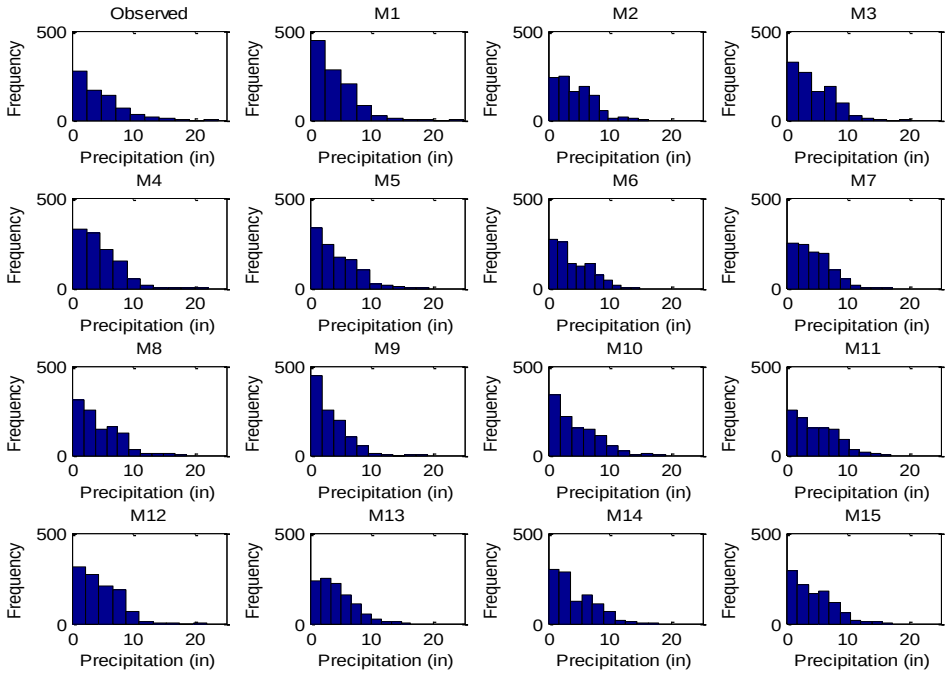

Figure 5-1: Histograms - Arcadia Observed (1951-2010) - Projected Precipitation Data (2011-2099)

To compare the projected vs. the observed precipitation values, the precipitation projection data was broken up into 4 periods, 2011-2030, 2031-2050, 2051-2070 and 2071-2099. Each of these periods was compared to the observed data using CDF plots. See Figure 5-2 through Figure 5-5 for CDF plots.

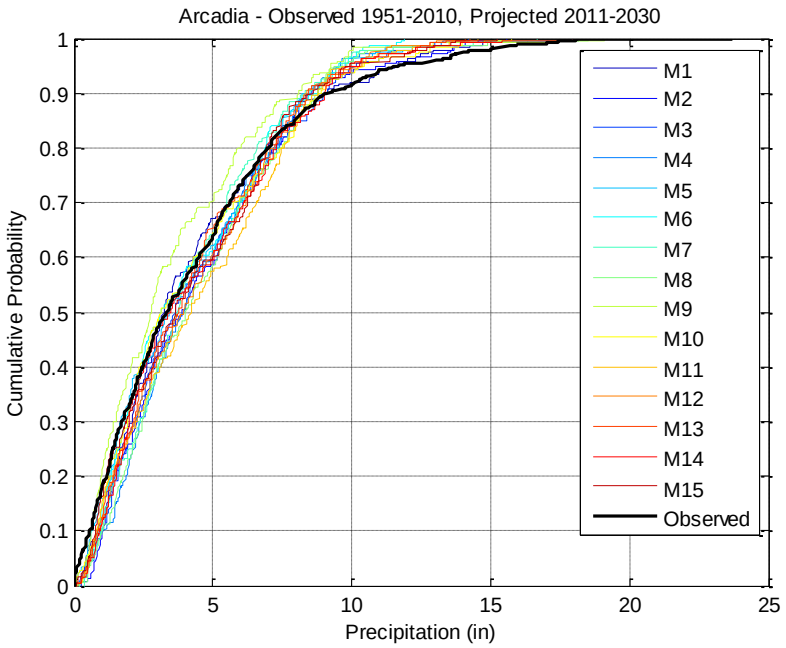

Figure 5-2: Arcadia Observed (1951-2010) - Projected Precipitation Data (2011-2030)

The first period plotted was 2011-2030, the graph illustrate that most of the models shows an increase in precipitation, except at the extremes where the trend is reversed. All models indicate reduced extreme values events (chance of having more precipitation is less).

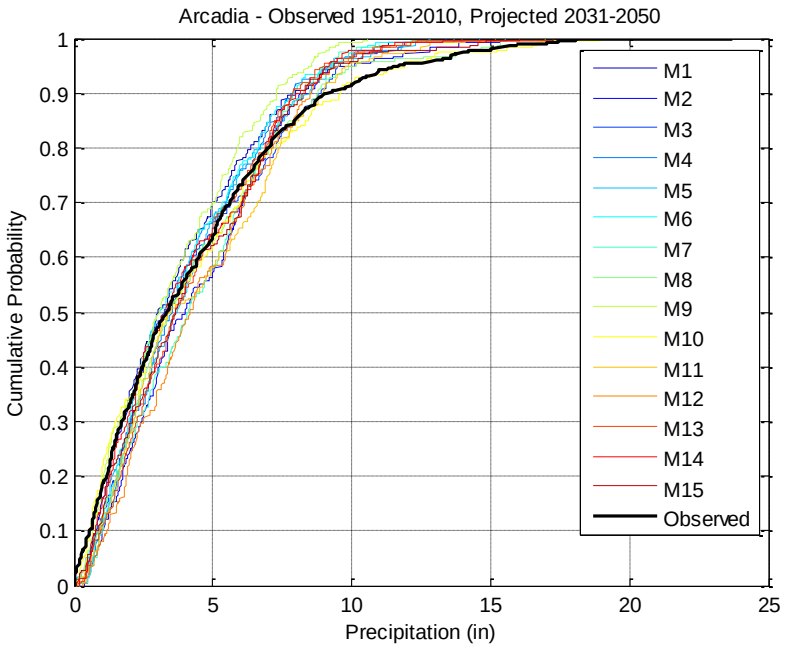

Figure 5-3: Arcadia Observed (1951-2010) - Projected Precipitation Data (2031-2050)

The next CDF plot (Figure 5-3) for period (2031-2050) followed the same pattern.

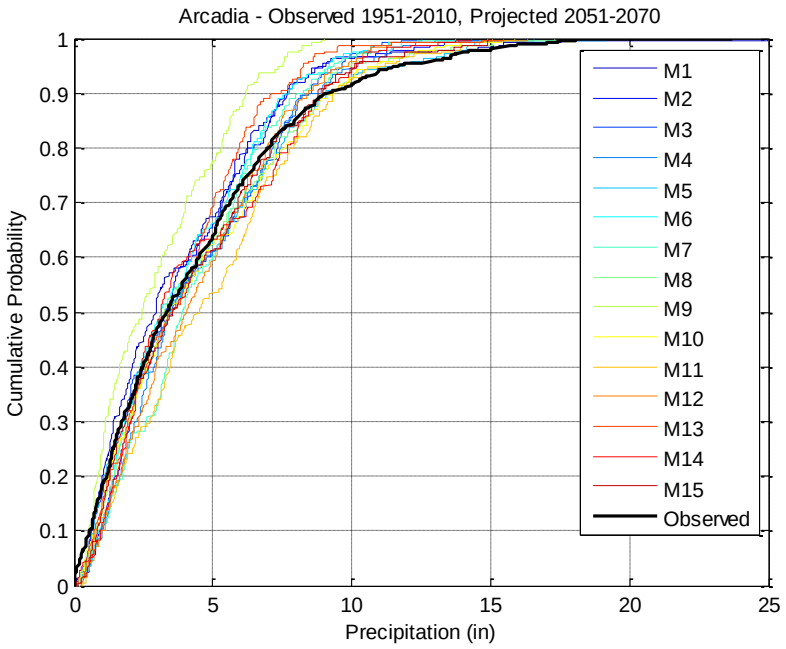

Figure 5-4: Arcadia Observed (1951-2010) - Projected Precipitation Data (2051-2070)

The plotted graphs also show that as time progresses, the CDF bands of the models widens. This is an indication that there is more variability among the models as time passes. One obvious model (M9) follows a different trend; the CDF plot shows that for all the time periods it is consistently underestimating the observed values. This trend was observed in plots for 2031-2050, 2051-2070 and 2071-2099.

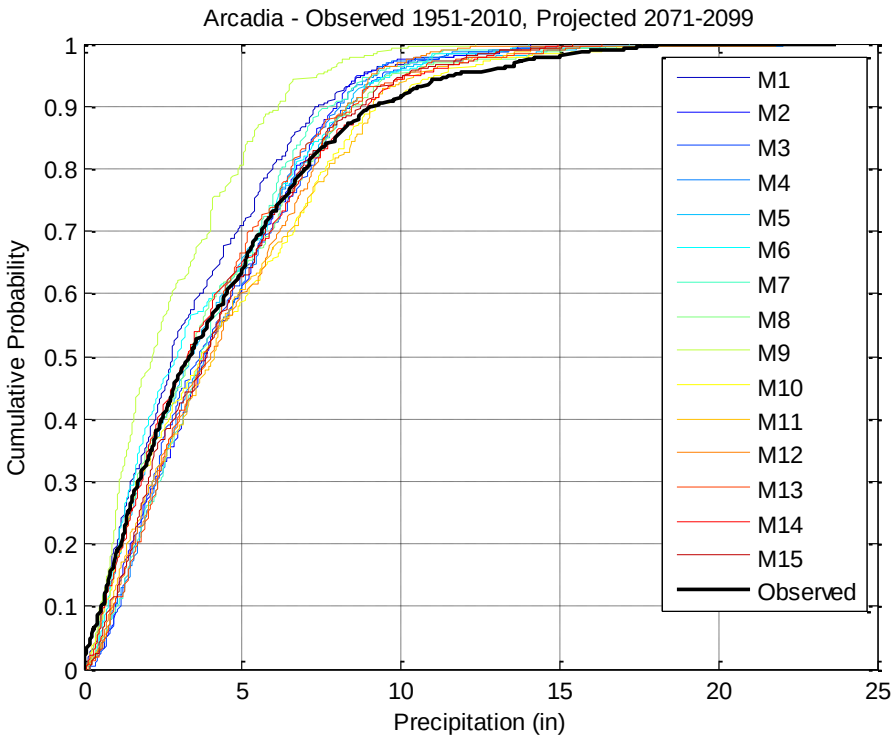

Figure 5-5: Arcadia Observed (1951-2010) - Projected Precipitation Data (2071-2099)

A scatter plot of the precipitation values for the observed values as well as for each model was done with a trend line added. The observed data (1951-2010) shows a slightly downward trend. Most of the models showed a decreasing trend or relatively no change. Model M10 was the only exception showing an increasing trend for future precipitation values.

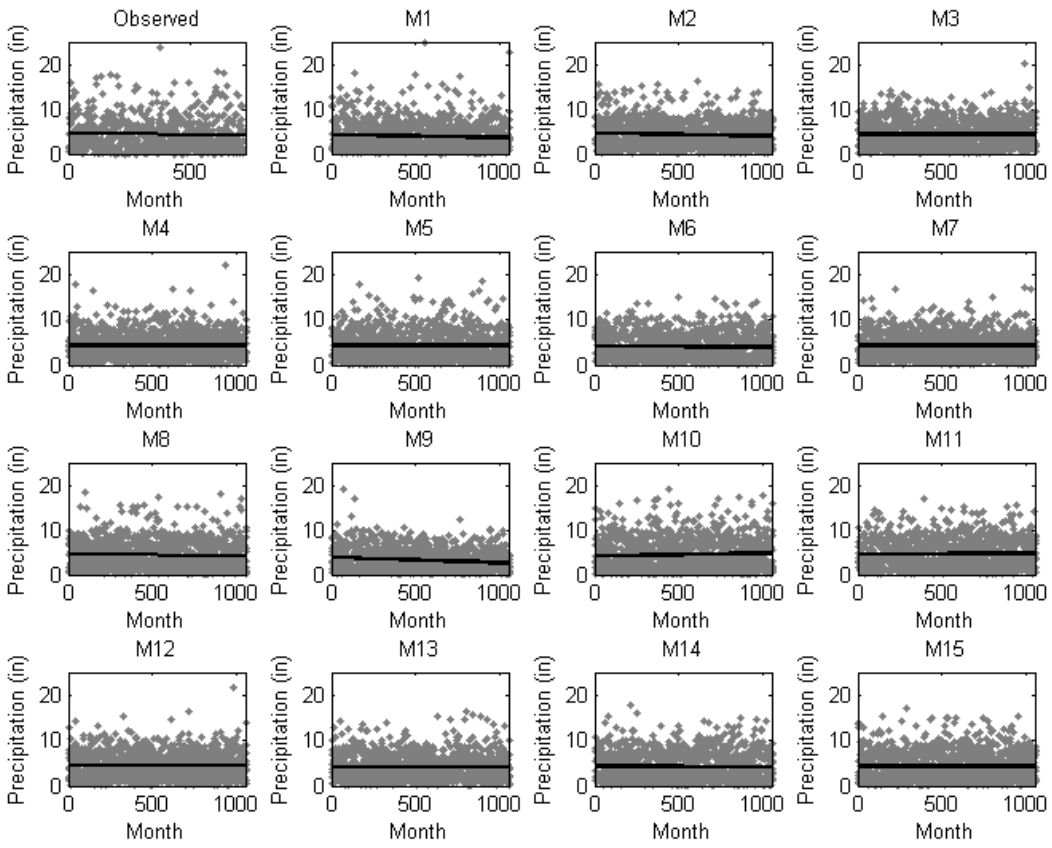

Figure 5-6: Scatter Plot - Arcadia Observed (1951-2010) - Projected Precipitation Data (2011-2099)

5.3.3 Arcadia - Temperature Data

For the temperature data, as was seen with the precipitation data, the models statistical summary shows that the models have similar results to those of the observed temperature values. All projected temperature data is slightly negatively skewed, this means that there are more occurrences of higher values. The standard deviation for all models ranged from 7.7 to 8.6 which is an indication that the data has a wide spread. This kurtosis values for all the models with values less than two (2) also supports that.

Table 5-3: Statistics - Arcadia Observed (1951-2010) - Projected Temperature Data (2011-2099)

Models	Mean	STD	Skewness	Kurtosis	Max	Min	Range
Observed	72.219	7.940	-0.327	1.877	83.800	51.100	32.700
M1	75.637	8.292	-0.317	1.953	89.348	53.816	35.532
M2	75.618	8.162	-0.304	1.858	89.195	52.817	36.378
M3	76.320	8.131	-0.337	1.942	89.978	56.777	33.201
M4	74.355	7.966	-0.308	1.898	87.971	54.194	33.777
M5	76.220	8.436	-0.289	1.872	89.906	53.456	36.450
M6	75.158	7.760	-0.289	1.797	87.026	57.029	29.997
M7	75.767	8.189	-0.263	1.862	88.898	57.020	31.878
M8	75.533	8.017	-0.269	1.856	89.222	54.023	35.199
M9	76.751	8.604	-0.293	1.839	90.203	53.879	36.324
M10	75.810	7.995	-0.379	2.030	88.160	53.645	34.515
M11	75.909	7.759	-0.314	2.072	89.204	54.131	35.073
M12	75.359	8.225	-0.239	1.860	88.736	54.923	33.813
M13	75.585	7.784	-0.349	1.928	87.854	55.787	32.067
M14	74.100	8.120	-0.411	1.985	86.018	52.835	33.183
M15	76.048	7.715	-0.332	1.922	87.719	54.428	33.291

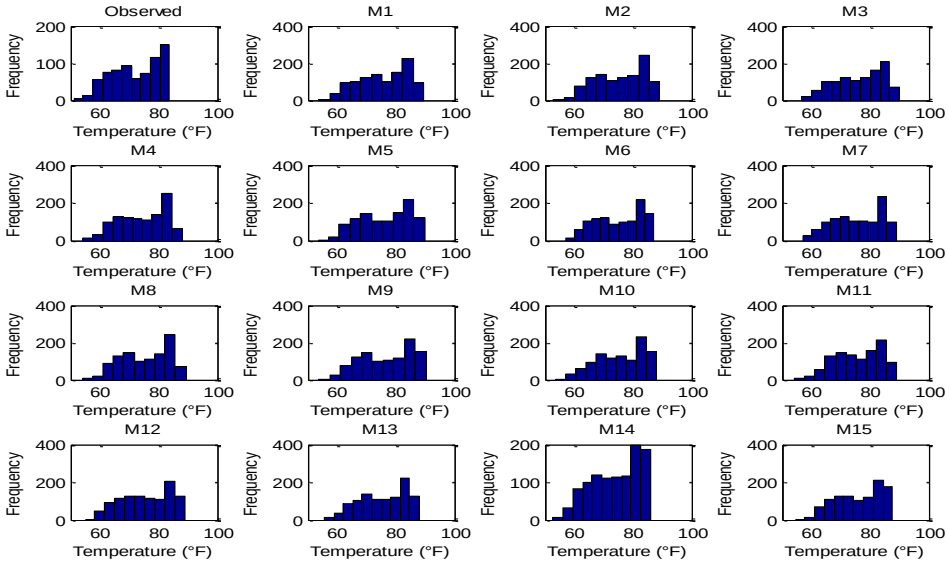

Figure 5-7: Histograms - Arcadia Observed (1951-2010) - Projected Temperature Data (2011-2099)

The histogram in Figure 5-7 provides a graphical illustration of temperature data distribution. A review of the graph supports the statistical summary results. As shown, the shape of the distribution is somewhat broad at the top, the kurtosis values for the observed and all the models were less than 3, which is an indication that its central peak is lower than that of a normal distribution, with shorter tail.

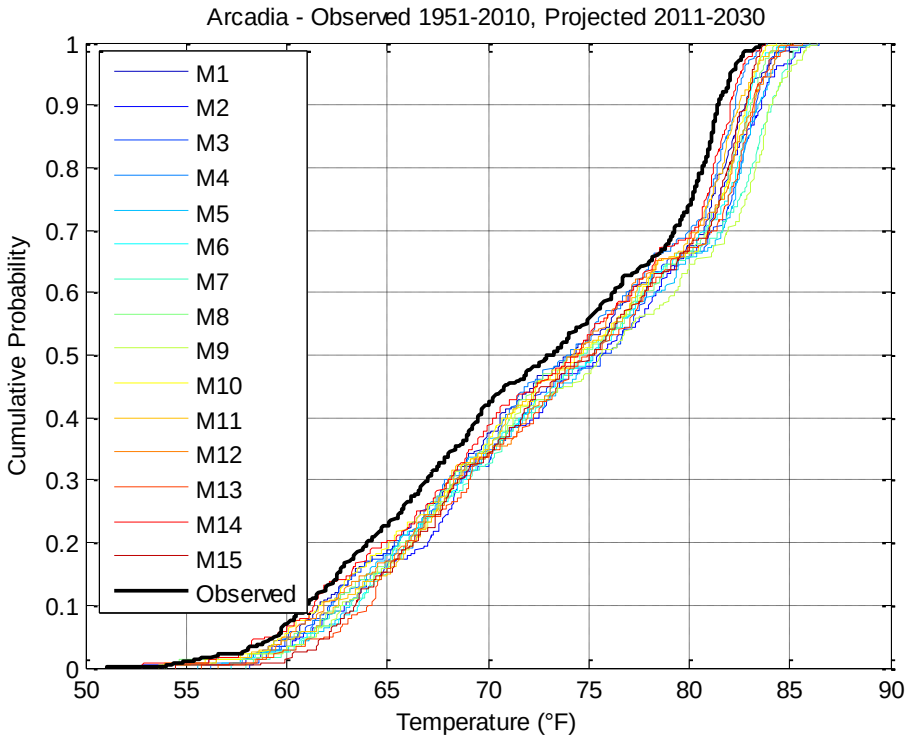

Figure 5-8: Arcadia Observed (1951-2010) - Projected Temperature Data (2011-2030)

The CDF plotted for the observed (1951-2010) and model predictions (2011-2030), shows that all models increases temperature. With Model M9 being the most excessive.

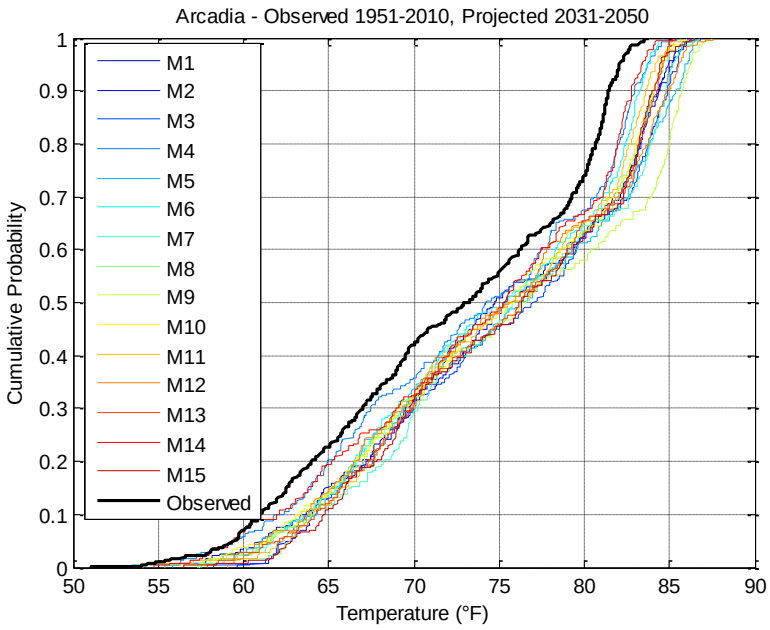

Figure 5-9: Arcadia Observed (1951-2010) - Projected Temperature Data (2031-2050)

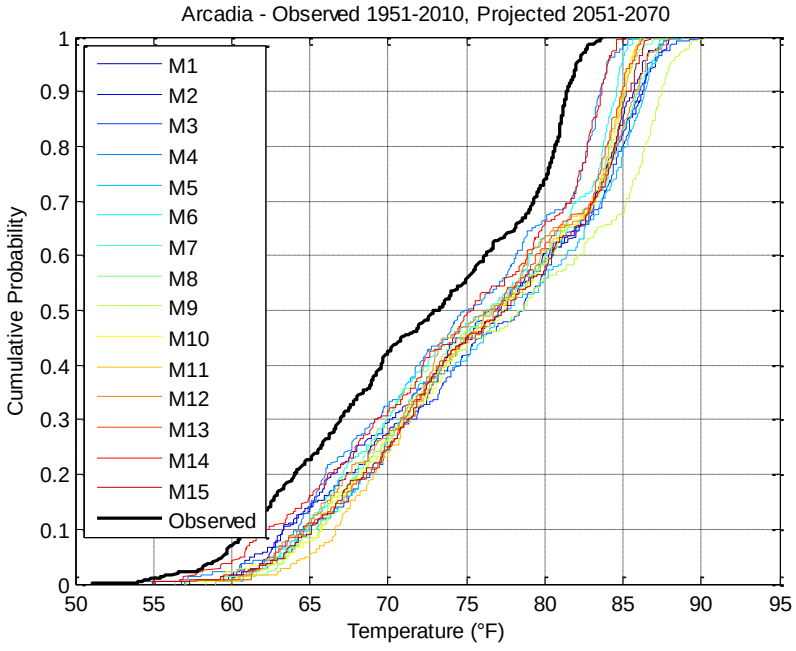

Figure 5-10: Arcadia Observed (1951-2010) - Projected Temperature Data (2051-2070)

As time progresses, the CDF bands of the models moves further away from the plotted observed cumulative probability band. This trend is can be seen in Figure 5-8 through Figure 5-11. This means that as time passes, temperature values are also increasing. Another observation is that the bands of the models widen as time progress, similar to those bands observed in the precipitation CDF plots. This is also an indication that there is more variability among the models as time passes. As seen in the earlier time period from 2011and up, model (M9) is predicting higher temperature values throughout.

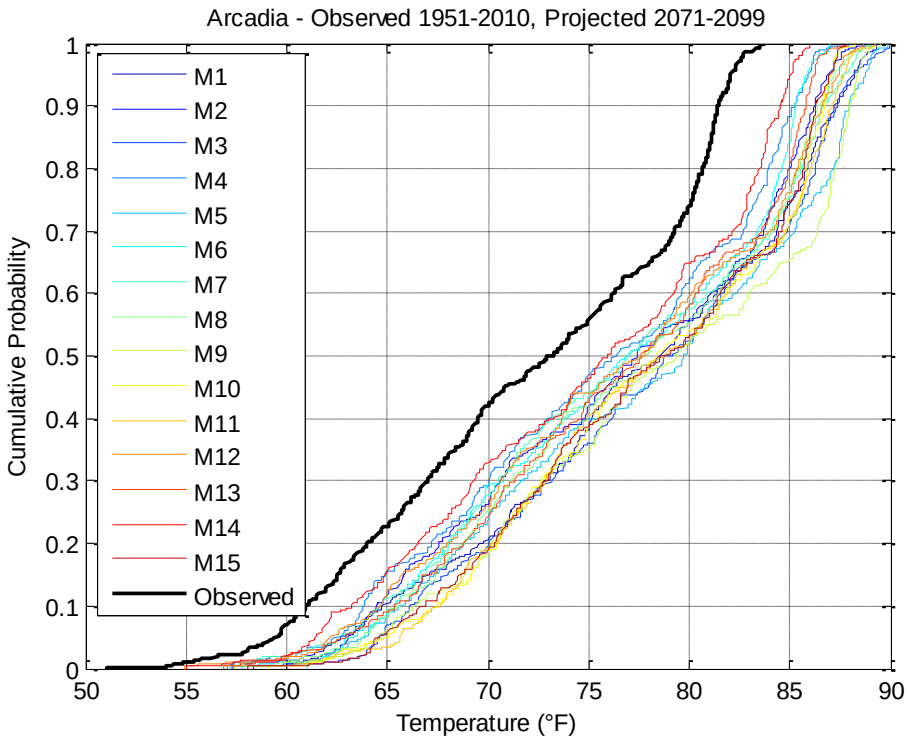

Figure 5-11: Arcadia Observed (1951-2010) - Projected Temperature Data (2071-2099)

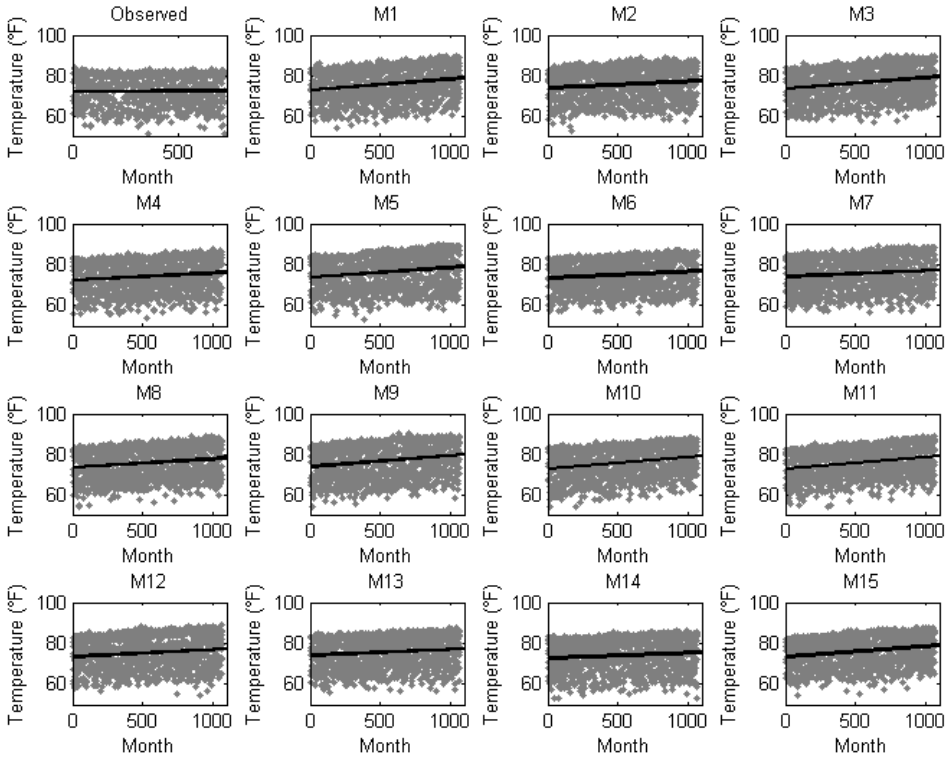

Figure 5-12: Scatter Plots - Arcadia Observed (1951-2010) - Projected Temperature Data (2011-2099)

The scatter plot of the temperature values for the observed values as well as for each model shows and increasing trend. The observed data (1951-2010) shows a slightly upward trend. Most of the models showed a steeper trend than that of the observed values. This could be due to the fact that the observed plot time period is shorter. Models M9 and M15 showed a much steeper trend line that the rest of the models.

5.3.4 Federal Point Precipitation Data

Table 5-4 below provides the statistical summary of the precipitation data collected for use in the model development and application for the Federal Point/South Fork Black Creek catchment. The table contains both the observed (1951-2010) and the projected precipitation values (2011-2099). The statistical measures show that the projected values more or less follows those of the observed values, similar to those seen for the Arcadia/Joshua Creek Catchment. The statistical measures show that all the models and the observed data sets are positively skewed. Kurtosis values for all the models were more than three.

Table 5-4: Statistics - Federal Point Observed (1951-2010) - Projected Precipitation Data (2011-2099)

Models	Mean	STD	Skewness	Kurtosis	Max	Min	Range
Observed	4.072	3.090	1.210	4.585	17.460	0.000	17.460
M1	4.164	2.982	1.307	5.698	22.546	0.052	22.495
M2	4.339	2.446	0.752	3.463	14.866	0.105	14.761
M3	4.327	2.712	1.432	7.258	23.163	0.142	23.021
M4	4.555	2.919	1.308	5.790	22.405	0.164	22.241
M5	4.614	3.311	1.370	5.858	23.127	0.129	22.998
M6	4.508	2.965	1.100	4.555	17.738	0.000	17.738
M7	4.266	2.469	0.985	4.326	15.943	0.263	15.681
M8	4.425	2.996	0.911	3.702	17.097	0.175	16.922
M9	3.364	2.204	1.149	4.780	14.434	0.146	14.288
M10	4.469	3.120	1.037	4.391	20.834	0.069	20.764
M11	4.828	3.080	0.840	3.439	17.813	0.078	17.735
M12	4.783	2.993	1.033	4.414	21.173	0.154	21.018
M13	4.591	2.879	0.796	3.386	16.518	0.145	16.373
M14	4.655	3.190	0.870	3.413	17.668	0.141	17.527
M15	4.817	3.193	0.942	3.716	20.109	0.051	20.058

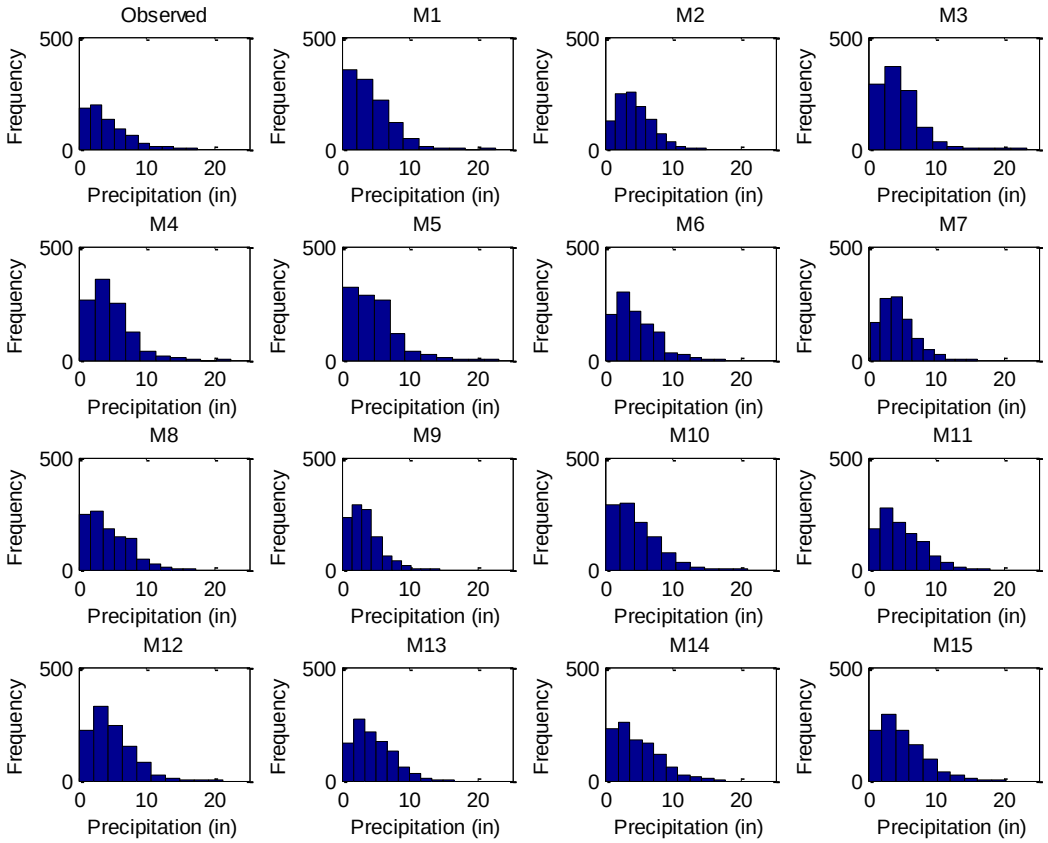

Figure 5-13: Histograms - Federal Point Observed (1951-2010) - Projected Precipitation Data (2011-2099)

The histogram in Figure 5-13 provides a graphical illustration of the precipitation data. As observed in the frequency values, there are higher incidences of getting lower precipitation values.

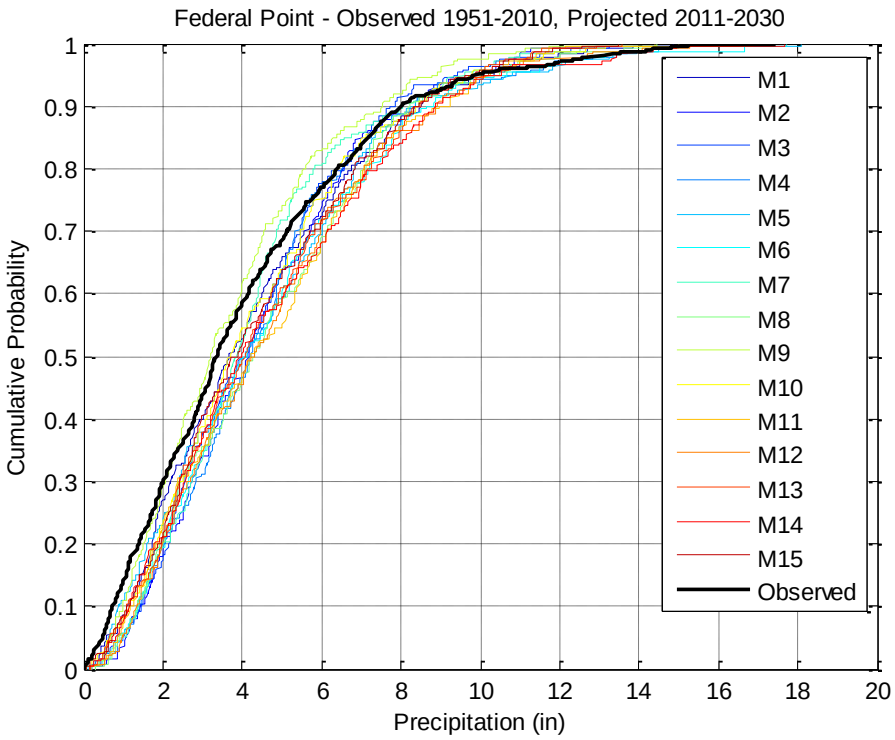

Figure 5-14: Federal Point Observed (1951-2010) - Projected Precipitation Data (2011-2030)

For period (2011-2030), the plotted CDF graph (Figure 5-14) illustrates that most of the models show increases in precipitation values for the better part of the range. Only at the extreme top of the range there was a reversal. Models M7 and M9 generally followed the tendency to predict less precipitation.

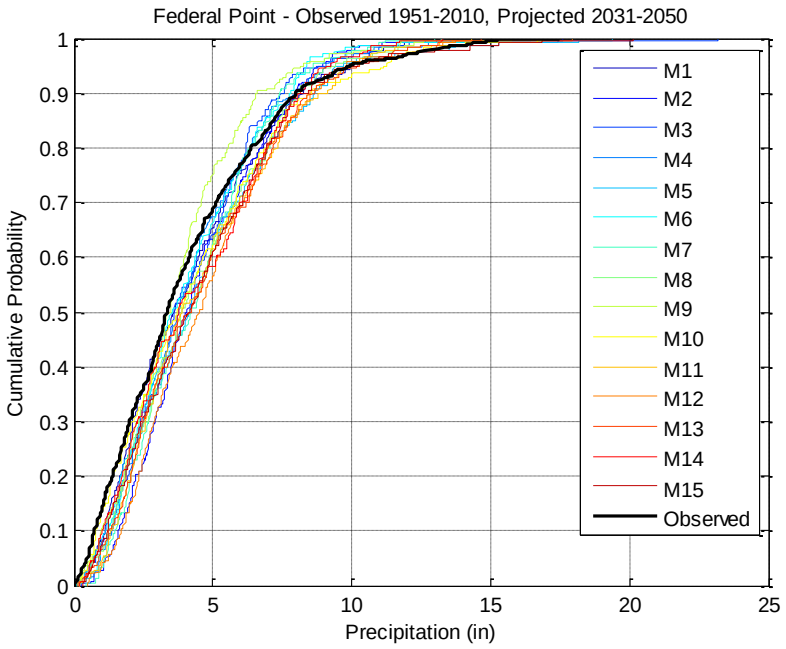

Figure 5-15: Federal Point Observed (1951-2010) - Projected Precipitation Data (2031-2050)

The trend observed in plots for 2011-2030 continues into the next period (Figure 5-15), the models shows increases in precipitation values at the lower values.

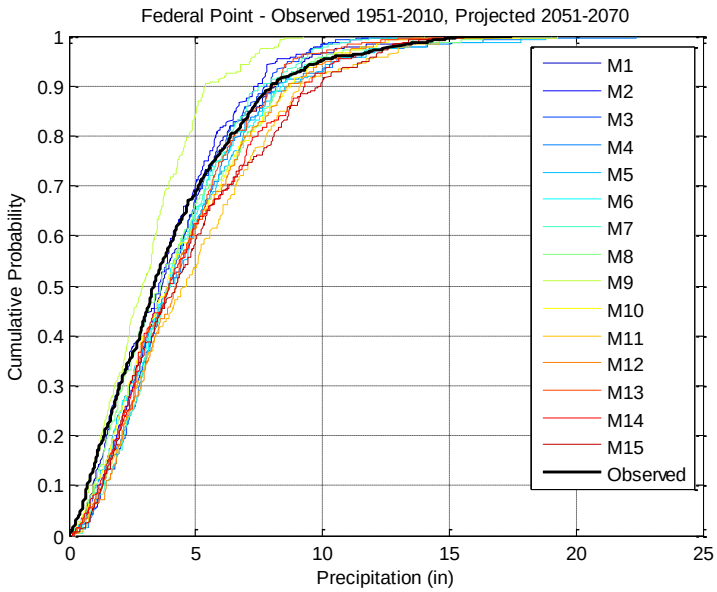

Figure 5-16: Federal Point Observed (1951-2010) - Projected Precipitation Data (2051-2070)

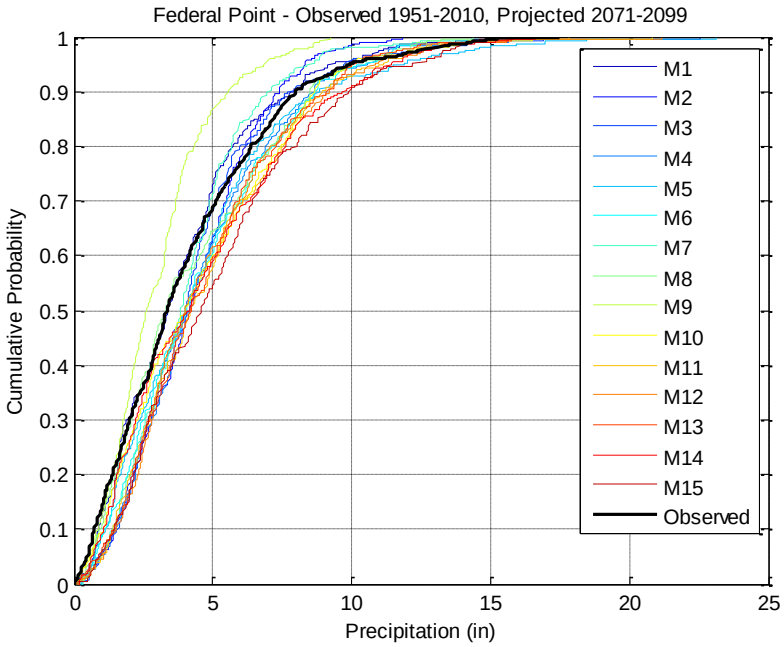

Figure 5-17: Federal Point Observed (1951-2010) - Projected Precipitation Data (2071-2099)

The scatter plot of the precipitation values for the observed values as well as for each model shows a slightly downward trend for most or no significant change… Models M10, M11 and M15 were the only noticeable exception showing an increasing trend for future precipitation values. See Figure 5-18 below.

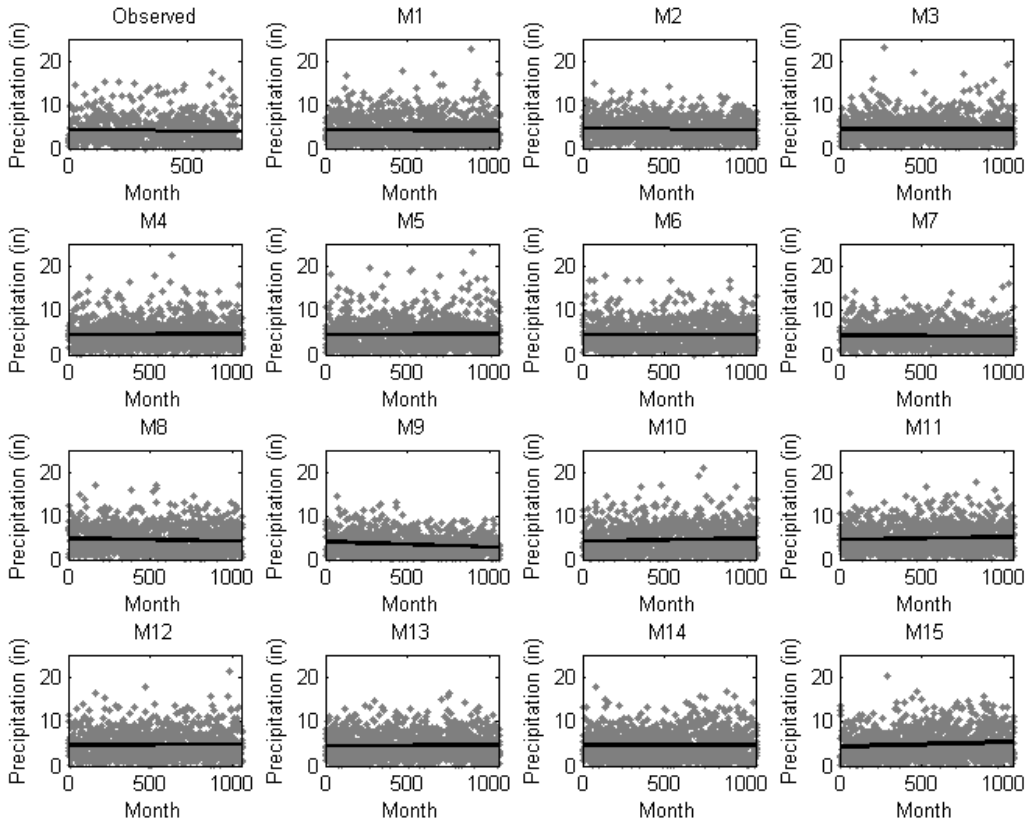

Figure 5-18: Scatter Plots - Federal Point Observed (1951-2010) - Projected Precipitation Data (2011-2099)

5.3.5 Federal Point Temperature Data

For the Federal Point temperature data, as was also seen with the Arcadia data, the analysis shows similar results. All projected temperature data is slightly negatively skewed, this means that there are more occurrences of higher values. The standard

deviation for all models ranged from 9.5 to 10.8 which is an indication that the data has a wide spread. This kurtosis values for all the models with values less than two (2) also supports that.

Table 5-5: Statistics - Federal Point Observed (1951-2010) - Projected Temperature Data (2011-2099)

Models	Mean	STD	Skewness	Kurtosis	Max	Min	Range
Observed	70.251	9.717	-0.256	1.761	86.800	48.600	38.200
M1	73.521	10.026	-0.291	1.889	91.814	51.440	40.374
M2	73.430	9.930	-0.242	1.784	89.456	46.706	42.750
M3	74.156	9.875	-0.287	1.893	92.948	50.630	42.318
M4	72.342	9.826	-0.240	1.831	89.411	49.190	40.221
M5	73.907	10.222	-0.241	1.781	90.977	49.550	41.427
M6	73.043	9.464	-0.201	1.740	89.636	51.215	38.421
M7	73.466	10.002	-0.205	1.764	89.330	52.043	37.287
M8	73.662	9.712	-0.265	1.872	90.446	45.608	44.838
M9	75.267	10.802	-0.168	1.763	94.307	48.308	45.999
M10	73.624	9.712	-0.295	1.877	89.204	49.721	39.483
M11	73.710	9.560	-0.251	1.927	91.436	49.703	41.733
M12	73.176	9.767	-0.275	1.815	89.213	48.632	40.581
M13	73.449	9.506	-0.311	1.846	87.935	51.242	36.693
M14	72.003	10.014	-0.358	1.904	89.204	45.419	43.785
M15	74.646	9.695	-0.252	1.849	93.227	50.513	42.714

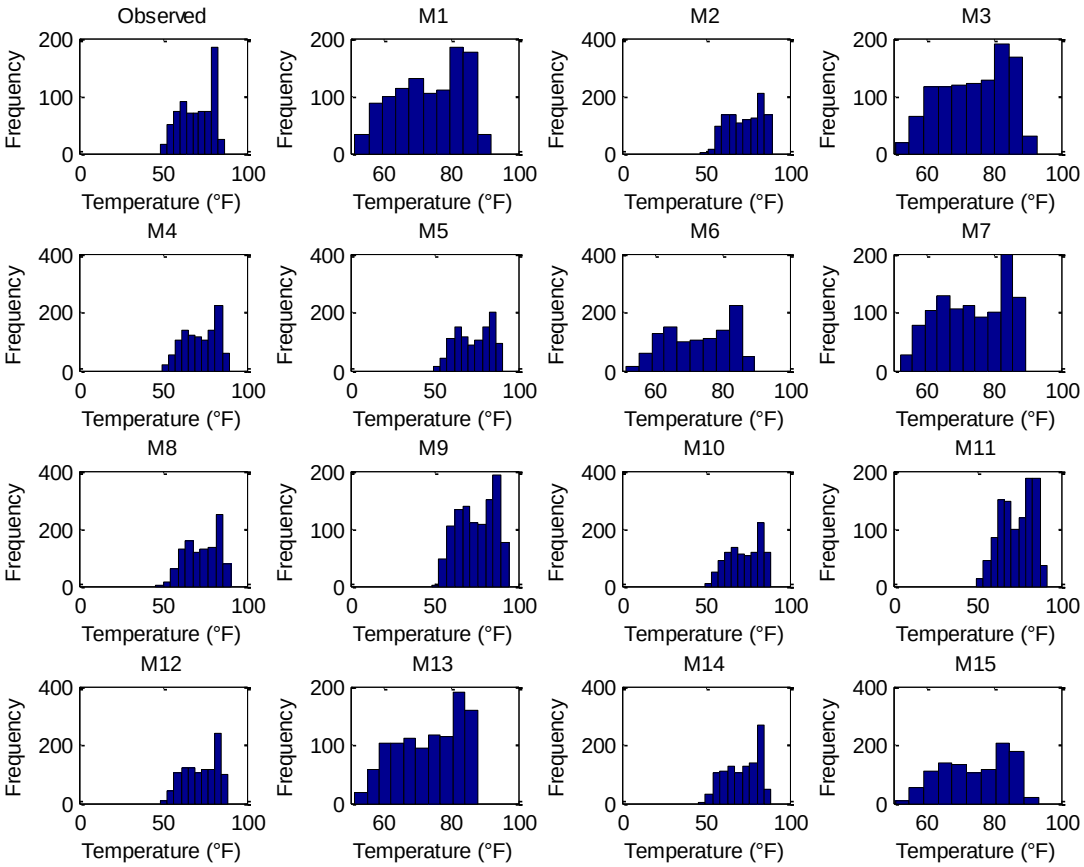

Figure 5-19: Histograms - Federal Point Observed (1951-2010) - Projected Temperature Data (2011-2099)

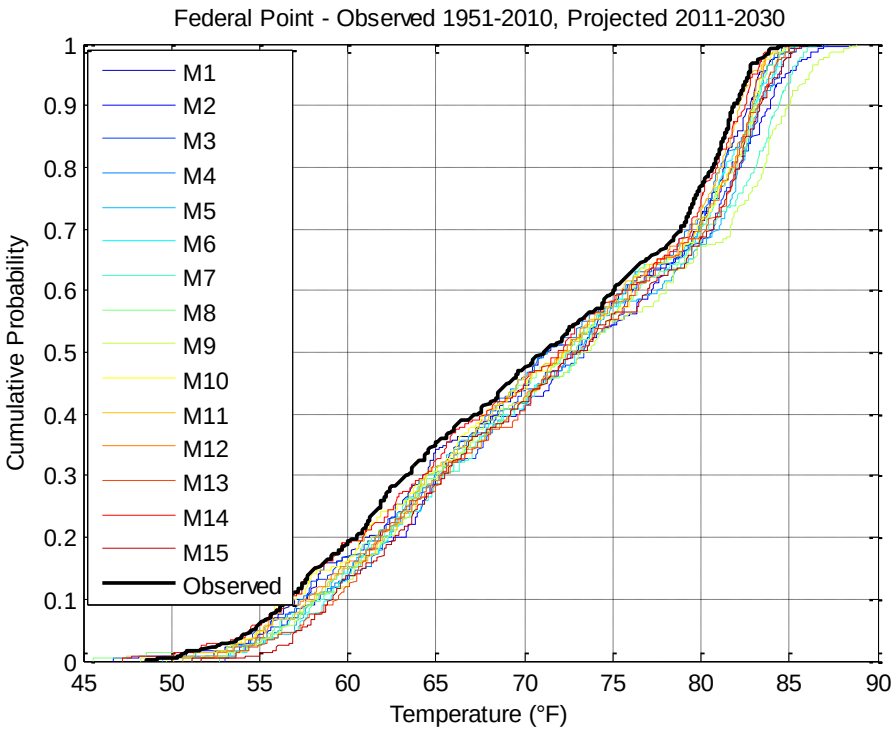

Figure 5-20: Federal Point Observed (1951-2010) - Projected Temperature Data (2011-2030)

The CDF plot of the observed (1951-2010) and the model predictions (2011-2030) show that all models increases in temperature. With Model M9 and M7 being the more excessive at higher temperatures.

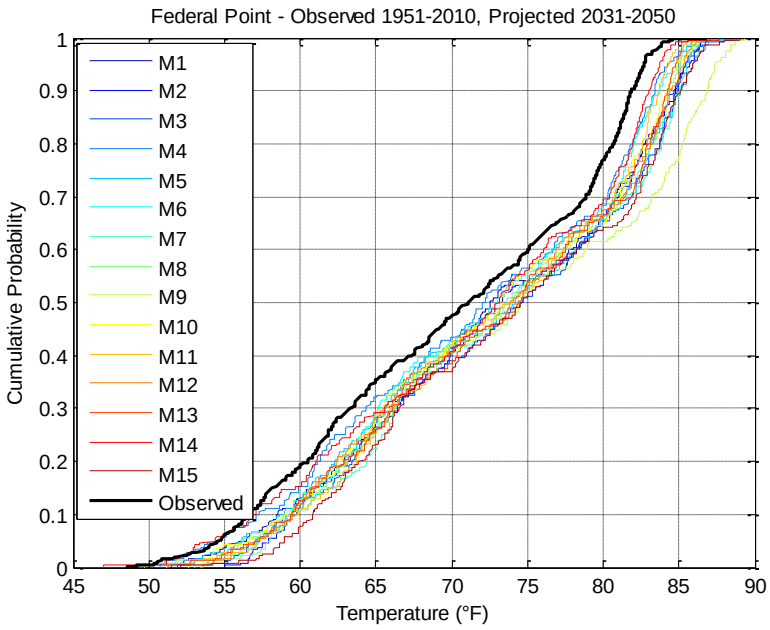

Figure 5-21: Federal Point Observed (1951-2010) - Projected Temperature Data (2031-2050)

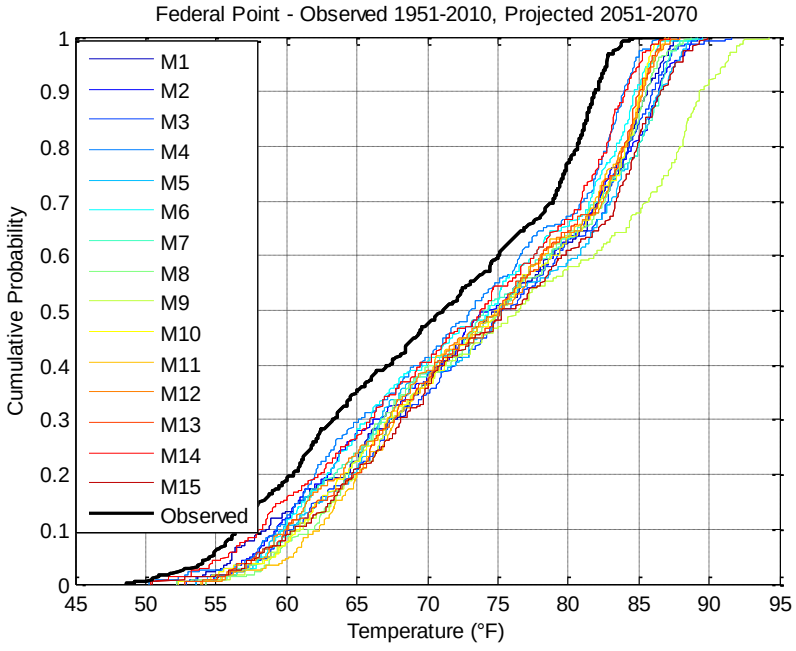

Figure 5-22: Federal Point Observed (1951-2010) - Projected Temperature Data (2051-2070)

As time progresses, the CDF bands of the models moves further away from the plotted observed cumulative probability band, indicating the increase in temperature. This trend is can be seen in Figure 5-20 through Figure 5-23

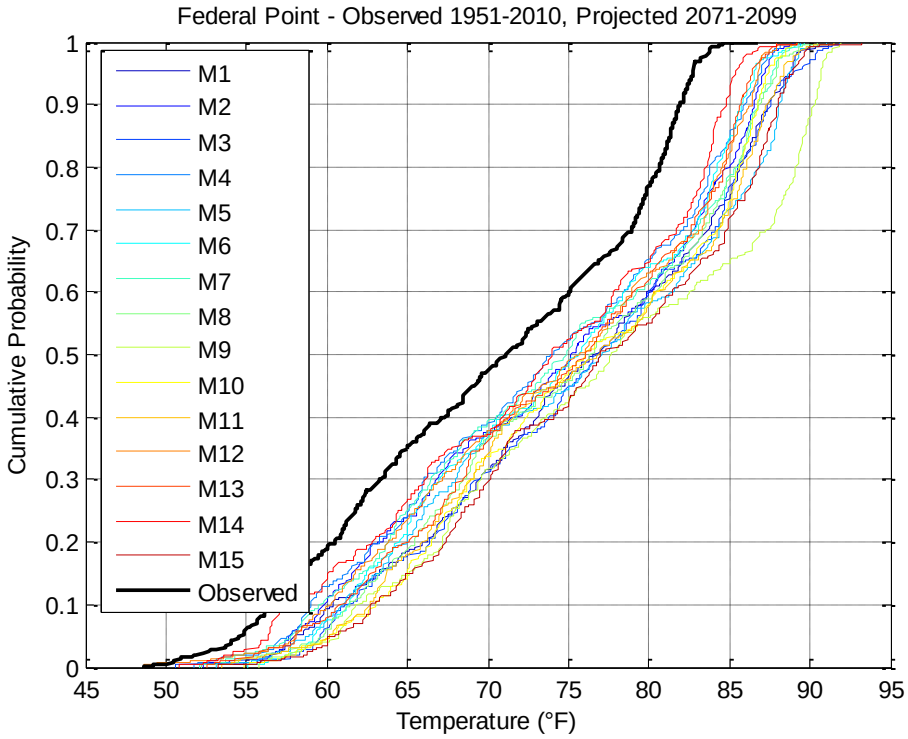

Figure 5-23: Federal Point Observed (1951-2010) - Projected Temperature Data (2071-2099)

The scatter plot of the temperature values for Federal temperature data shows a slightly upward trend for all the models. Most of the models showed a steeper trend than that of the observed values. This could be due to the fact that the observed plot time period is shorter. Models M9 and M15 showed a much steeper trend line that the rest of the models.

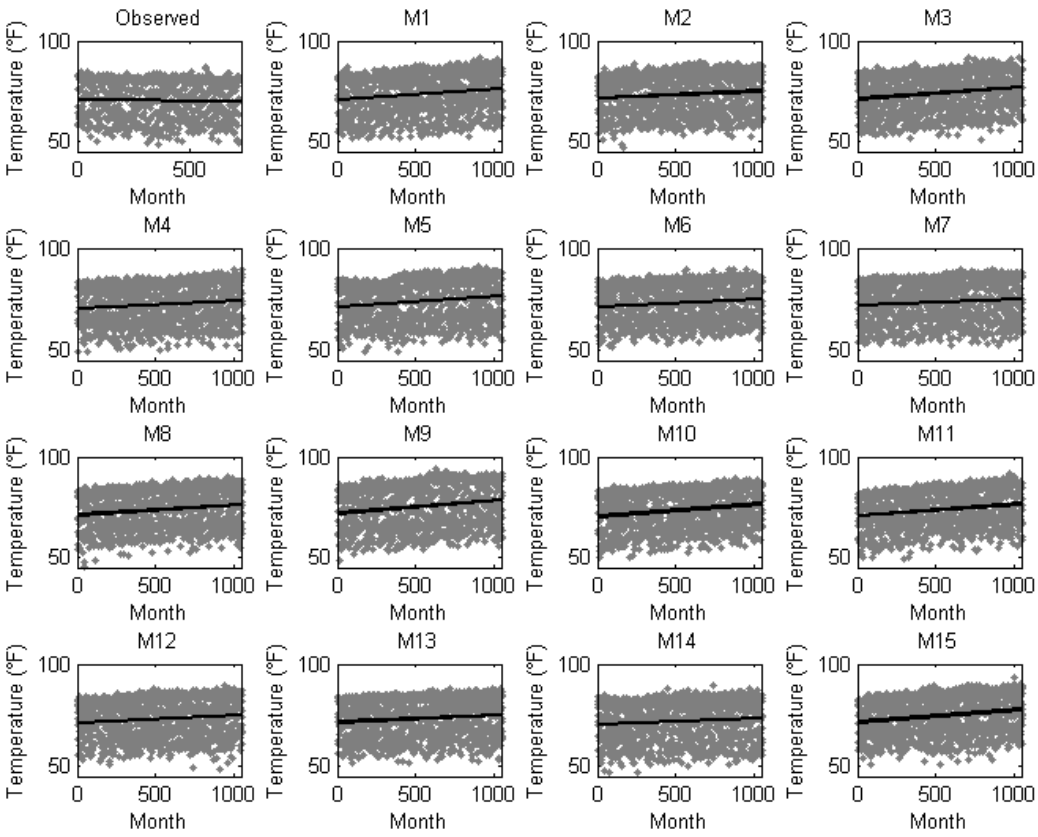

Figure 5-24: Scatter Plots - Federal Point Observed (1951-2010) - Projected Temperature Data (2011-2099)

5.3.6 Tarpon Springs Precipitation Data

Table 5-6 below provides the statistical summary of the precipitation data collected for Tarpon Springs/Anclote River Catchment. The table contains both the observed (1951-2010) and the projected precipitation values (2011-2099). The statistical measures show that the projected values more or less follows those of the observed values, similar to those seen in the other two catchments being analyzed. The statistical measures show that all the models and the observed data sets are positively skewed. Kurtosis values for all the models were more than three.

Table 5-6: Statistics - Tarpon Spring Observed (1951-2010)

– Projected Precipitation Data (2011-2099)

Models	Mean	STD	Skewness	Kurtosis	Max	Min	Range
Observed	4.303	3.619	1.318	4.793	20.760	0.000	20.760
M1	4.087	3.182	1.427	6.116	24.873	0.046	24.827
M2	4.426	2.890	0.954	3.865	17.242	0.091	17.150
M3	4.363	2.881	0.859	3.246	15.471	0.055	15.415
M4	4.405	2.806	0.860	3.442	15.681	0.110	15.571
M5	4.510	3.447	1.293	5.457	24.924	0.055	24.870
M6	4.298	2.889	0.928	3.413	15.920	0.069	15.851
M7	4.406	2.884	1.050	4.750	20.931	0.136	20.795
M8	4.453	3.204	0.980	3.645	18.286	0.082	18.204
M9	3.264	2.415	1.326	5.454	17.360	0.053	17.307
M10	4.451	3.337	0.987	3.656	19.324	0.022	19.302
M11	4.821	3.264	0.781	3.006	16.911	0.023	16.888
M12	4.620	2.966	0.844	3.502	18.716	0.091	18.625
M13	4.561	2.970	0.835	3.378	15.732	0.053	15.678
M14	4.454	3.287	0.922	3.246	16.522	0.111	16.411
M15	4.537	3.176	0.945	3.755	20.160	0.069	20.091

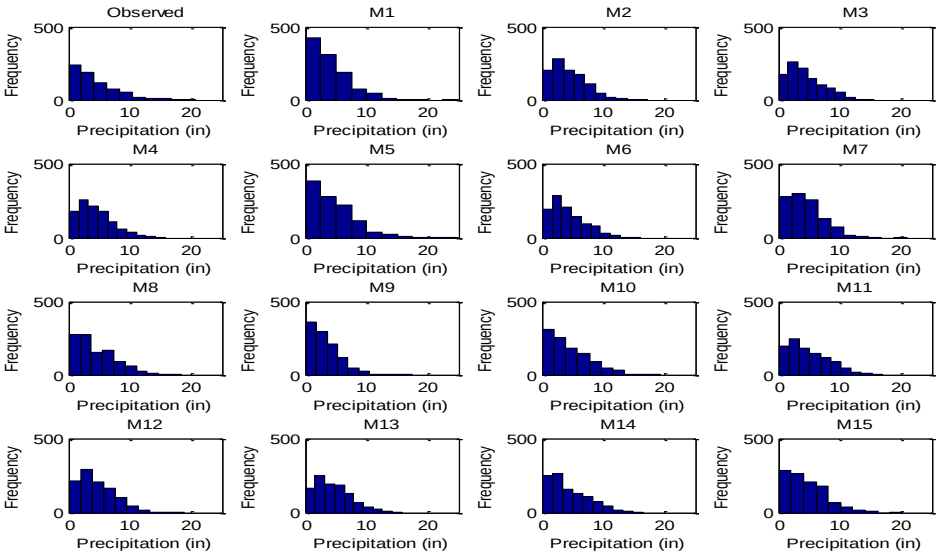

Figure 5-25: Histograms - Tarpon Spring Observed (1951-2010) – Projected Precipitation Data (2011-2099)

The histogram in Figure 5-25 provides a graphical illustration of the precipitation data. The graphs show higher incidences of lower precipitation values.

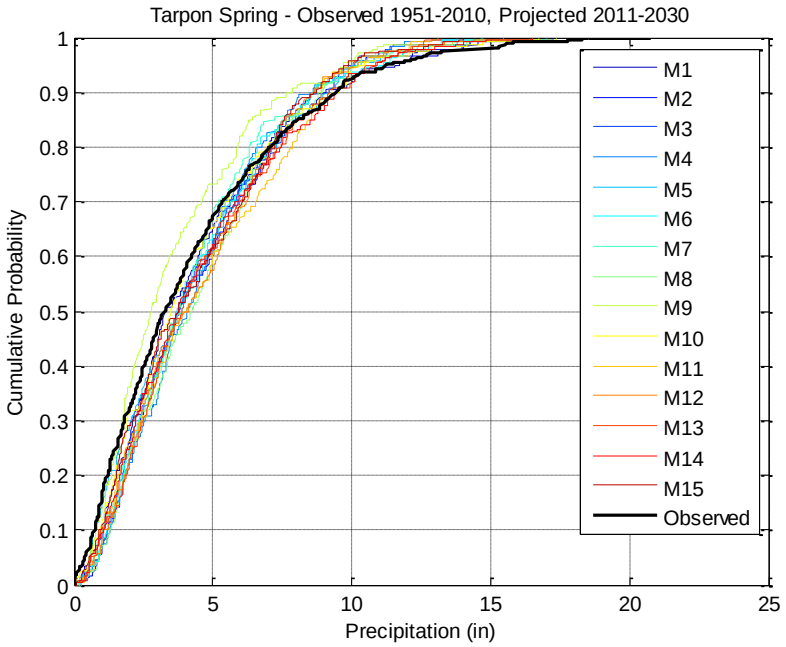

Figure 5-26: Tarpon Spring Observed (1951-2010) – Projected Precipitation Data (2011-2030)

The CDF graphs show an increase in precipitation, except at the extremes where the trend is reversed. This was typical for all the selected catchments. All models indicate reduced extreme values events. The plotted graphs also show that as time progresses, the CDF bands of the models widens. Model (M9) follows a different trend; the CDF plot shows, as seen in the other two the catchments, it is consistently underestimating the values at both low and high values. See Figure 5-26 through Figure 5-29 for CDF plots.

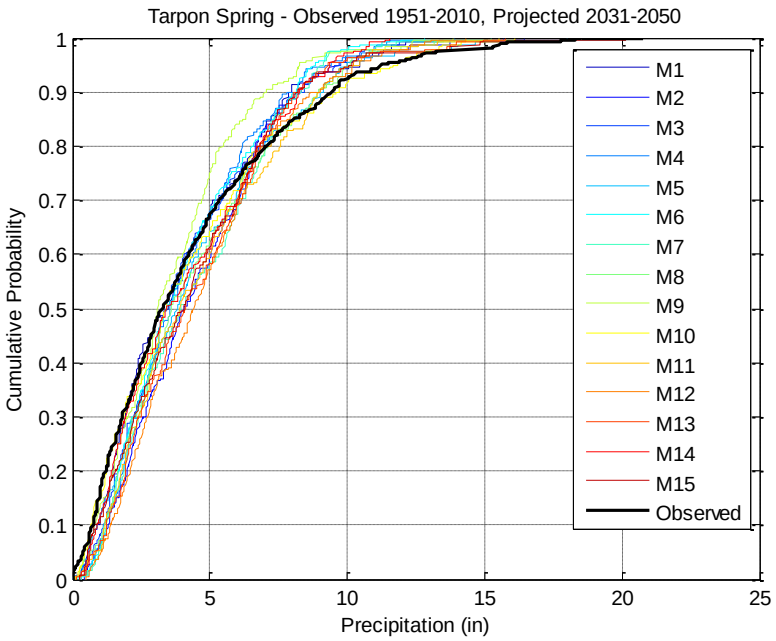

Figure 5-27: Tarpon Spring Observed (1951-2010) – Projected Precipitation Data (2031-2050)

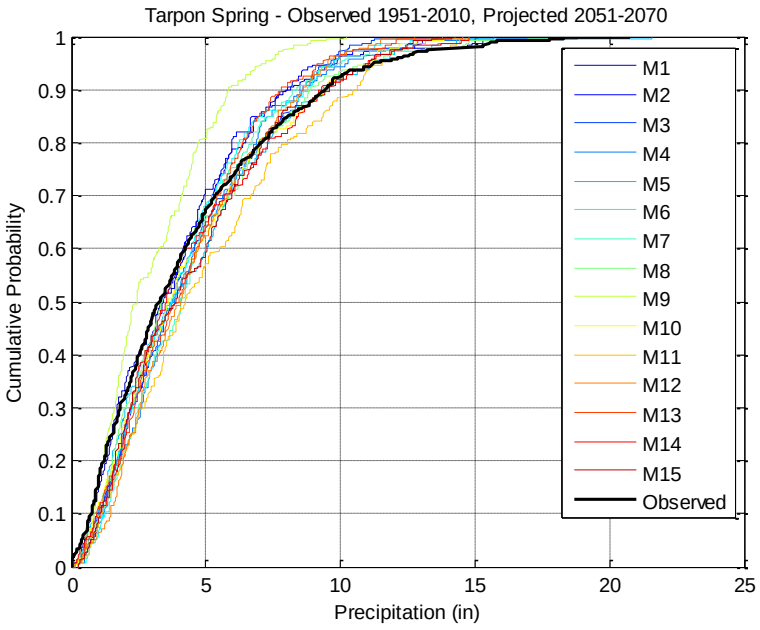

Figure 5-28: Tarpon Spring Observed (1951-2010) – Projected Precipitation Data (2051-2070)

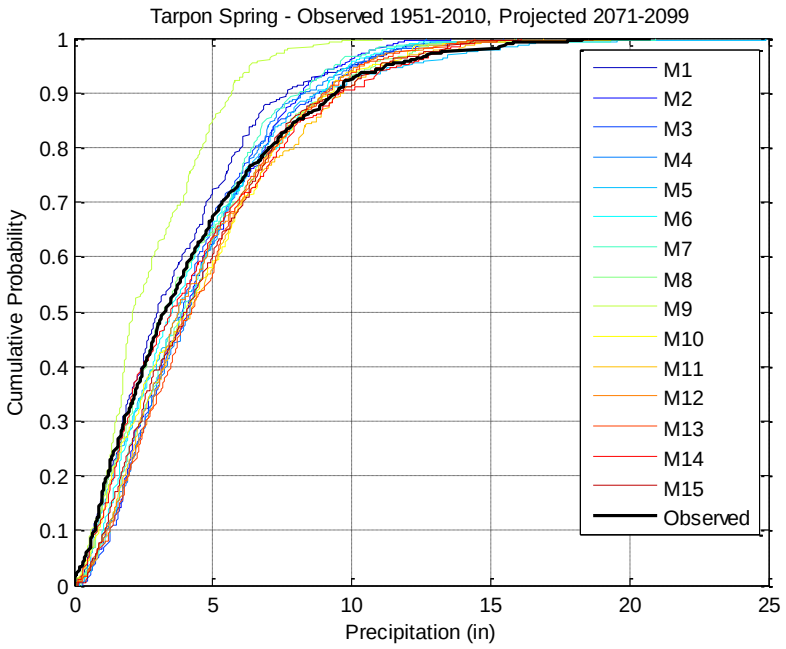

Figure 5-29: Tarpon Spring Observed (1951-2010) – Projected Precipitation Data (2071-2099)

For Tarpon Springs/Anclote River, the scatter plot (Figure 5-30) of the precipitation values shows a slightly downward trend for the observed data. Most of the models showed a decreasing trend or relatively no change. Models M10 and M11 were the only exceptions showing an increasing trend for future precipitation values.

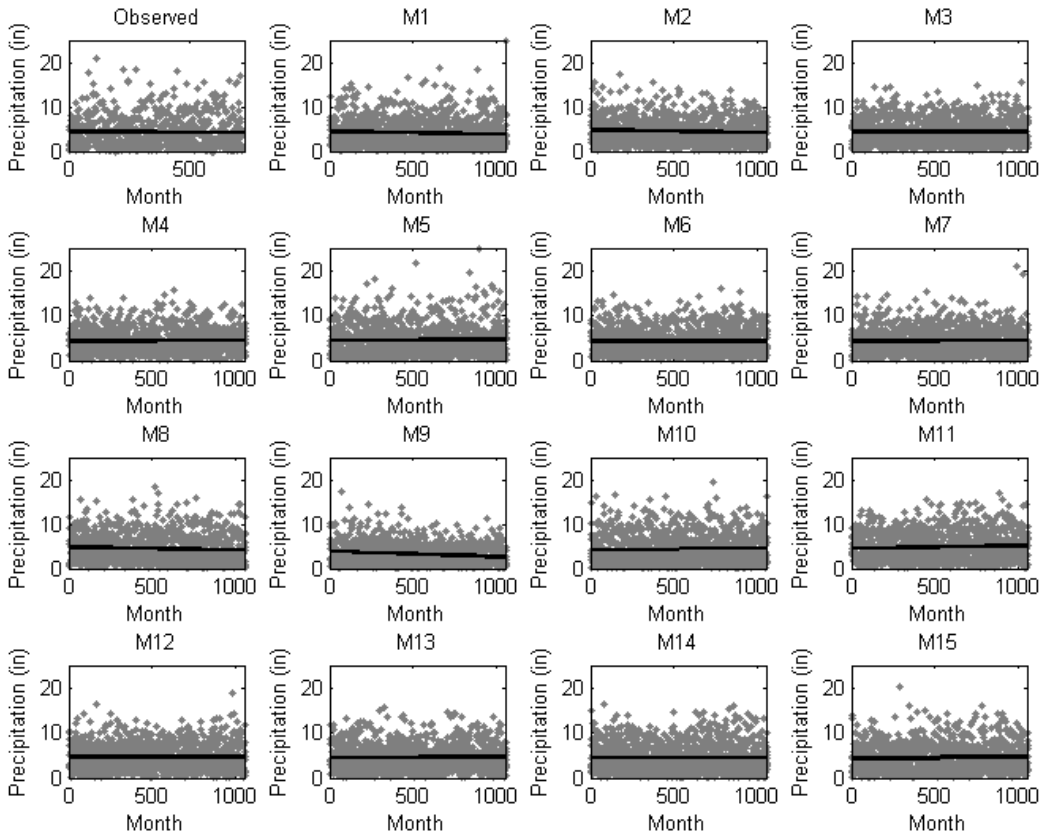

Figure 5-30: Scatter Plots - Tarpon Spring Observed (1951-2010) – Projected Precipitation Data (2011-2099)

5.3.7 Tarpon Springs Temperature Data

The temperature data for Tarpon Springs/Anclote River shows that the 15 models have similar results to those of the observed temperature values. The models statistical summary (Table 5-7) shows that all projected temperature data is slightly negatively skewed, this means that there are more occurrences of higher values. This kurtosis values for all the models were less than two (2). The histogram in Figure 5-31 provides a graphical illustration of temperature data distribution.

Table 5-7: Statistics - Tarpon Spring Observed (1951-2010) - Projected Temperature Data (2011-2099)

Models	Mean	STD	Skewness	Kurtosis	Max	Min	Range
Observed	71.253	8.860	-0.314	1.856	84.300	48.700	35.600
M1	75.335	9.030	-0.326	1.910	90.905	53.528	37.377
M2	75.413	9.091	-0.291	1.831	90.230	50.351	39.879
M3	76.035	8.910	-0.330	1.890	91.004	55.355	35.649
M4	74.179	8.886	-0.280	1.856	89.024	52.412	36.612
M5	75.805	9.241	-0.288	1.823	90.077	52.079	37.998
M6	74.963	8.542	-0.252	1.745	87.881	54.734	33.147
M7	75.227	8.847	-0.276	1.827	89.672	54.770	34.902
M8	75.505	8.829	-0.281	1.871	90.284	50.225	40.059
M9	76.698	9.558	-0.242	1.787	92.183	51.665	40.518
M10	75.580	8.819	-0.360	1.976	89.015	52.070	36.945
M11	75.719	8.634	-0.299	2.017	90.950	52.358	38.592
M12	75.149	8.986	-0.262	1.829	89.456	52.376	37.080
M13	75.451	8.590	-0.343	1.893	88.502	54.797	33.705
M14	73.886	9.006	-0.394	1.932	87.719	50.567	37.152
M15	76.235	8.670	-0.305	1.885	90.860	53.168	37.692

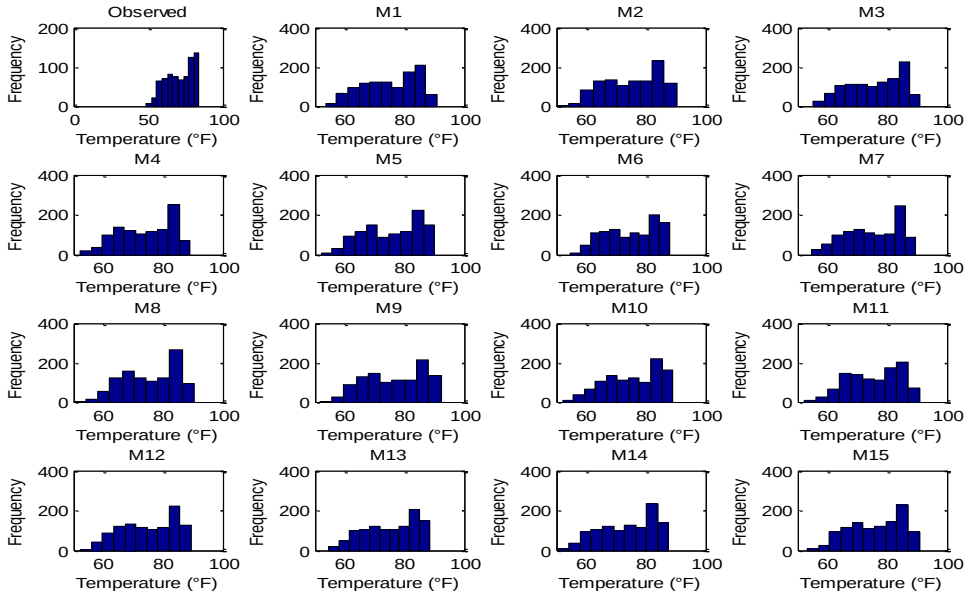

Figure 5-31: Histograms - Tarpon Spring Observed (1951-2010) - Projected Temperature Data (2011-2099)

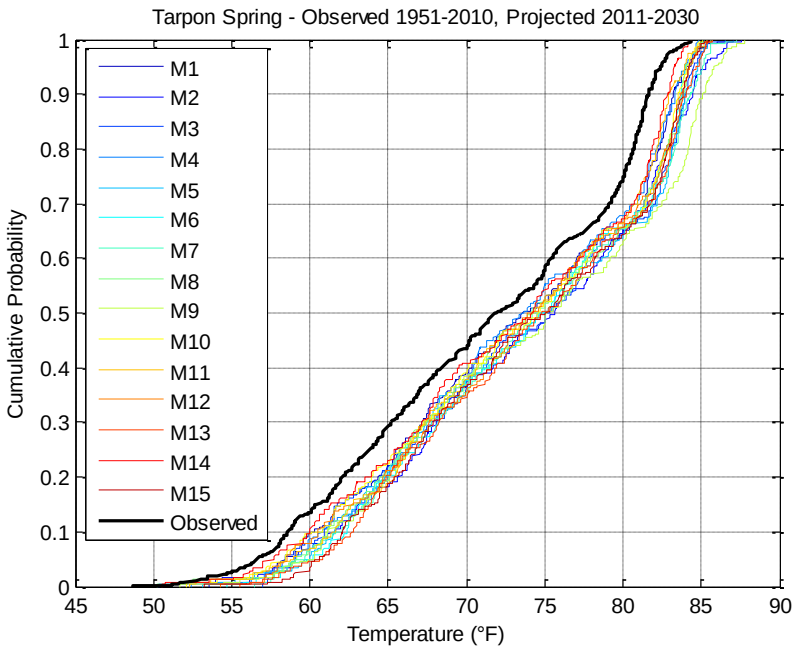

Figure 5-32: Tarpon Spring Observed (1951-2010) - Projected Temperature Data (2011-2030)

The CDF plots for the Tarpon Springs/Anclote River Catchment shows that all models are increasing in temperature values as time progresses. The bands of the models typical for all three catchments, moves further away from the plotted observed cumulative probability band and widens, meaning that as time passes, temperature values are also increasing. This is also an indication that there is more variability among the models as time passes. This trend is can be seen in Figure 5-32 through Figure 5-35. As seen in the earlier time period from 2011and up, model (M9) is predicting higher temperature values throughout all three catchments.

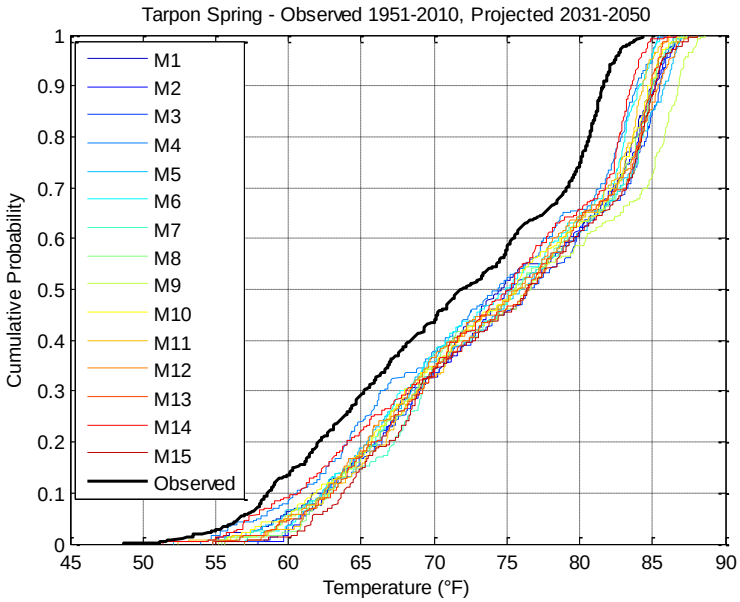

Figure 5-33: Tarpon Spring Observed (1951-2010) - Projected Temperature Data (2031-2050)

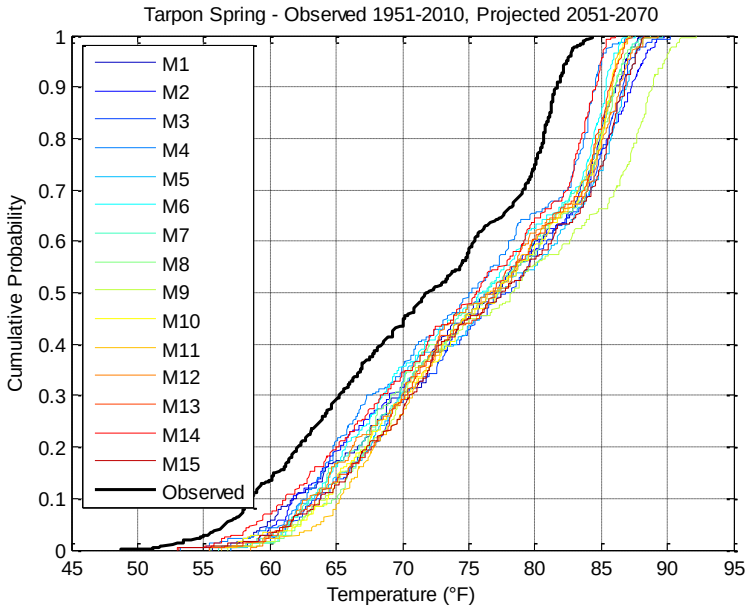

Figure 5-34: Tarpon Spring Observed (1951-2010) - Projected Temperature Data (2051-2070)

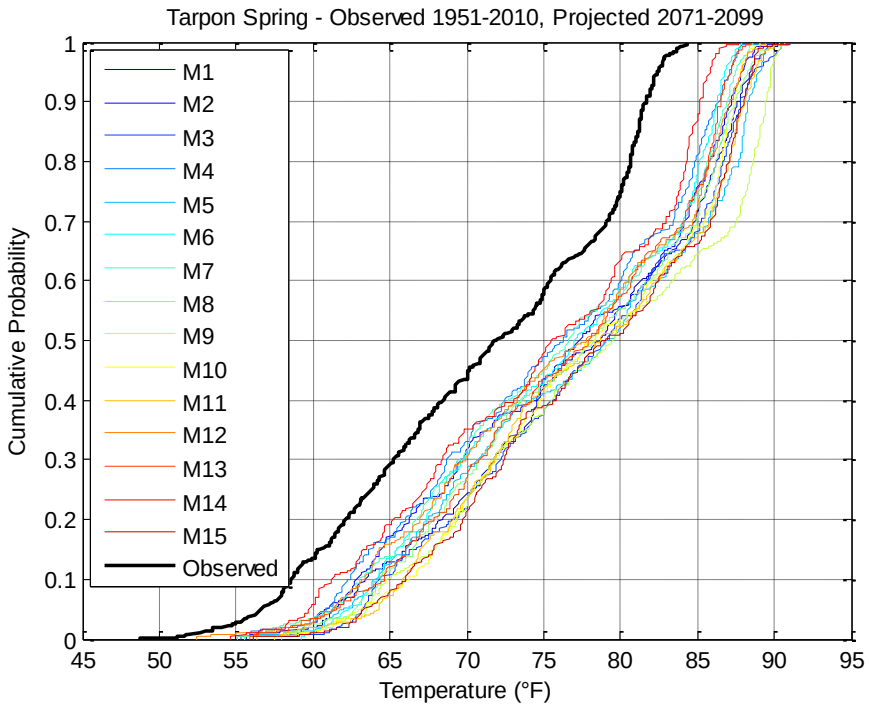

Figure 5-35: Tarpon Spring Observed (1951-2010) - Projected Temperature Data (2071-2099)

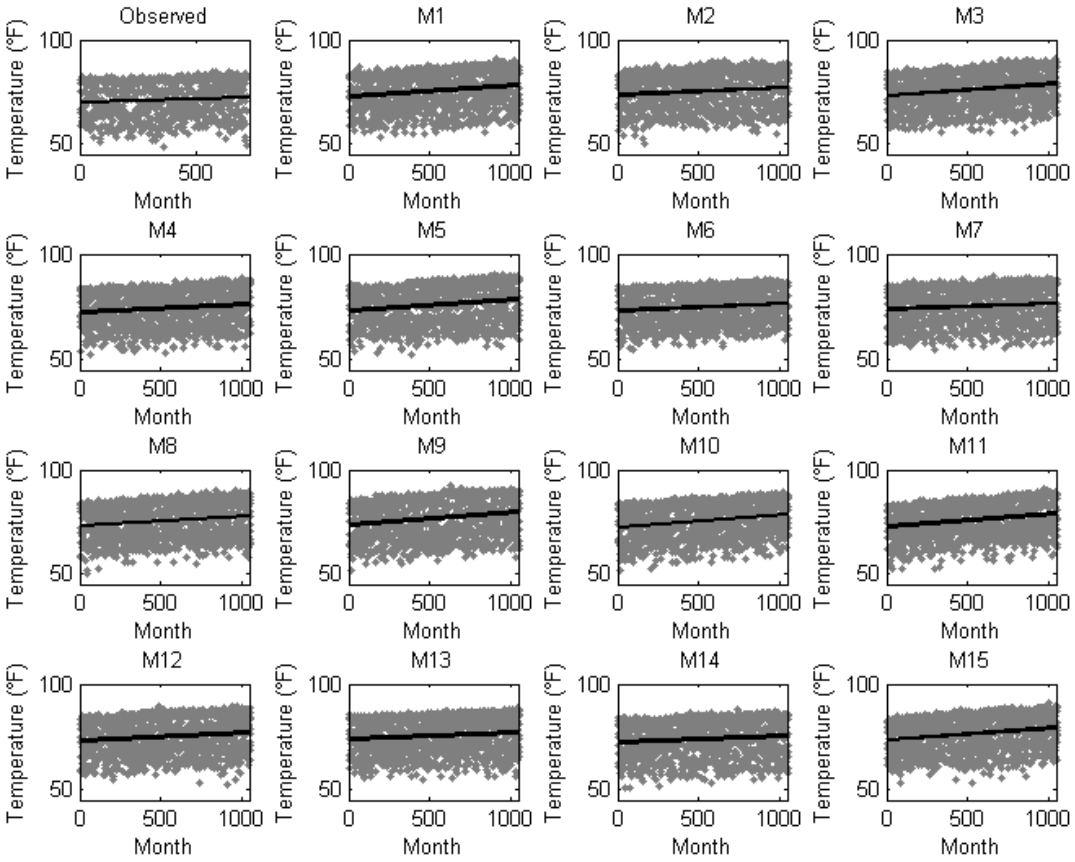

Figure 5-36: Scatter Plots - Tarpon Spring Observed (1951-2010) - Projected Temperature Data (2011-2099)

The scatter plot (Figure 5-36) of the temperature values for the observed values as well as for each model shows and increasing trend. Models M9 and M10 showed a much steeper trend line that the rest of the models

CHAPTER 6. MODEL DEVELOPMENT AND APPLICATION

6.1 Arcadia/Joshua Creek Catchment

For the Arcadia/Joshua Creek Catchment the model discharge predictions were compared to their corresponding observed values.

6.1.1 Model Calibration Results & Discussion

The Thomas Model was calibrated for period January 1951-December 2000. As previously stated in the case study application, this long time period was chosen in order to develop a realistic and reliable model. Calibrating a model with a narrow time window can bias the model due to the fact the within that said time period an extreme event may have taken place that will result in unrealistic predictions. The calibration was done using the evolutionary function within the Microsoft Excel Solver tool. This method mimics the process of natural evolution. It is a search technique used to find true or approximate solutions to optimization and search problems.

The first objective function (obj.) used to minimize the errors was absolute error (AE). Both predicted and observed values were plotted along a 45 degree line to provide a graphical illustration of how the model is performing (see Figure 6-1). A review of the graph indicates that the plotted points generally follow the path of the 45 degree line and they are mostly evenly distributed across the line. This suggests that the model is performing relatively well. More of the plotted points on the graph appear on the left of

the 45 degree line, which suggest that the model is slightly under predicting. The calibrated model parameters were, a = .9547, b = 12.1848, c = 0.6424, and d = 0. Initial soil and ground water storage was 3.56 and 205.27 mm respectively. Parameter value b is high, given its physical interpretation as the upper limit of the sum of evapotranspiration and soil moisture storage (Thomas et al., 1983; Alley, 1984). The AE objective function produced a correlation of coefficient of approximately 0.70. This shows that the predicted and observed flows (data points) are highly correlated being that the range is from 0 to 1, with 0 meaning no relationship and 1 meaning that they are perfectly related. To further illustrate the model performance, a line plot was also done for the observed vs. predicted flows (Figure 6-2). The graph shows that the predicted values, tries to mimic those of the observed values, indicating a relatively moderate to a good fit. The graph also illustrates that the model in under predicting the extreme events. The maximum observed monthly discharge value within the calibration period for this catchment was 1133 cfs, the maximum discharge the model predicted was 787.73 cfs. These two values were for the same month of the same year, which was in June 1983.

The next objective function (obj.) used to minimize the errors was squared error (SE) also known as the sum of squared error (SSE). As was done for the AE both predicted and observed values were plotted along a 45 degree line. A review of the graph indicates that the plotted points followed a similar trend. The calibrated model parameters were, a = 0.7798, b = 10.9866, c = 0.5781, and d = 0. Initial soil and ground water storage was 4.49 and 296.24 mm respectively. The SE objective function produced a correlation of coefficient of approximately 0.71. The time series line plot shown in Figure

6-3 shows that the projected monthly discharges is doing better when compared to the observed values. The maximum discharge value the model produced was 916.93 cfs. This is much closer to the highest observed value of 1133 cfs than what was projected using the AE objective function. The other two objective functions RMSE and MAE were used to optimize the model and the calibrated parameters are summarized in Table 6-1 below.

Table 6-1: Arcadia/Joshua Creek Catchment – Model Calibration Parameters

Objective Function (min)	Initial Soil Storage (mm)	Initial Groundwater Storage (mm)	a	b	c	d
Model - Absolute Error (AE)	3.6535	205.2746	0.9547	12.1848	0.6424	0.0000
Model - Squared Error (SE)	4.4897	296.2379	0.7798	10.9866	0.5781	0.0000
Model - Root Mean Squared Error (RMSE)	3.8076	250.1934	0.8857	15.0000	0.5435	0.0000
Model - Mean Absolute Error (MAE)	4.2044	252.0138	0.9710	14.9191	0.5979	0.0001

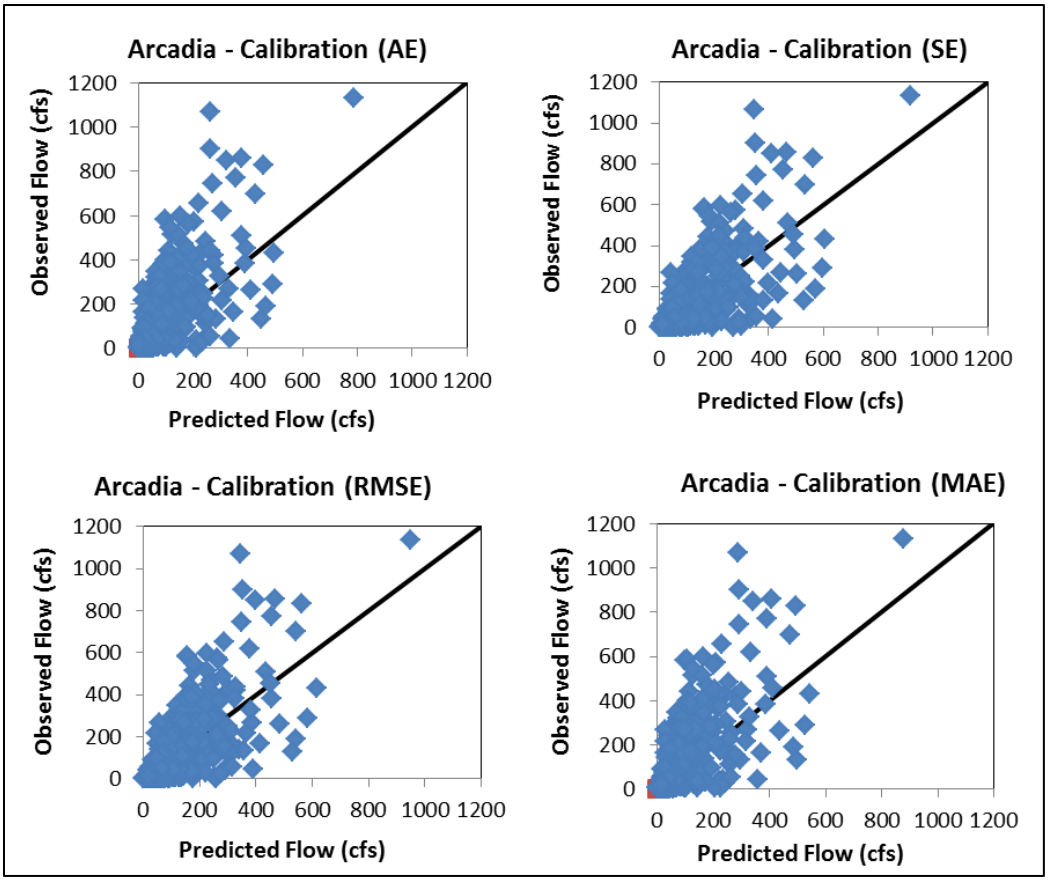

Figure 6-1: Arcadia/Joshua Creek Catchment – Model Calibration

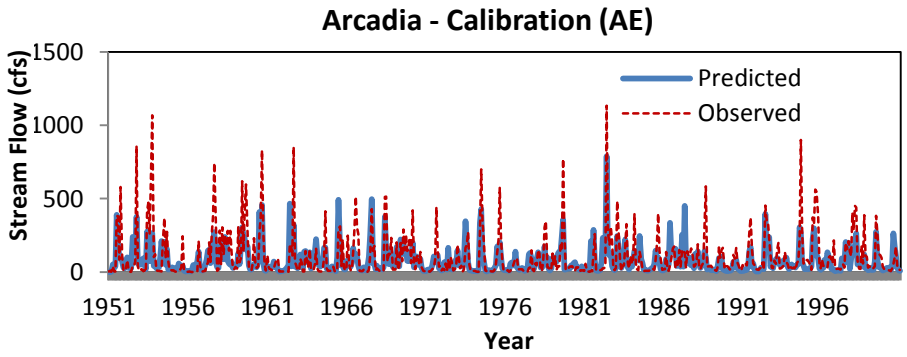

Figure 6-2: Arcadia/Joshua Creek Catchment – Model Calibration (AE)

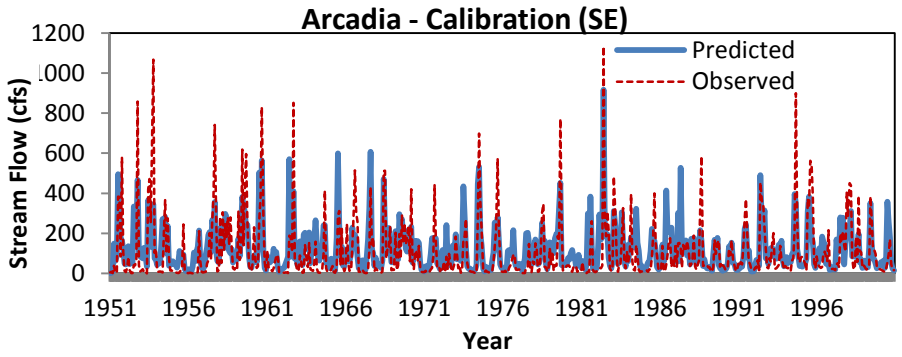

Figure 6-3: Arcadia/Joshua Creek Catchment – Model Calibration (SE)

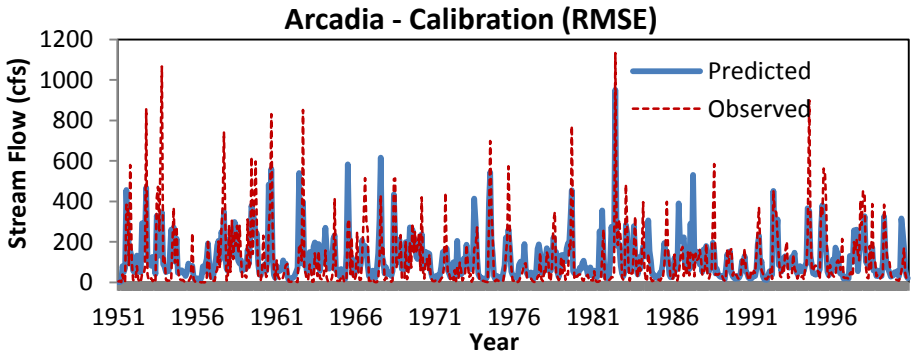

Figure 6-4: Arcadia/Joshua Creek Catchment – Model Calibration (RMSE)

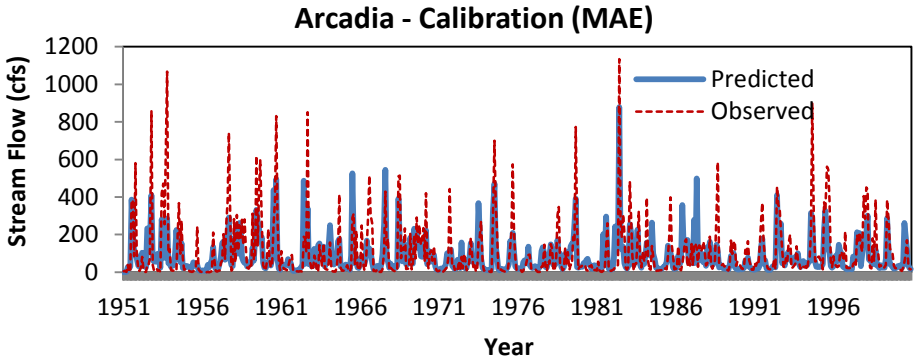

Figure 6-5: Arcadia/Joshua Creek Catchment – Model Calibration (MAE)

6.1.2 Model Validation Results and Discussion

Validation of the calibrated parameter set provides a means of evaluating the developed calibrated model. An acceptable validation result indicates that the calibrated parameter set is suitable for the intended applications. In this study, a successful validation of the calibrated parameter set would indicate that, within certain conditions identified in the calibration process, the parameter set is suitable for simulating stream-flows on the above mention catchment area. The model validation period was from January 2001 to December 2010.

The result of the model validation is illustrated in the graph below (Figure 6-6). As was observed in the calibration results, the plotted points along the 45 degree line were relatively balanced with a slight leaning to the left. Once again, as seen in the calibration period, the model tends to slightly under predict the observed values especially when it comes to the extreme data values. The validation result however shows that the model is performing reasonably well, because out of 120 data point, only about 4 to 6 points had large differences. The line plot of the observed vs. predicted discharge, shows the model predictions fit the observed data point with the exception of the extremes values previously mentioned. Using the AE parameters set by the calibration period, the validated result showed a correlation of coefficient of 0.81. The validation results using the SE objective function were similar to that of the AE model validation. The model validation predicted a maximum discharge of 598.43 cfs. This was more than the maximum produced using the AE objective function which was 489.5cfs. This is an

indication that the model is performing better in that it is trying to reach the observed extreme values.

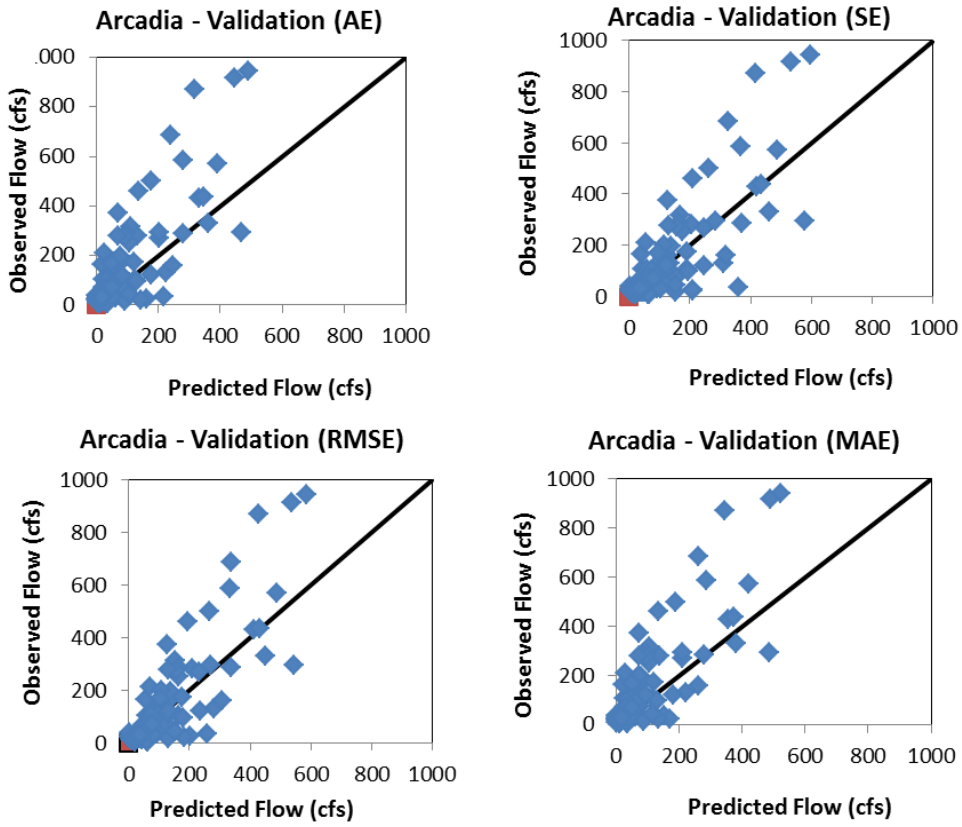

Figure 6-6: Arcadia/Joshua Creek Catchment – Model Validation

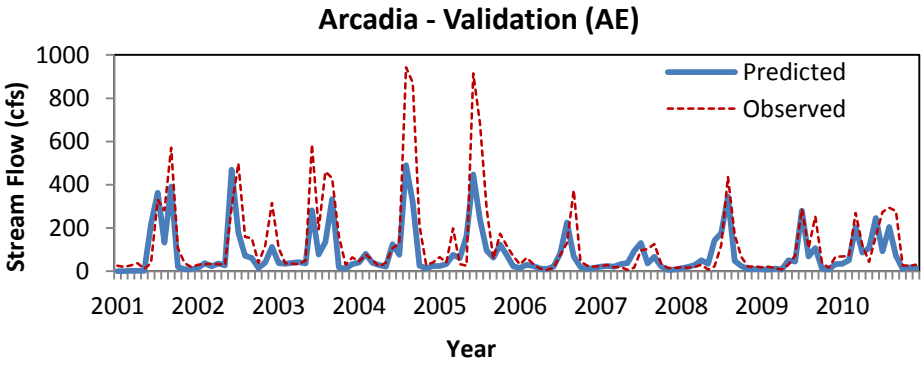

Figure 6-7: Arcadia/Joshua Creek Catchment – Model Validation (AE)

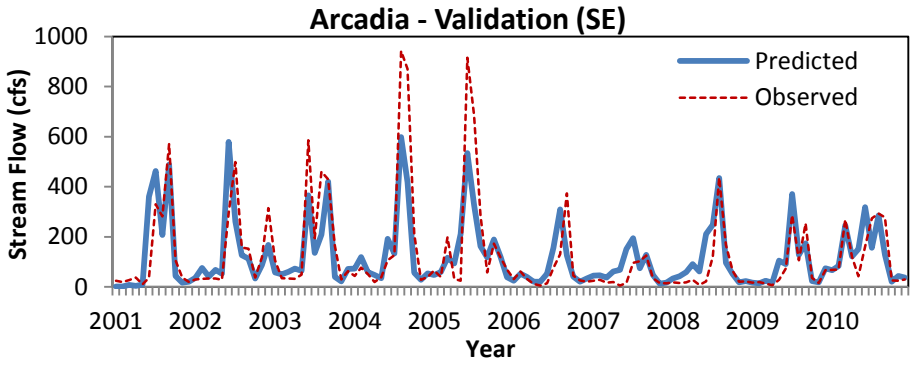

Figure 6-8: Arcadia/Joshua Creek Catchment – Model Validation (SE)

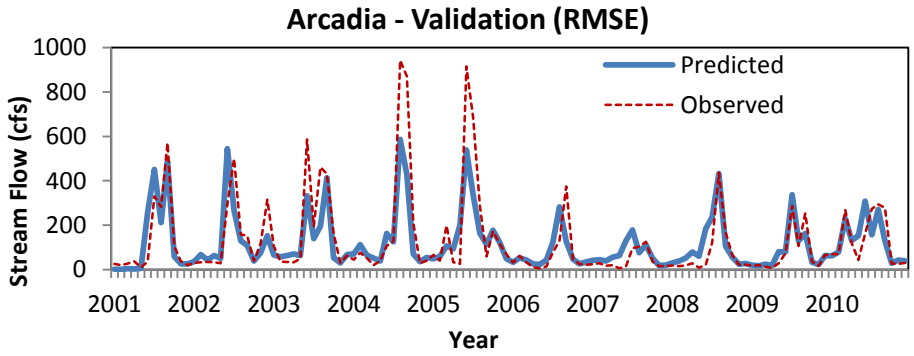

Figure 6-9: Arcadia/Joshua Creek Catchment – Model Validation (RMSE)

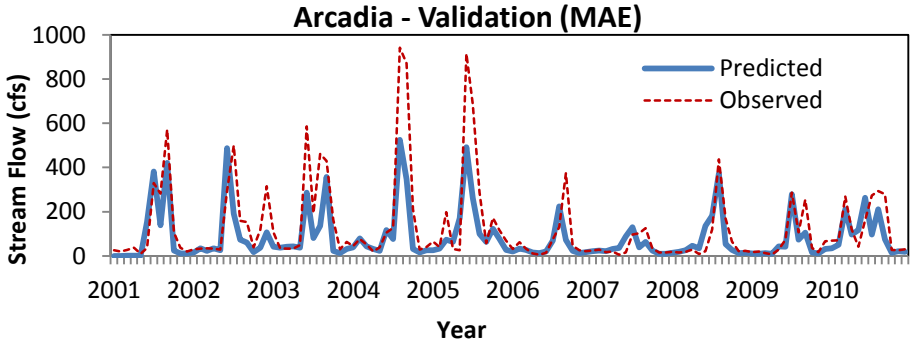

Figure 6-10: Arcadia/Joshua Creek Catchment – Model Validation (MAE)

As outlined in the methodology, a scoring system was developed in order to compare the various methods used. The methods were ranked based on the assessed score from lowest to highest, with the one with the lowest score being the best method. Based on this

scoring system, the calibrated parameter set producing the best results was optimization RMSE method with a score of 3.404. The results are tabulated and ranked below (Table 6-2)

Table 6-2: Arcadia/Joshua Creek Catchment – Model Ranking

Objective Function (min)	Performance Measures					Score
	Absolute Error (AE)	Squared Error (SE)	Root Mean Squared Error (RMSE)	Mean Absolute Error (MAE)	1- Correlation Coefficient	
Root Mean Squared Error (RMSE)	7188.815	1315117.604	104.687	59.907	0.159	3.404
Squared Error (SE)	7632.339	1444508.392	109.716	63.603	0.189	3.649
Mean Absolute Error (MAE)	7985.799	1716038.637	119.584	66.548	0.169	3.935
Absolute Error (AE)	8383.677	1889385.159	125.479	69.864	0.185	4.185

6.2 Federal Point/South Fork Black Creek near Penney Farms, FL

6.2.1 Model Calibration Results & Discussion

All procedures described in the calibration of the Arcadia/Joshua Creek catchment were applied to the Federal Point/South Fork catchment. All four objective functions AE, SE, RMSE and MAE were used to calibrate the model. Both predicted and observed values were plotted along a 45 degree line. A review of the graph indicates that the plotted points followed a similar trend. The calibrated model parameters of the best performing model were, $a = 0.8995$, $b = 13.2807$, $c = 0.5019$, and $d = 0$. Initial soil and ground water storage was 3.7523 and 293.6885 mm respectively. The AE objective

function produced a correlation of coefficient of approximately 0.6. The time series line plot shown in Figure 6-12 shows that the projected monthly discharges is doing better when compared to the observed values than the other methods. The calibrated parameters sets are summarized in Table 6-3 below.

Table 6-3: Federal Point/South Fork Black Creek – Model Calibration Parameters

Objective Function (min)	Initial Soil Storage (mm)	Initial Groundwater Storage (mm)	a	b	c	d
Absolute Error (AE)	3.7523	293.6885	0.8995	13.2807	0.5019	0.0000
Squared Error (SE)	3.7177	206.9973	0.3620	15.0000	0.5377	0.0000
Root Mean Squared Error (RMSE)	3.6574	269.8357	0.7882	15.0000	0.5165	0.0003
Mean Absolute Error (MAE)	3.9571	269.4335	0.8872	14.9830	0.4949	0.0001

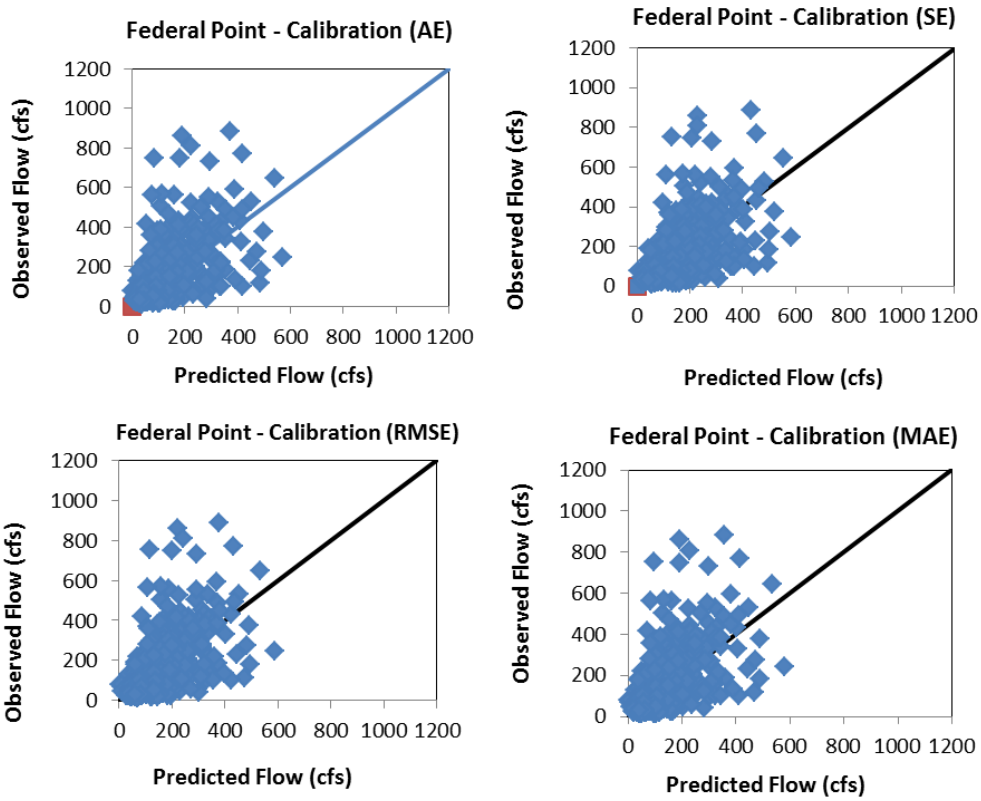

Figure 6-11: Federal Point/South Fork Black Creek – Model Calibration

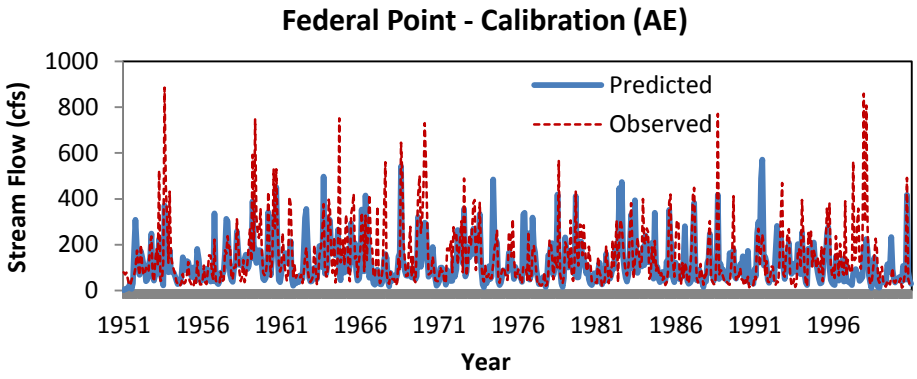

Figure 6-12: Federal Point/South Fork Black Creek – Model Calibration (AE)

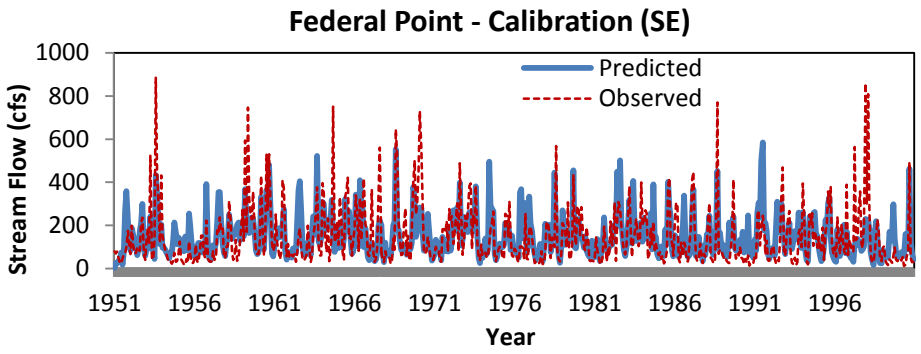

Figure 6-13: Federal Point/South Fork Black Creek – Model Calibration (SE)

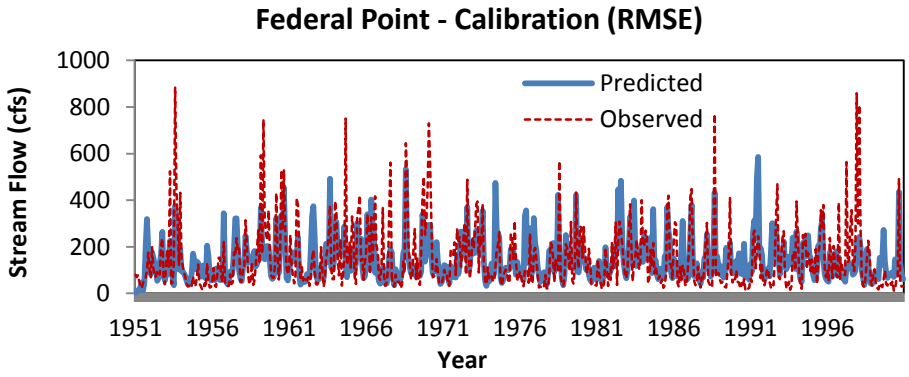

Figure 6-14: Federal Point/South Fork Black Creek – Model Calibration (RMSE)

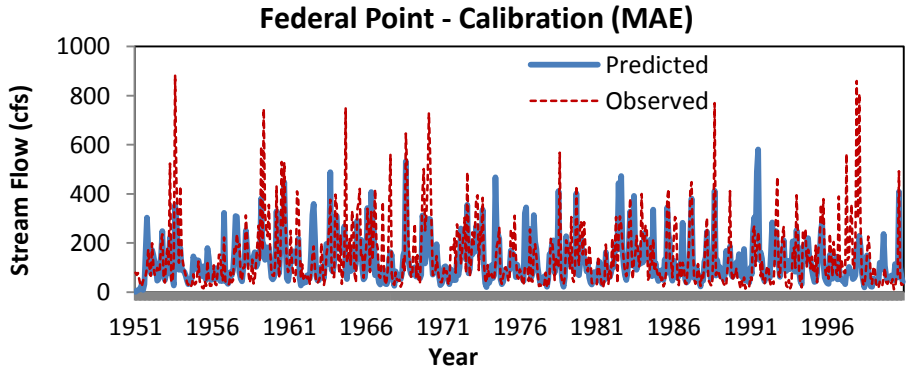

Figure 6-15: Federal Point/South Fork Black Creek – Model Calibration (MAE)

6.2.2 Model Validation Results & Discussion

The results of the model validation are illustrated in the graphs below (Figure 6-16). The calibrated 45 degree plot shown a slight inclination to the left, which would suggest the model was slightly under predicting, however with validation, the plotted observed vs. predicted points along the results 45 degree line were relatively balanced. As stated earlier the best performing model was using the AE parameter set. The AE validation results had a correlation of coefficient of 0.7. as oppose to the calibrated model of 0.6. Using this performance measure only for comparison, suggests that the validation period model predictions was performing better. The line plot of the observed vs. predicted discharge, shows the model predictions fit the observed data point with the exception of only one point. This point may be an outlier.

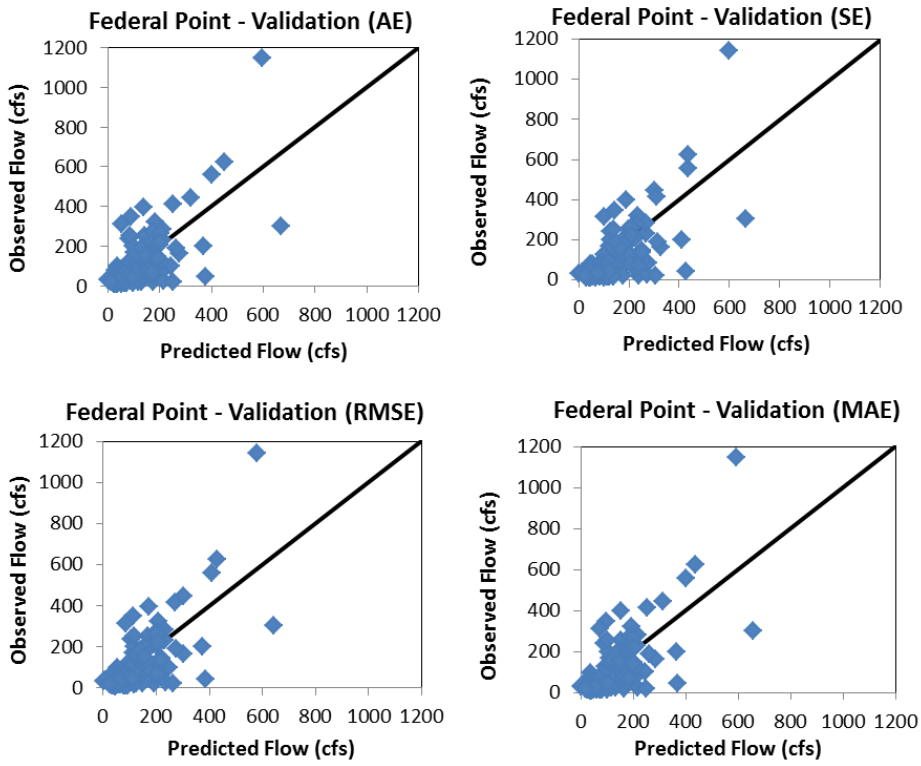

Figure 6-16: Federal Point/South Fork Black Creek – Model Validation

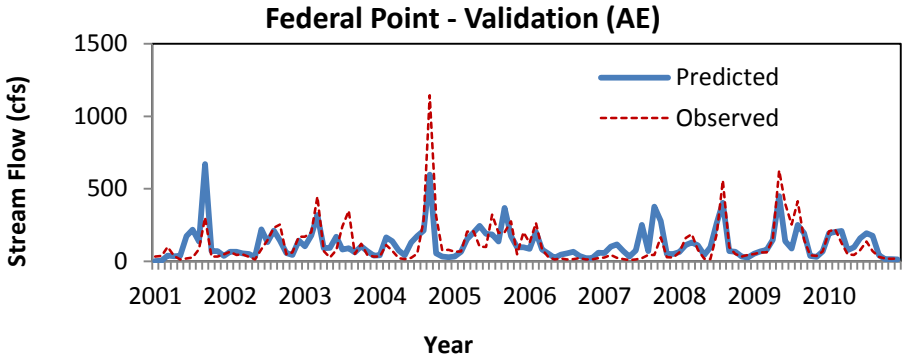

Figure 6-17: Federal Point/South Fork Black Creek – Model Validation (AE)

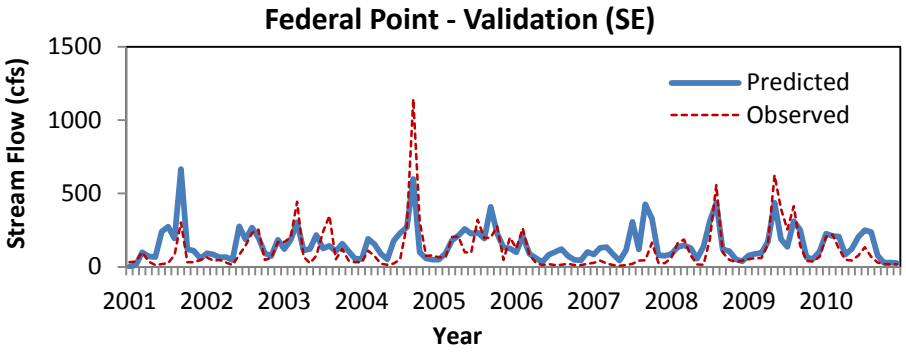

Figure 6-18: Federal Point/South Fork Black Creek – Model Validation (SE)

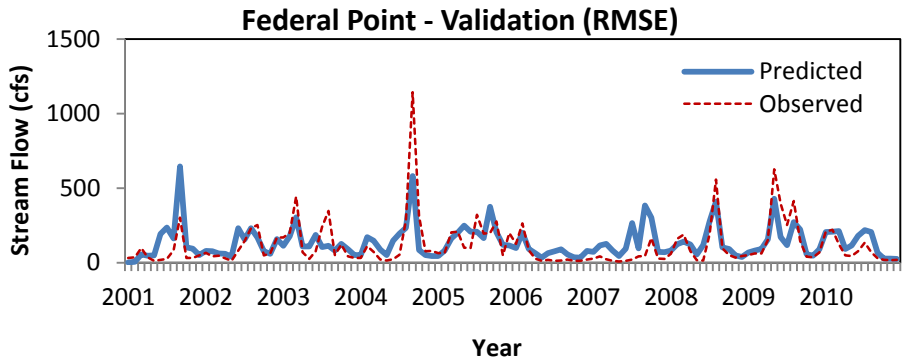

Figure 6-19: Federal Point/South Fork Black Creek – Model Validation (RMSE)

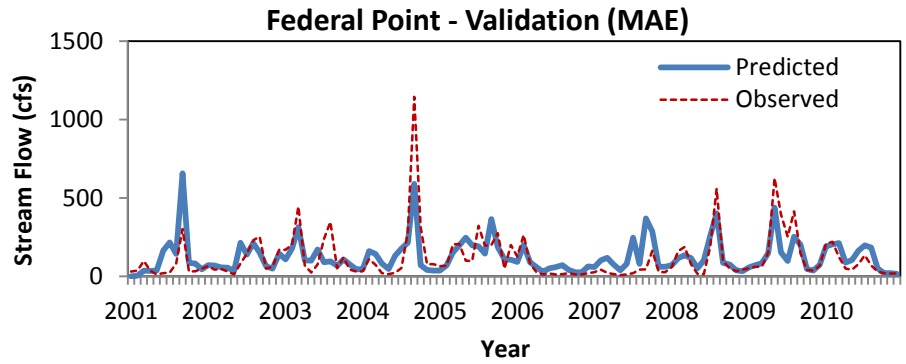

Figure 6-20: Federal Point/South Fork Black Creek – Model Validation (MAE)

Table 6-4: Federal Point/South Fork Black Creek – Model Ranking

Objective Function (min)	Performance Measures					Score
	Absolute Error (AE)	Squared Error (SE)	Root Mean Squared Error (RMSE)	Mean Absolute Error (MAE)	1- Correlation Coefficient	
Absolute Error (AE)	7896.277	1332350.187	105.370	65.802	0.291	3.732
Mean Absolute Error (MAE)	8055.157	1314750.575	104.672	67.126	0.285	3.742
Root Mean Squared Error (RMSE)	8576.727	1382977.700	107.354	71.473	0.293	3.928
Squared Error (SE)	9451.019	1569532.881	114.365	78.758	0.313	4.313

6.3 Tarpon Spring/Anclote River near Elfers FL

6.3.1 Model Calibration Results & Discussion

All four objective functions AE, SE, RMSE and MAE were used to calibrate the model for Tarpon Spring/Anclote River catchment. Similar to what was done with the two previous catchments, both predicted and observed values were plotted along a 45 degree line. A review of the graphs (Figure 6-21) indicates that the plotted points followed a similar trend. The calibrated model parameters of the best performing model (RMSE) were, a = 0..9594, b = 14.9962, c = 0.4505, and d = 0. Initial soil and ground water storage was 4.01mm and 261.26 mm respectively. The RMSE objective function produced a correlation of coefficient of approximately 0.73. The time series line plot shown in Figure 6-24 shows that the projected monthly discharges relatively "good fit" when compared to the observed values with the exception of some extreme values. The

calibrated parameters sets are summarized in Table 6-5 below.

Table 6-5: Tarpon Spring/Anclote River – Model Calibration Parameters

Objective Function (min)	Initial Soil Storage (mm)	Initial Groundwater Storage (mm)	a	b	c	d
Model - Absolute Error (AE)	3.5689	300.3662	0.9792	8.7970	0.6080	0.0000
Model - Squared Error (SE)	3.8659	269.2410	0.8773	13.0038	0.4519	0.0000
Model - Root Mean Squared Error (RMSE)	4.0109	261.2614	0.9595	14.9962	0.4505	0.0000
Model - Mean Absolute Error (MAE)	4.1463	234.2322	0.9909	15.0000	0.5509	0.0000

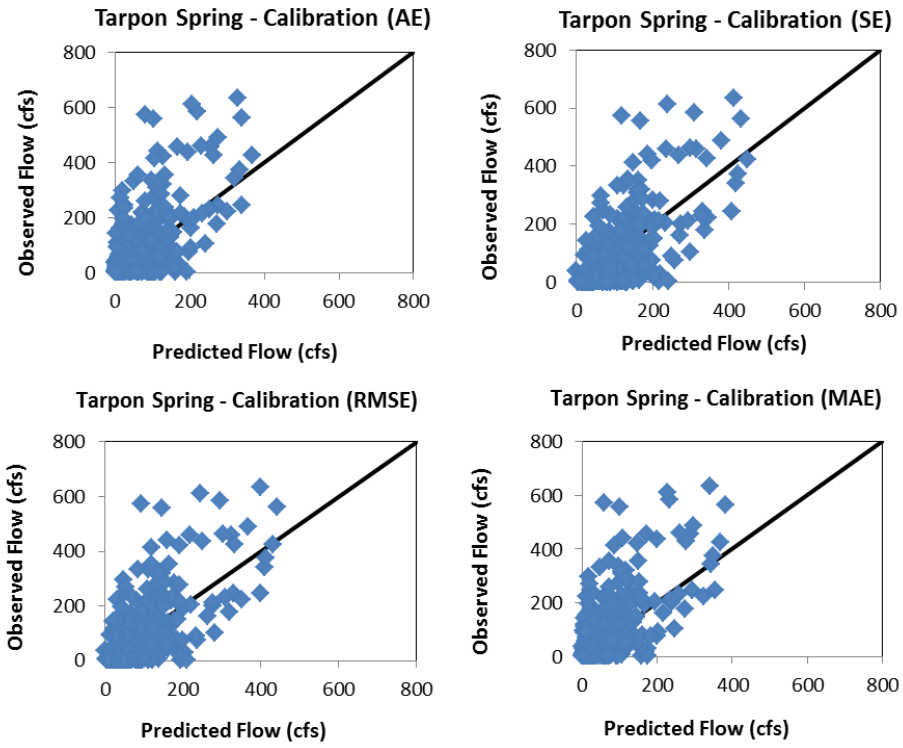

Figure 6-21: Tarpon Spring/Anclote River – Model Calibration

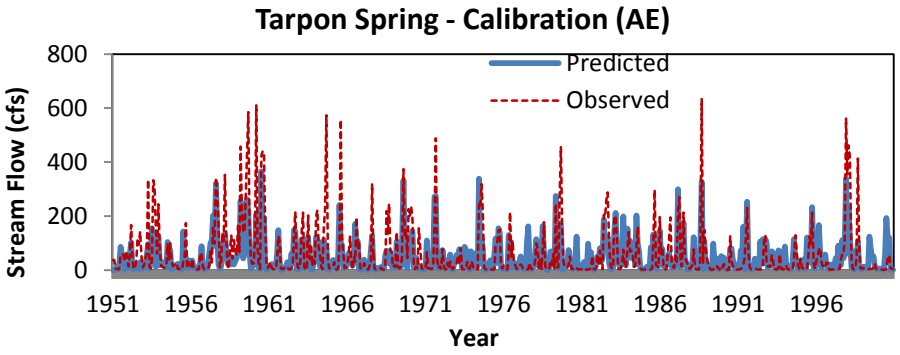

Figure 6-22: Tarpon Spring/Anclote River – Model Calibration (AE)

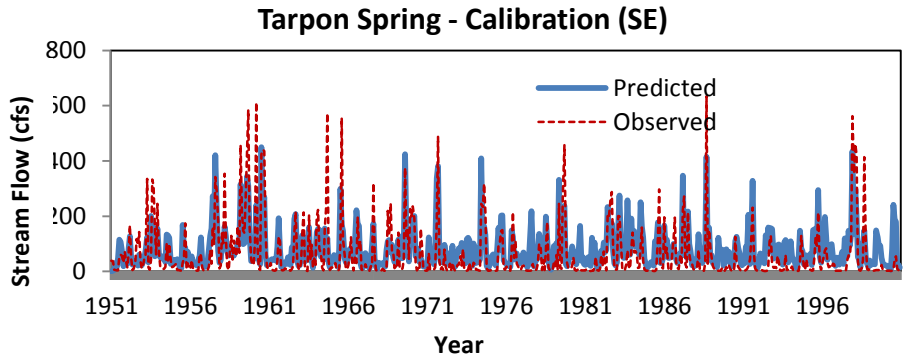

Figure 6-23: Tarpon Spring/Anclote River – Model Calibration (SE)

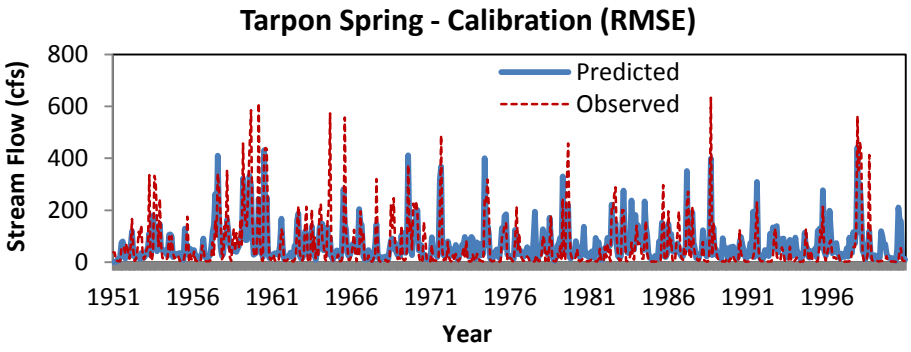

Figure 6-24: Tarpon Spring/Anclote River – Model Calibration (RMSE)

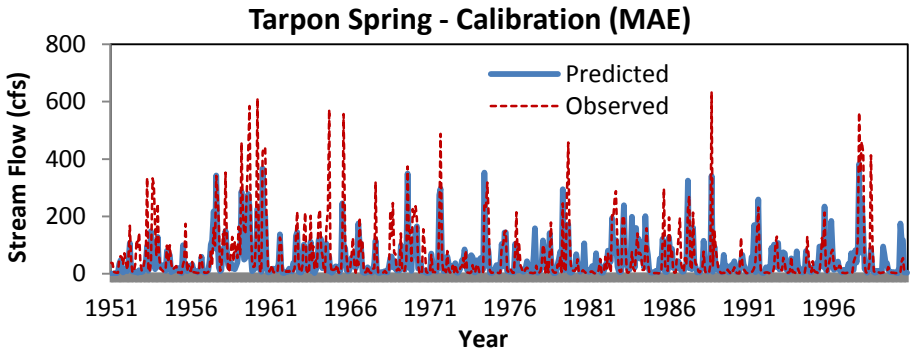

Figure 6-25: Tarpon Spring/Anclote River – Model Calibration (MAE)

6.3.2 Model Calibration Results & Discussion

For Tarpon Springs/Anclote river catchment, the calibrated 45 degree plot shows a relatively balanced distribution along the line with the exception of three to four data points, which would suggest that the model is not bias. However between the years 2003 to 2005 there were high discharge values that the model failed to predict. There may be many reasons why this model is not performing at its best, some of these reasons could be that the precipitation values may not be accurate or the PE values were not actual values because they were estimated using the Thornthwaite and Wilm Method, which may have had some errors because it is a temperature base estimating method. Another reason could be the length of the calibration period. That is, because of the longer time period the probability for errors in the data are greater. All these errors can be compounding and there might be errors in the calibration as well as the validation.

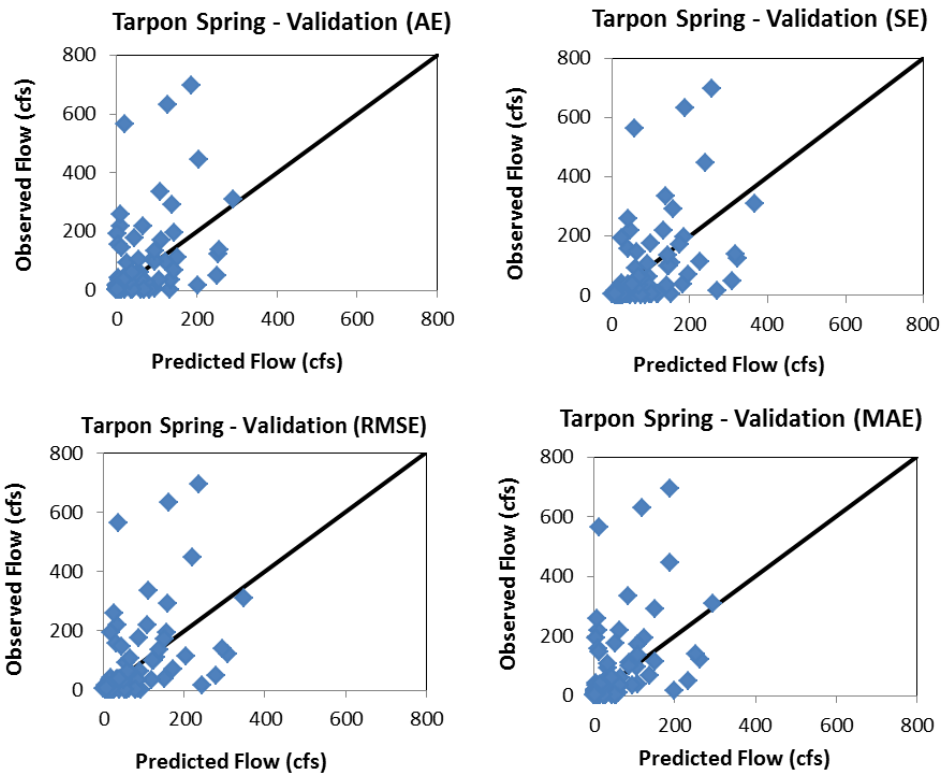

Figure 6-26: Tarpon Spring/Anclote River – Model Validation

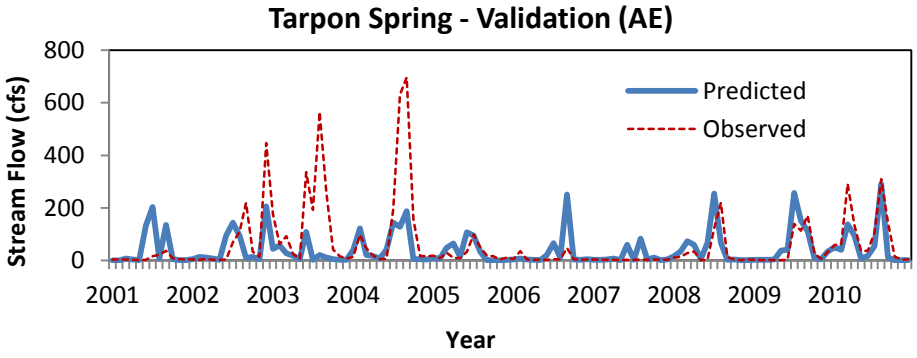

Figure 6-27: Tarpon Spring/Anclote River – Model Validation (AE)

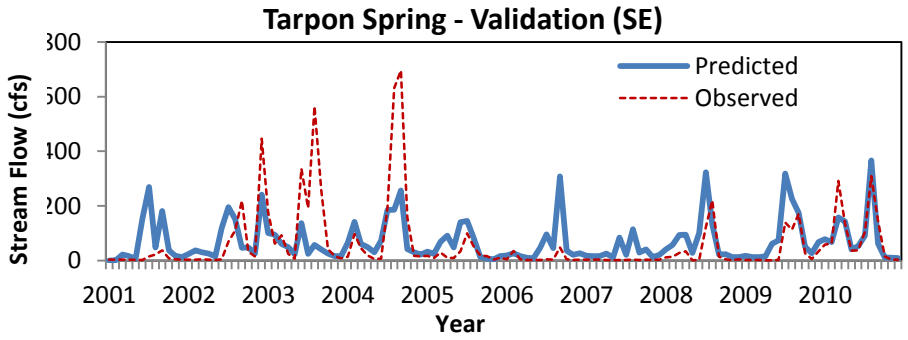

Figure 6-28: Tarpon Spring/Anclote River – Model Validation (SE)

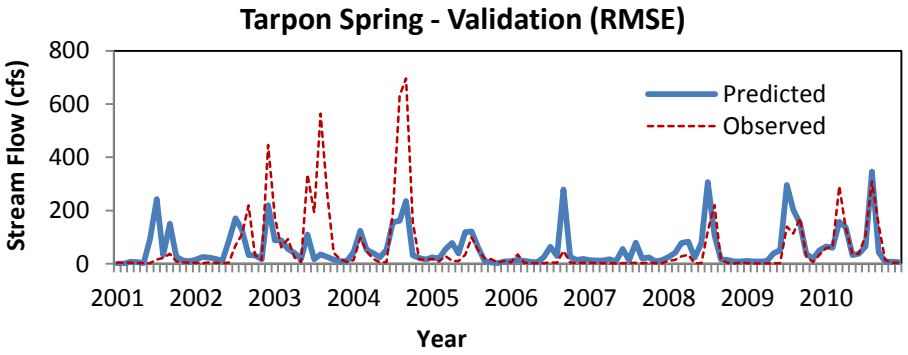

Figure 6-29: Tarpon Spring/Anclote River – Model Validation (RMSE)

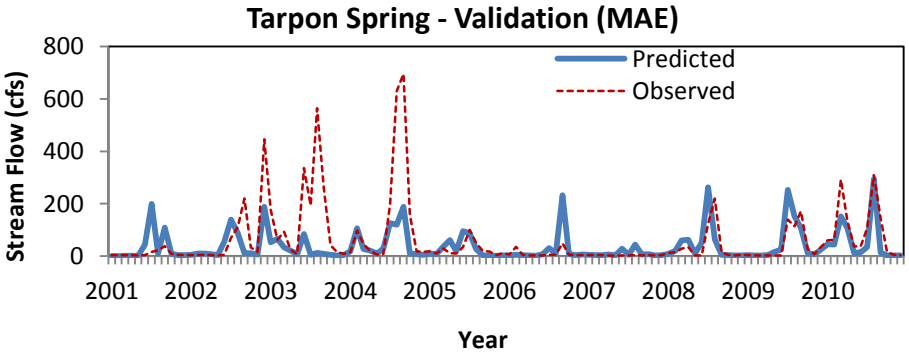

Figure 6-30: Tarpon Spring/Anclote River – Model Validation (AE)

As stated earlier the best performing model was using the RMSE parameter set. The RSME validation results had a correlation of coefficient of 0.53, which is not the best result on a scale of 0 to 1. However, the model was accepted based on other performance measures.

Table 6-6: Tarpon Spring/Anclote River – Model Ranking

Objective Function (min)	Performance Measures					Score
	Absolute Error (AE)	Squared Error (SE)	Root Mean Squared Error (RMSE)	Mean Absolute Error (MAE)	1-Correl. Coeff.	
Root Mean Squared Error (RMSE)	6069.407	1268122.473	102.799	50.578	0.472	4.114
Mean Absolute Error (MAE)	5539.105	1350036.604	106.067	46.159	0.485	4.163
Absolute Error (AE)	5938.665	1368527.734	106.791	49.489	0.508	4.222
Squared Error (SE)	6928.792	1295539.944	103.905	57.740	0.476	4.396

CHAPTER 7. RESULTS AND DISCUSSION

7.1 Results - Arcadia/Joshua Creek Catchment

The results presented in Table 7-1 suggests that the developed water balance model performed satisfactorily in the simulation of monthly discharges (streamflow) in the Joshua Creek Catchment. The table contains both the observed (1951-2010) and the projected precipitation values (2011-2099). The statistical analysis shows that the projected values produces varying results, however they more or less follow those of the observed values of the historical period. The mean of the observed values is 109.673 cfs, the closest model to the observed mean was M11 with a value of 111.827 cfs. The model producing the lowest mean was M9. The mean discharge value of model M9 was approximately 50% less than that of the observed values. The kurtosis value of 30.194 and the highest Skewness value of 3.669 for model M9 projections also indicate that this model is producing more incidences of lower values when compared to the others. Model M1 follow closely behind with kurtosis of 19.525 (second highest of all the model projections) and with skewness of 3.247. This may be related to the fact that the data analysis of the precipitation and temperature data in section 5.3 of this report indicated that M9 continually predicted higher temperature values and lower precipitation values throughout the time period than all the other models. The statistics also show that all the model discharge predictions and the observed data sets are positively skewed, which is an indication that the majority of the discharge values fall within the lower ranges.

Table 7-1: Statistics - Arcadia Observed (1951-2010) - Projected Discharge Data (2011-2099)

Models	Mean	STD	Skewness	Kurtosis	Max	Min	Range
Observed	109.673	161.187	2.766	12.400	1133.000	0.520	1132.480
M1	83.565	77.371	3.247	19.525	753.899	0.472	753.428
M2	99.603	71.391	2.007	8.770	486.685	6.656	480.029
M3	93.990	72.083	1.735	7.582	595.213	0.084	595.129
M4	104.296	74.861	2.460	14.562	764.335	6.069	758.266
M5	92.885	77.693	2.180	10.135	606.092	0.197	605.894
M6	86.791	64.026	1.670	6.722	437.157	0.361	436.796
M7	97.086	64.899	2.079	10.132	540.014	0.119	539.895
M8	100.195	81.692	2.233	10.208	673.991	0.452	673.540
M9	54.376	48.938	3.669	30.194	585.055	4.774	580.281
M10	101.807	88.436	1.936	7.868	581.579	4.774	576.805
M11	111.827	80.342	1.407	5.464	501.529	10.049	491.479
M12	104.944	69.261	1.833	10.992	732.530	2.222	730.308
M13	93.161	68.350	2.045	8.974	525.639	2.043	523.597
M14	101.474	78.969	1.678	6.557	571.720	2.131	569.589
M15	97.242	74.744	1.873	7.837	556.727	2.506	554.221

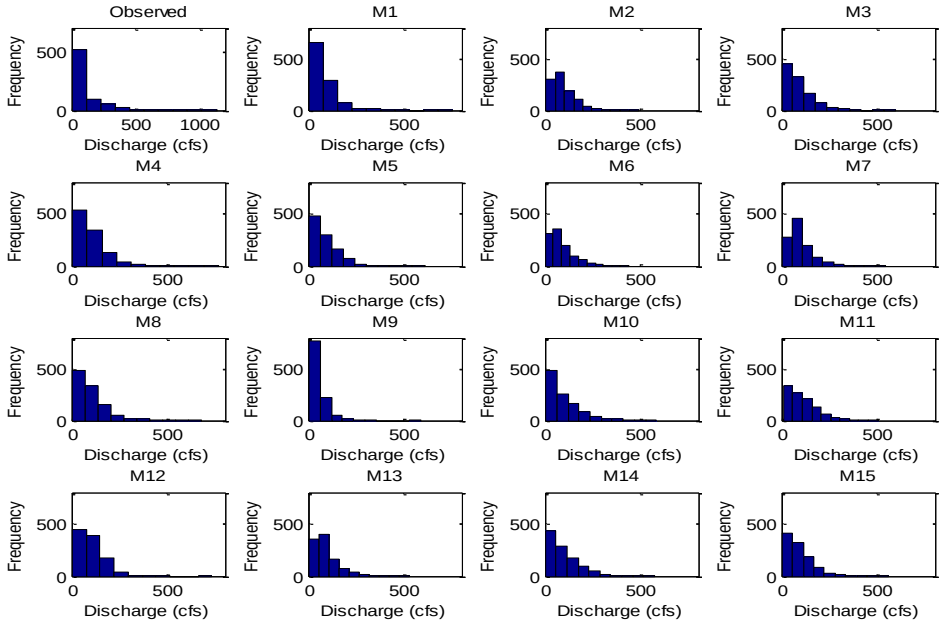

Figure 7-1: Histograms - Arcadia Observed (1951-2010) - Projected Discharge Data (2011-2099)

The histogram in Figure 7-1 provides a graphical illustration of this, as the graphs shows, model M9 had higher frequencies of lower discharge values. M11 was at the other extent. It had the lowest kurtosis and skewness values of all the projections. As observed the distribution is relatively sloped and has a flatter peak than those of the other models.

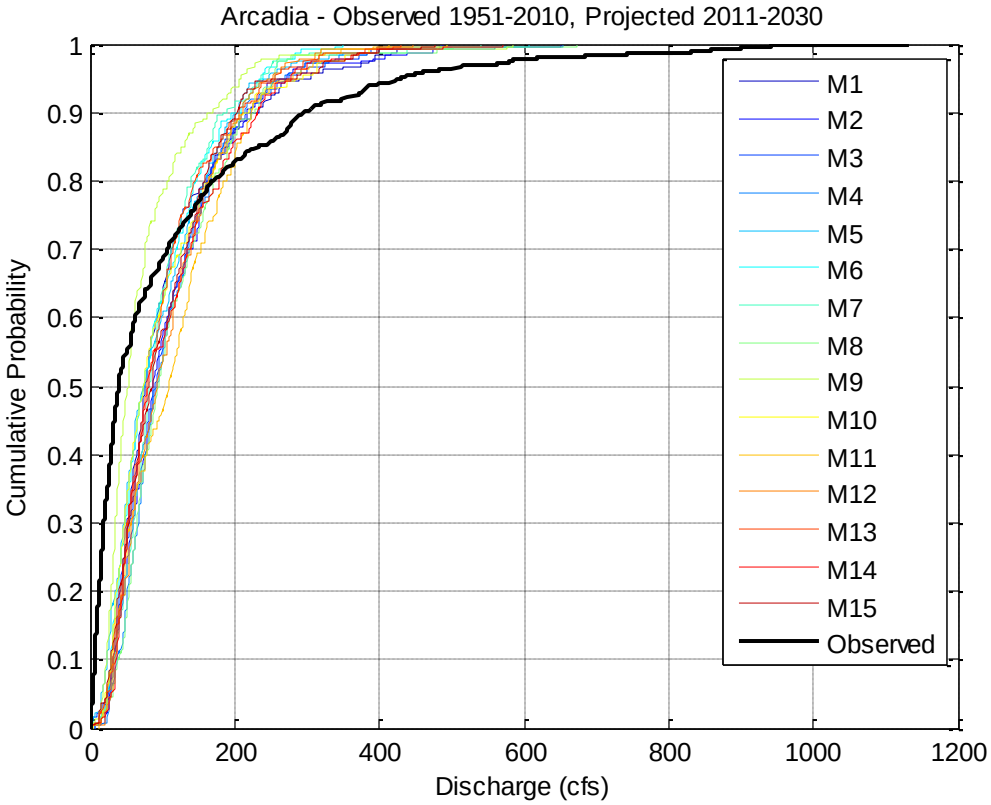

Figure 7-2: Arcadia Observed (1951-2010) - Projected Discharge Data (2011-2030)

Similar to what was done for the temperature and precipitation data analysis, the projected discharge values were broken up into 4 periods, 2011-2030, 2031-2050, 2051-2070 and 2071-2099. Each of these periods was compared to the observed data using CDF plots. See Figure 7-2 through Figure 7-5 for CDF plots. The first period plotted (2011-2030), shows an increase in discharge at the lower ranges. As the values get higher

the trend is reversed. This followed a similar pattern with the corresponding precipitation data for the same period. All models indicate reduced extreme values events.

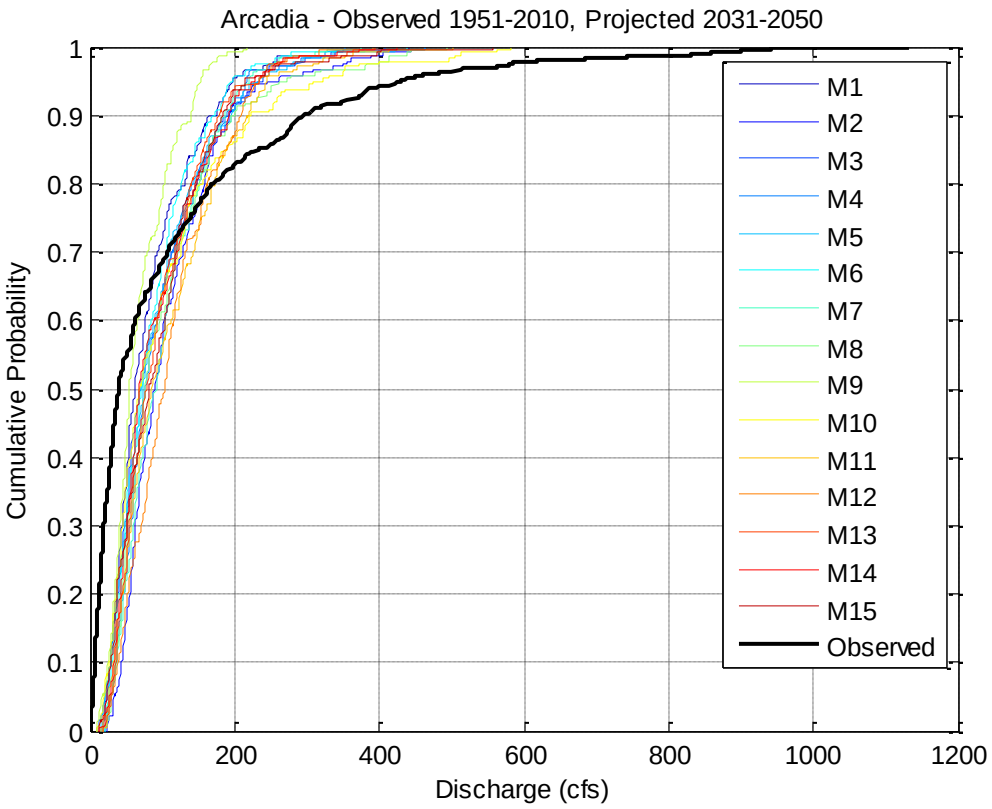

Figure 7-3: Arcadia Observed (1951-2010) - Projected Discharge Data (2031-2050)

A similar trend was observed in plots for 2031-2050, 2051-2070 and 2071-2099 periods, As time progresses, the CDF bands of the models widens, indicating that there is more variability among the models as time passes. Model M1 and M9 in period 2071-2099 (Figure 7-5) had much higher percentage of producing lower extreme values.

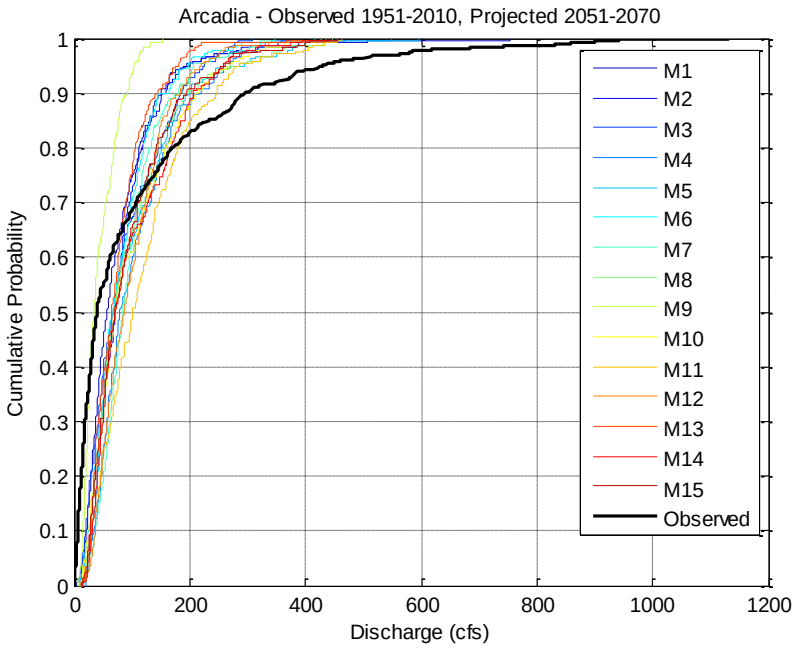

Figure 7-4: Arcadia Observed (1951-2010) - Projected Discharge Data (2051-2070)

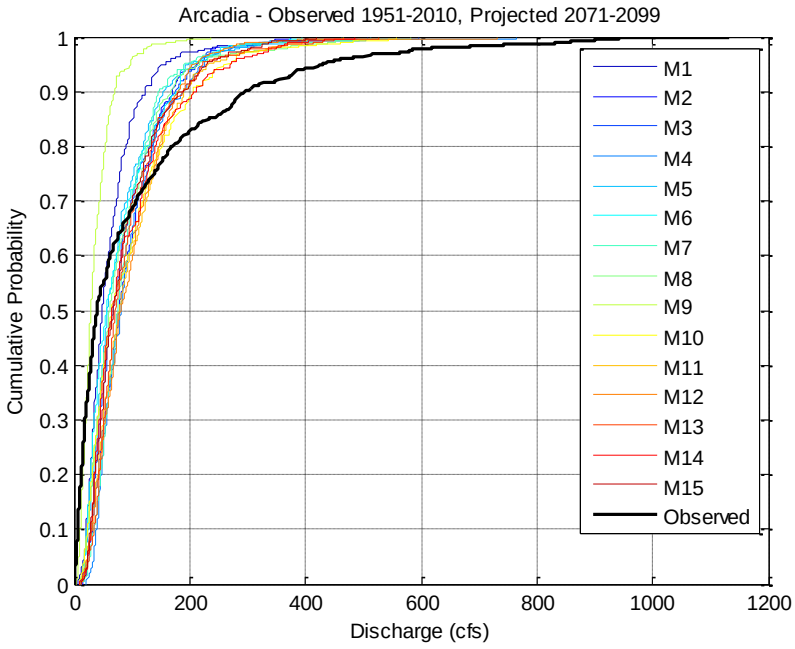

Figure 7-5: Arcadia Observed (1951-2010) - Projected Discharge Data (2071-2099)

The scatter plot (Figure 7-6) of the discharge values shows relatively no change for the observed data. All models showed a decreasing trend. The graph shows models M1 and M9 with a relatively steeper falloff than the other models.

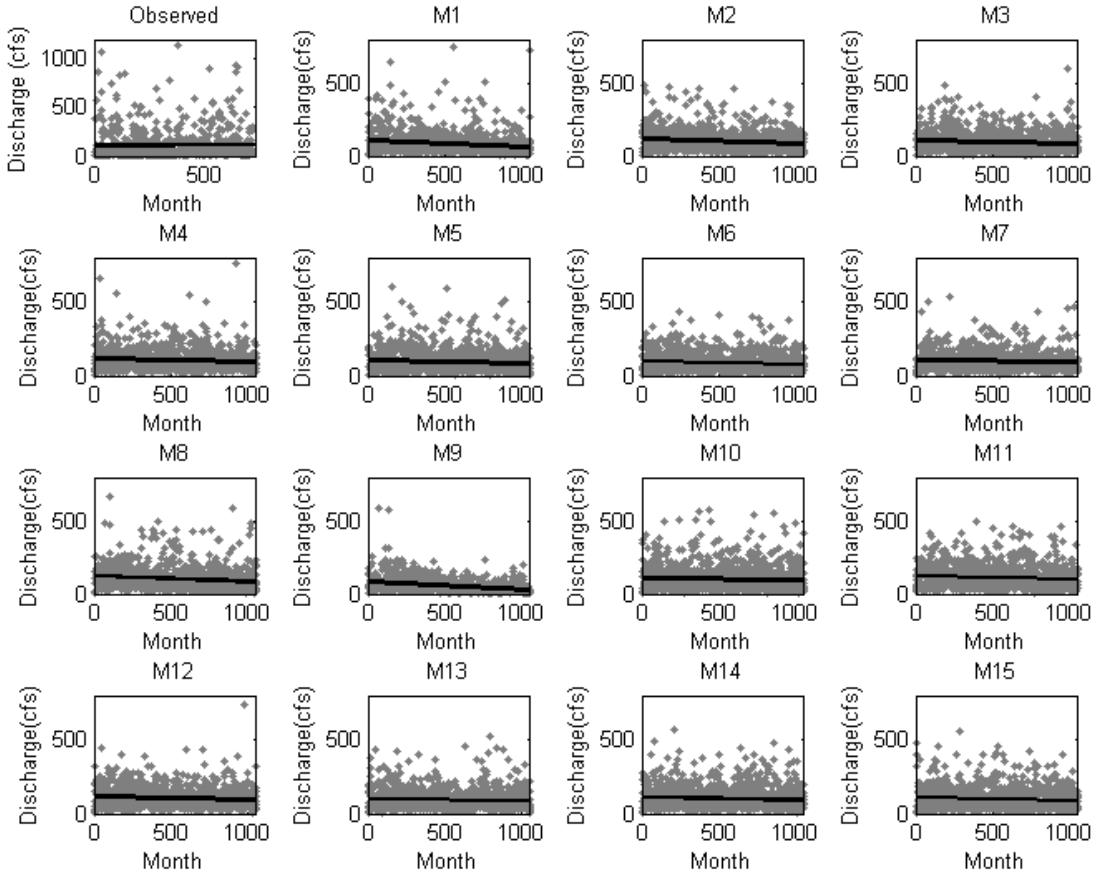

Figure 7-6: Scatter Plots - Arcadia Observed (1951-2010) - Projected Discharge Data (2011-2099)

7.2 Results Federal Point/South Fork Black Catchment

The statistical analysis for Federal Point/South Fork Black Catchment shows that the projected values also produce varying results. The mean of the observed values is 140.219 cfs. Like Arcadia/Joshua Creek, most of the models did not produced such a

high average; the closest model to the observed mean was M12 with a value of 136.519 cfs. The model producing the lowest mean was M9. The mean discharge value of model M9 was approximately 52% less than that of the observed values. The statistics also show that all the model discharge predictions and the observed data sets are positively skewed.

Table 7-2: Statistics - Federal Point Observed (1951-2010) - Projected Discharge Data (2011-2099)

Models	Mean	STD	Skewness	Kurtosis	Max	Min	Range
Observed	140.219	139.704	2.363	11.111	1144.000	8.300	1135.700
M1	108.439	85.655	2.467	13.408	835.670	2.038	833.632
M2	115.043	68.558	1.681	7.191	515.464	12.772	502.692
M3	111.738	84.336	3.001	21.083	1028.176	1.310	1026.867
M4	130.522	93.982	2.395	11.949	893.212	7.070	886.142
M5	126.356	105.223	2.397	11.260	831.041	3.271	827.771
M6	124.607	87.963	2.047	9.415	674.930	0.227	674.703
M7	112.300	69.725	1.775	7.253	481.305	0.436	480.869
M8	117.205	86.508	2.169	10.516	722.706	0.907	721.798
M9	67.969	50.719	2.628	16.013	552.163	4.172	547.991
M10	117.051	85.278	2.351	12.928	828.105	9.040	819.065
M11	135.273	91.534	1.496	5.820	604.375	5.839	598.536
M12	136.519	90.367	1.881	8.630	751.352	3.029	748.323
M13	125.103	79.551	1.572	6.259	539.995	3.438	536.558
M14	133.778	92.327	1.723	7.115	676.489	6.074	670.414
M15	130.318	92.985	1.717	7.136	759.314	3.438	755.876

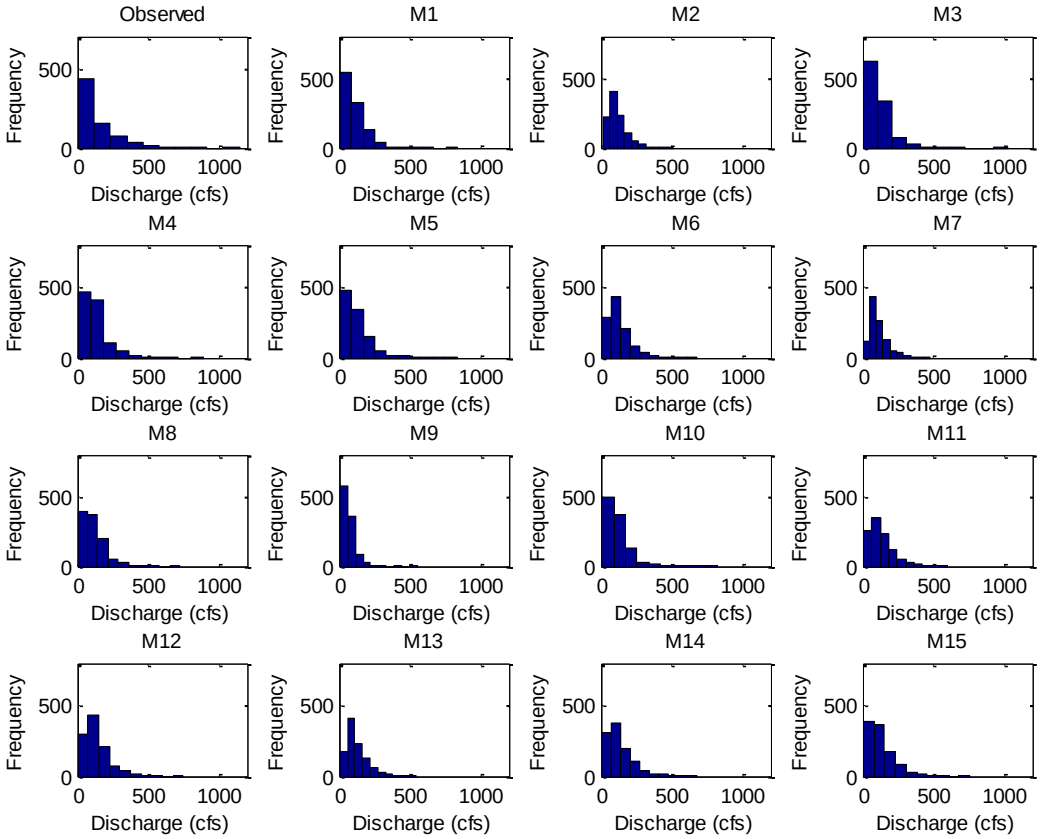

Figure 7-7: Histograms - Federal Point Observed (1951-2010) - Projected Discharge Data (2011-2099)

The histogram in Figure 7-7 provides a graphical illustration of the discharge data. As observed in the frequency values, there are higher incidences of getting lower discharge values.

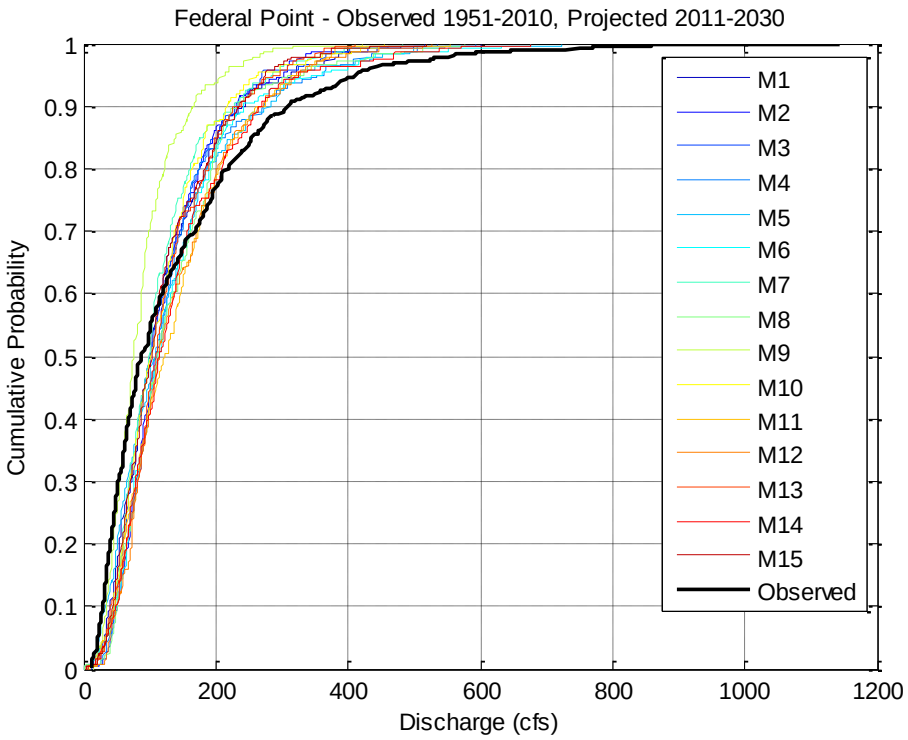

Figure 7-8: Federal Point Observed (1951-2010) - Projected Discharge Data (2011-2030)

For period (2011-2030), the plotted CDF graph (Figure 7-8) illustrates that most of the models shows increases in discharge at the lower values. Extreme are less. Model M9 generally followed the tendency to predict less discharge, which is proportional to precipitation. The trend was typical for periods 2031-2050, 2051-2070 and 2071-2099. As time progresses, the CDF bands of the models widens and moves toward the left indicting lower values. See Figure 7-9 through Figure 7-11 for the remainder of the CDF plots for Federal Point/South Fork Black Creek Catchment.

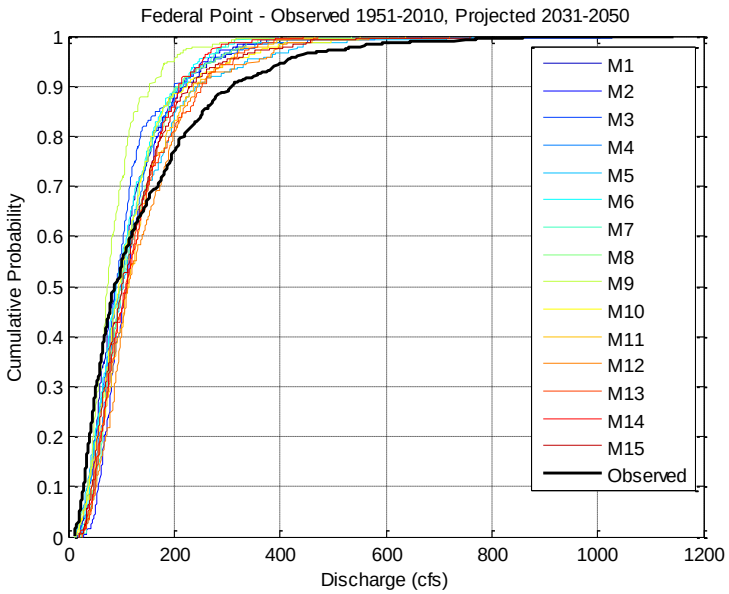

Figure 7-9: Federal Point Observed (1951-2010) - Projected Discharge Data (2031-2050)

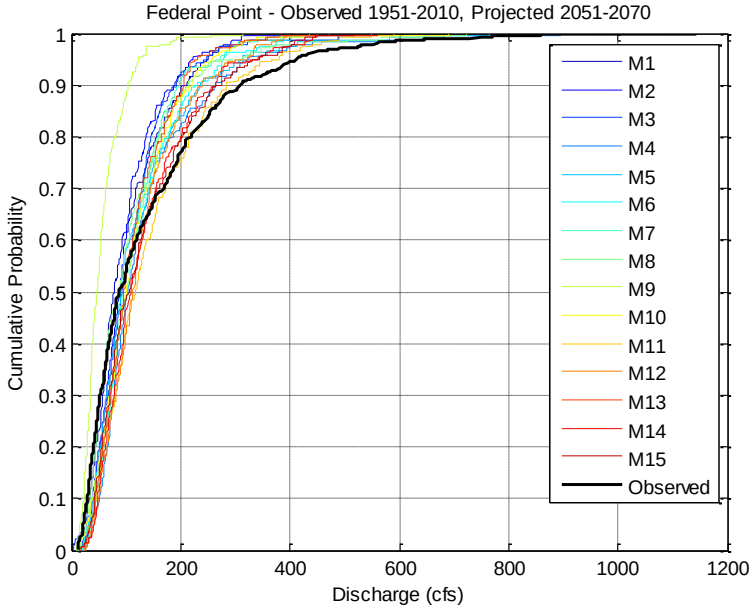

Figure 7-10: Federal Point Observed (1951-2010) - Projected Discharge Data (2051-2070)

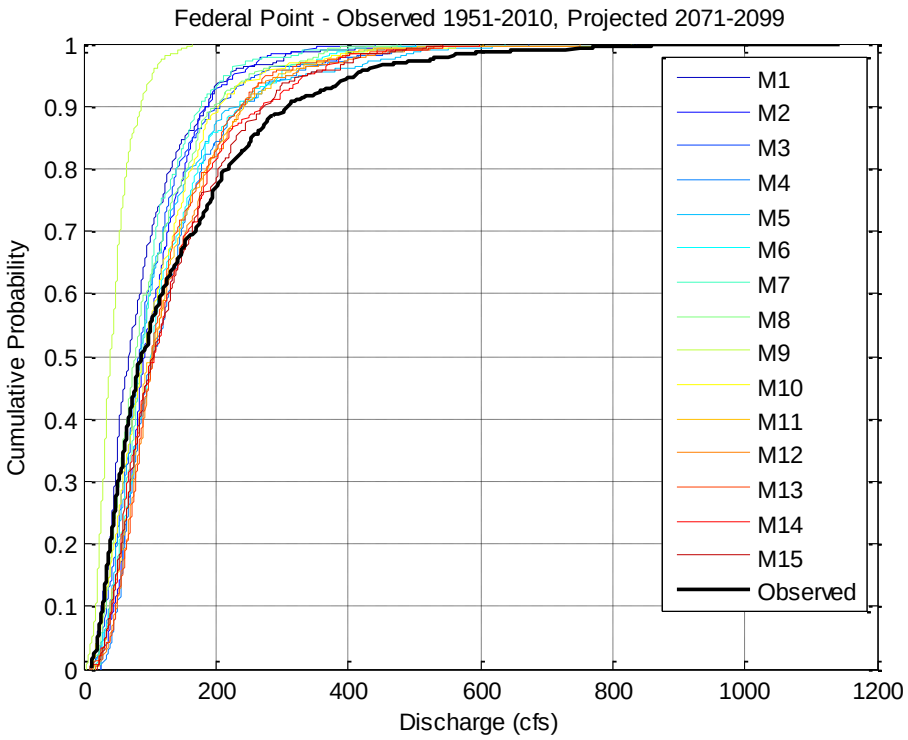

Figure 7-11: Federal Point Observed (1951-2010) - Projected Discharge Data (2071-2099)

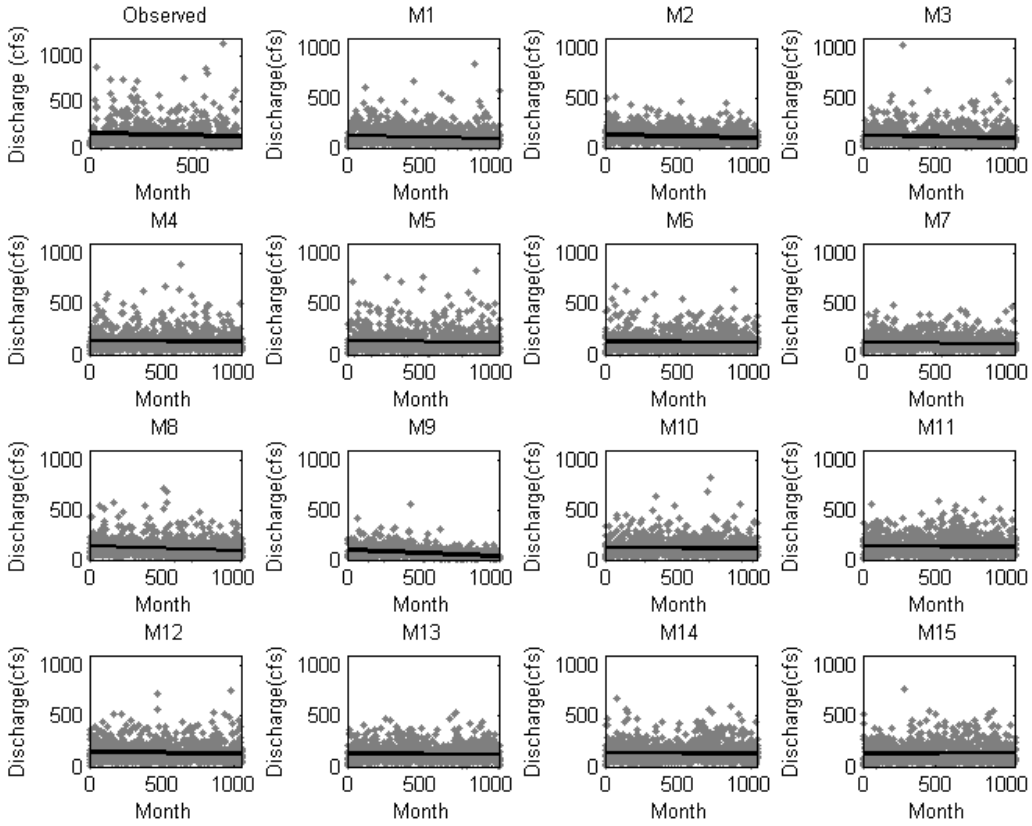

Figure 7-12: Scatter Plots - Federal Point Observed (1951-2010) - Projected Discharge Data (2011-2099)

The scatter plot (Figure 7-12) of the discharge values shows relatively a decreasing trend for the observed discharge data. Most of the models showed a decreasing trend or relatively no change. M15 was the only model that showed a marginal increase in trend. This was in line with the precipitation projections as seen in the analysis done on that data set in section 5.3.4 of this report.

7.3 Results - Tarpon Springs/Anclote River Catchment

Table 7-3 below provides the statistical summary of the streamflow (discharge) for Tarpon Springs/Anclote River Catchment. Similar to what was done in for the Arcadia/Joshua Creek and Federal Point/South Fork Black Catchments, the table contains both the observed (1951-2010) and the projected discharge values (2011-2099). The statistical measures show that all the models and the observed data sets are positively skewed with high kurtosis values. Typical throughout this report, regarding temperature, precipitation and discharge projections, M9 data sets continually produces anomalous statistical results.

Table 7-3: Statistics - Tarpon Spring Observed (1951-2010) - Projected Discharge Data (2011-2099)

Models	Mean	STD	Skewness	Kurtosis	Max	Min	Range
Observed	61.427	105.475	2.937	12.884	695.600	1.430	694.170
M1	46.41	48.56	3.41	21.79	557.04	0.25	556.79
M2	54.25	48.25	2.48	11.68	402.53	2.30	400.23
M3	49.76	44.28	2.23	9.73	319.63	0.12	319.51
M4	56.97	46.17	2.02	7.88	322.33	1.59	320.74
M5	55.32	58.16	2.85	14.95	531.17	0.34	530.83
M6	51.11	41.90	2.12	8.98	282.45	0.09	282.36
M7	54.70	47.96	2.63	12.97	413.08	0.02	413.06
M8	53.71	50.44	2.80	15.58	523.66	0.11	523.55
M9	25.04	28.02	4.41	32.59	325.58	1.27	324.31
M10	52.38	48.95	2.46	11.84	430.29	2.20	428.10
M11	62.46	53.61	1.68	6.07	356.31	3.01	353.30
M12	59.05	46.10	1.95	8.59	340.35	0.85	339.50
M13	56.09	44.90	2.04	8.61	352.25	1.15	351.10
M14	58.57	51.27	2.01	7.96	358.17	0.74	357.43
M15	53.49	49.17	2.40	11.47	449.68	0.79	448.89

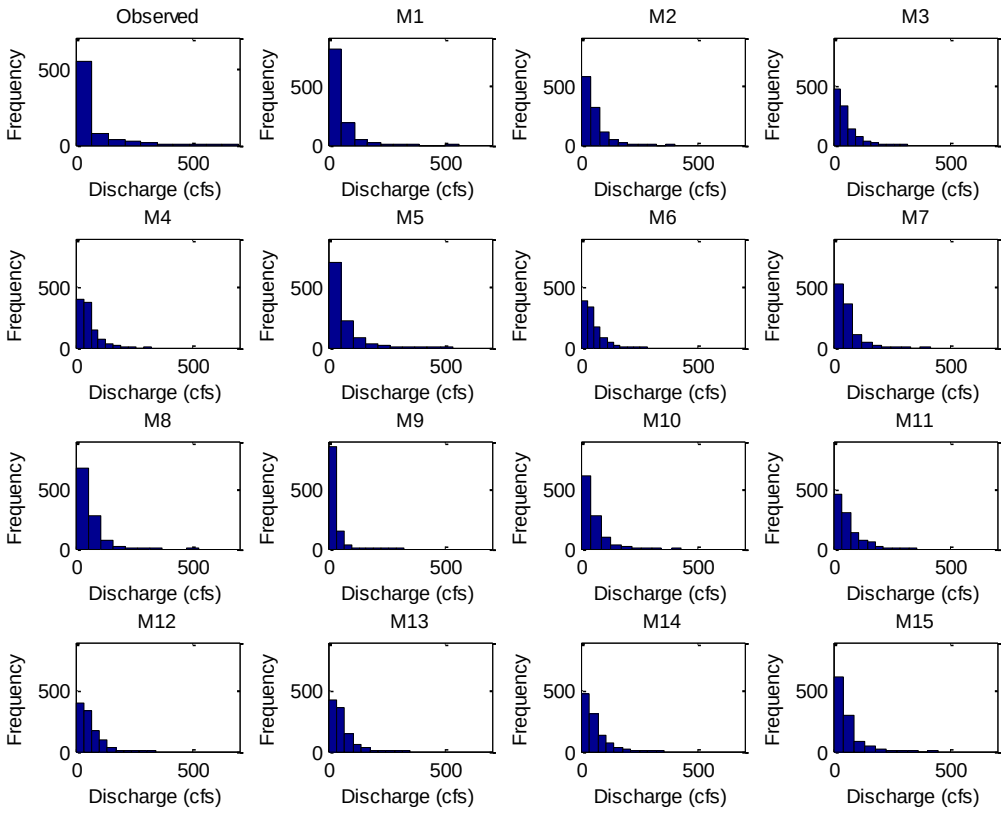

Figure 7-13: Histograms - Tarpon Spring Observed (1951-2010) - Projected Discharge Data (2011-2099)

The histogram in Figure 7-13 provides a graphical illustration of the projected discharge values for Tarpon Springs/Anclote River Catchment. The graph shows that there are higher incidences of getting lower discharge values.

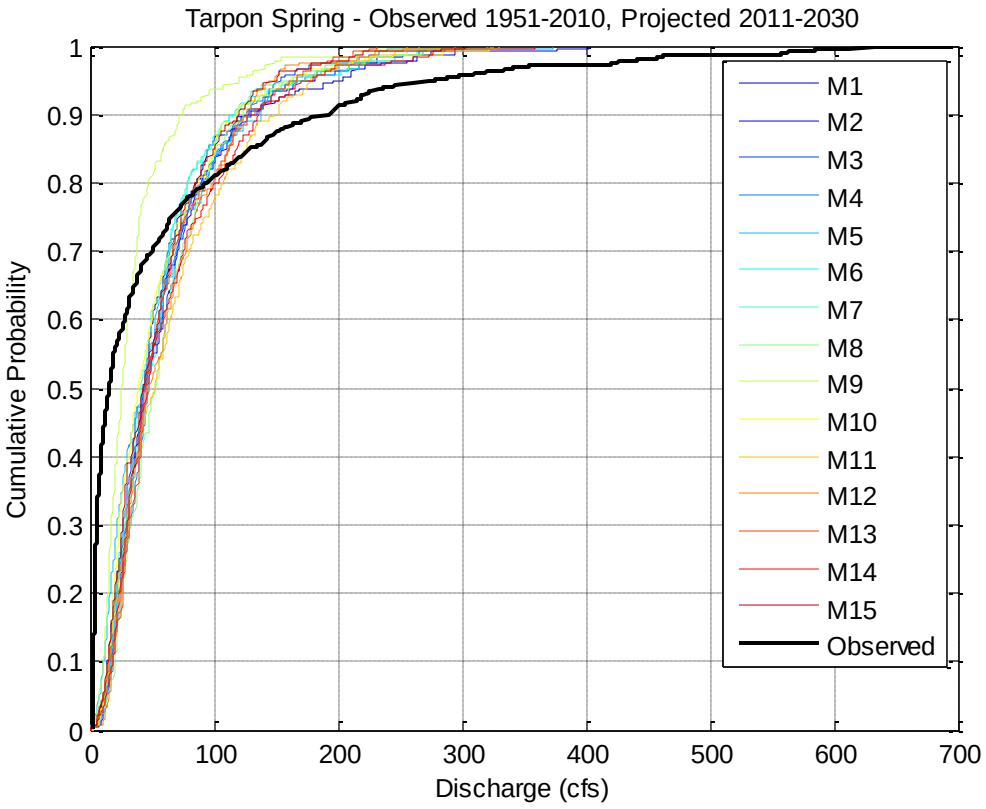

Figure 7-14: Tarpon Spring Observed (1951-2010) - Projected Discharge Data (2011-2030)

The plotted CDF graphs illustrate that most of the models shows increases in discharge at the lower values with a reversal in trend for higher values (chances of having more discharge is less). Typical in all three study areas, a similar trend was also observed for periods 2031-2050, 2051-2070 and 2071-2099. See Figure 7-14 through Figure 7-17 for the CDF plots. The graphs also indicated that there were much more variability in the projections for this catchment when compared to the other two.

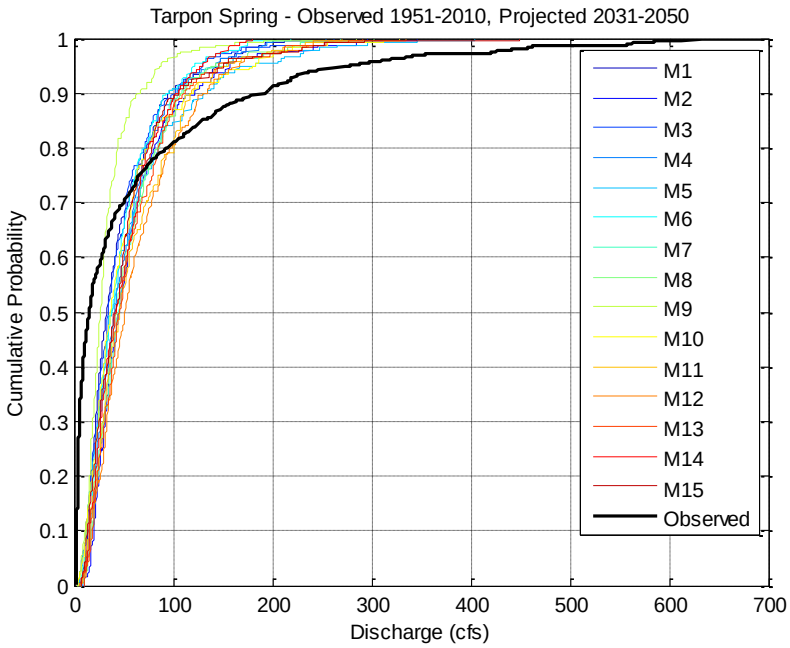

Figure 7-15: Tarpon Spring Observed (1951-2010) - Projected Discharge Data (2031-2050)

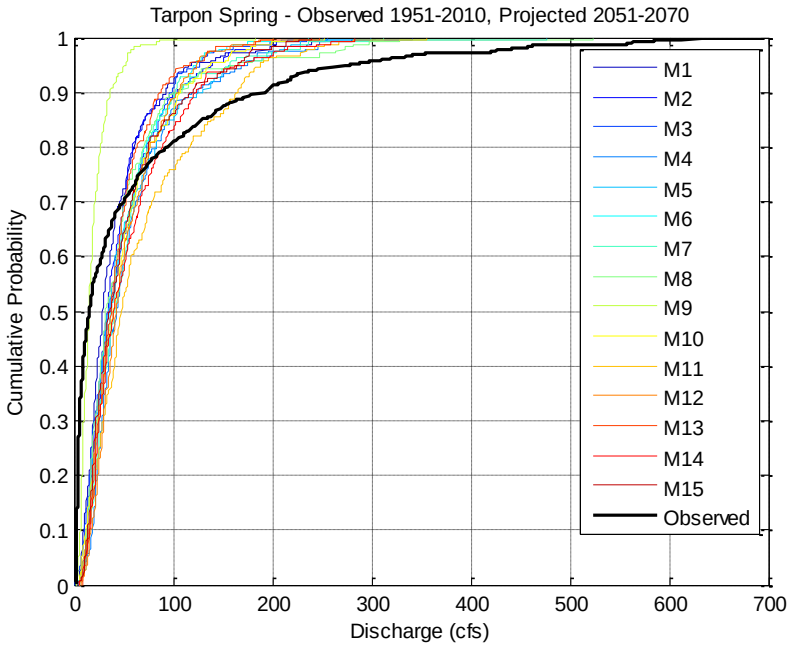

Figure 7-16: Tarpon Spring Observed (1951-2010) - Projected Discharge Data (2051-2070)

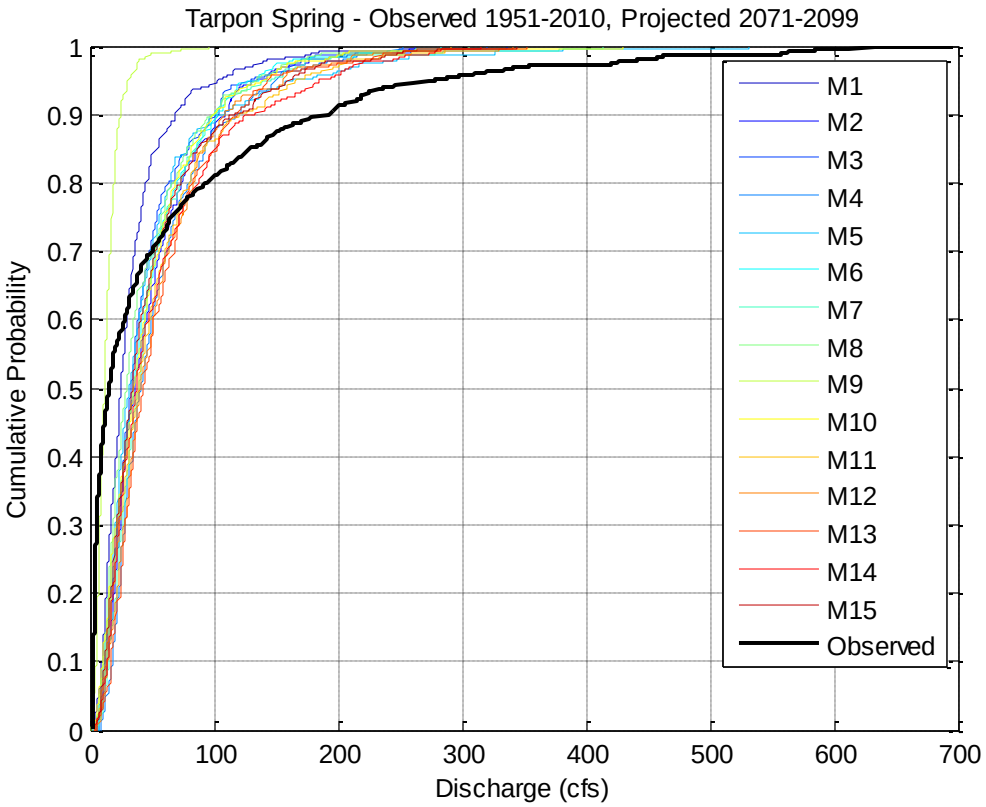

Figure 7-17: Tarpon Spring Observed (1951-2010) - Projected Discharge Data (2071-2099)

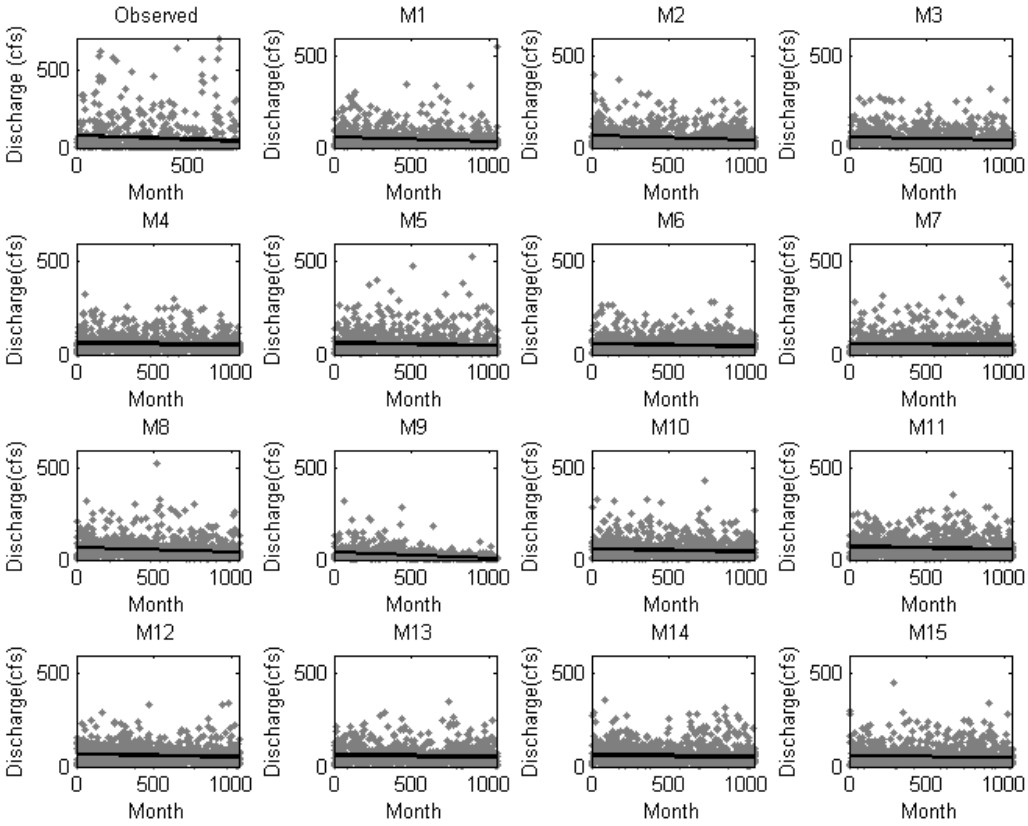

Figure 7-18: Scatter Plots - Tarpon Springs Observed (1951-2010) - Projected Discharge Data (2011-2099)

The scatter plot (Figure 7-18) of the discharge values shows a decreasing trend for the observed discharge data. All models showed a decreasing trend or relatively no change.

CHAPTER 8. CONCLUSIONS

The main objective of this research was to use an established rainfall runoff model to help predict future stream-flows based on various climate change scenario projections, in order to assist with future decisions, planning, design and control of water resource systems. With this information, water management districts and other governmental agencies can plan and develop strategies to mitigate against any potential negative impacts based on these predictions.

Three small catchments were selected for analysis. These catchments hydraulic units were located (1) Joshua Creek at Nocatee, FL, (2) South Fork Black Creek near Penney Farms, FL, and (3) Anclote River near Elfers, FL. Their respective associated weather station where the temperature and precipitation data was obtained for each unit was (1) Arcadia, (2) Federal Point, and (3) Tarpon Spring. The models were developed systematically and applied to these catchments. The models were calibrated with four different optimization techniques, Absolute Error (AE), Squared Error (SE), Root mean Squared Error (RMSE), and Mean Absolute Error (MAE) to efficiently obtain the best model parameter sets.

After each model was calibrated and the parameters estimated, it was then tested to see how well it will perform on a different data set. Five performance measures were used to validate the model, root mean squared error (RMSE), squared error (SE), mean absolute error (MAE), absolute error (AE), and coefficient of correlation (ρ). Each

optimization technique was ranked based on an assessed score from lowest to high, with the one with the lowest score being the best method.

The optimization technique producing the best model parameter sets for each catchment were RMSE for Arcadia/Joshua Creek, AE for Federal Point/ South Fork Black Creek, and RMSE for Tarpon Springs/Anclote River. The developed models were then applied to their respective catchment using the 15 model projections for temperature and precipitation based on the A1B climate change scenario.

The model discharge projections suggest that there is a direct relationship between temperature rise and discharge rates. The projection values following the A1B scenario storyline show that climatic change could have serious hydrologic consequences for any one of the catchments. Most of the models in all three catchments predicted a downward trend for future steam-flows. This will make it more difficult for water management authorities to satisfy water demands for various applications. However, these water managers can use the discharge projections form these models to prepare for and mitigate against the effects of climate change on their local hydrologic resources.

This research confirms that water balance models, modified to local conditions and calibrated with historic data, can be used as a tool to assess and predict future hydrologic conditions and stream-flow in an effort to better prepare and manage the impacts of climate change on these vital resources.

8.1 Main Limitations of the Model

Results of simulation model depend on optimal set of parameters (a, b, c, and d) and accurate inputs such as temperature and precipitation and the method used for

estimation of PE. Accurate data collection is essential to any model development. No model can be calibrated or even used without good quality data.

However, precipitation data quality is critical for accurate simulation of peaks. In calibration and validation phases of the model, the model under-predicted several peaks even though the correlation coefficient is moderately high and acceptable. Under estimation is possible due to inaccurate precipitation values or high values of PE being estimated in the time intervals of concern. Improved PE estimation is recommended to be obtaining better results in calibration and validation. Proximity of rain gage to the watershed or location of rain gage inside the watershed may improve the results. Radar data can be used for calibration; however, reliable data from radar sources are available only from 1995. The peaks that were underestimated were during major hurricane events in validation phase. Uniform rainfall assumed over the watershed derived from a rain gage located outside the watershed may be the reasons for such underestimations. The Thomas model has reasonably simulated the values of monthly discharge that are adequate for water management decisions at such a coarser temporal resolution. The possibility of lateral flows or flows from upstream basins may have led to higher observed discharges. This issues needs to be investigated thoroughly in future.

8.2 Contributions of this Research

Three optimization models are developed for calibration of Thomas model for streamflow predictions and future projections. Four different objective functions and two optimization solvers are adopted for development of optimal parameter values.
The BCSD-based statistical downscaling models for temperature and precipitation for

one scenario and for three watersheds were assessed to determine various trends. Future streamflow projections in three watersheds/catchments in Florida were developed and analyzed.

8.3 Recommendations for Future Research

- This research focused only on one scenario. The application of other types of climate change scenarios of may be a subject of interest.
- Future streamflow projections have only been evaluated for only three catchments in Florida. Extension of the methodology to other watersheds where water resources management is critical is another option that can be explored in the future.
- Uncertainty assessment of the Thomas model parameters.
- Uncertainty assessments of multi-model (climate change models) projections providing temperature and precipitation data.
- Assessment of scenario and model projection uncertainty.

REFERENCES

Bader, D.C., et al. 2008. Climate models: An assessment of strengths and limitations. *A Report by the U.S. Climate Change Science Program and the Subcommittee on Global Change Research*. Department of Energy, Office of Biological and Environmental Research, Washington, D.C.

Caldwell H., Quinn K.A., Meunier J., Suhrbier J. And Grenzeback L., 2002. Impactsof global climate change on freight. Proceedings, Federal Research Partnership Workshop"The potential impacts of climate change on transportation." *U.S. Department of TransportationCenter for Climate Change and Environmental Forecasting*, p. 3-32.

Chen, Y.D., 2011. Assessing hydrological impacts of climate change using monthly water balance models. *Department of Geography and Resource Management Centre of Strategic Environmental Assessment for China The Chinese University of Hong Kong, China*

Collins, W.D., C.M. Bitz, M.L. Blackmon, G.B. Bonan, C.S. Bretherton, J.A. Carton, P. Chang, S.C. Doney, J.J. Hack, T.B. Henderson, J.T. Kiehl, W.G. Large, D.S. McKenna, B.D. Santer, and R.D. Smith (2006) The Community Climate System Model Version 3 (CCSM3). J Climate, 19(11):2122-2143.

Delworth, T.L. et al (2005) GFDL's CM2 global coupled climate models part 1: formulation and simulation characteristics. *J Climate 19:643-674.*

Diansky, N.A., and E.M. Volodin (2002) Simulation of present-day climate with a coupled atmosphere-ocean general circulation model. *Izv Atmos Ocean Phys (Engl Transl) 38(6):732-747.*

Flato, G.M. and G.J. Boer (2001) Warming Asymmetry in Climate Change Simulations. *Geophys. Res. Lett., 28:195-198.*

Francisco, P.J., Filho, A., Sun, L., and Kwon, H., 2009. A Streamflow Forecasting Framework Using Multiple Climate and Hydrological Models. *Journal of the American Water Resources Association (JAWRA) 45(4):828-843. DOI: 10.1111/ j.1752-1688.2009.00327.x*

Furevik, T., M. Bentsen, H. Drange, I.K.T. Kindem, N. G. Kvamsto and A. Sorteberg (2003). Description and evaluation of the bergen climate model: *ARPEGE coupled with MICOM. Clim Dyn 21:27-51.*

Gordon C., C. Cooper, C.A. Senior, H.T. Banks, J.M. Gregory, T.C. Johns, J.F.B. Mitchell, and R.A. Wood (2000). The simulation of SST, sea ice extents and ocean heat transports in a version of the Hadley Centre coupled model without flux adjustments. *Clim Dyn 16:147-168.*

Gordon H.B., L.D. Rotstayn, J.L. McGregor, M.R. Dix, E.A. Kowalczyk, S.P. O'Farrell, L.J. Waterman, A.C. Hirst, S.G. Wilson, M.A. Collier, I.G. Watterson, and T.I. Elliott (2002). The CSIRO Mk3 climate system model, CSIRO Atmospheric Research Technical Paper No.60, CSIRO. *Division of Atmospheric Research, Victoria, Australia, 130 pp.*

Hallegatte,S., Mason, J., Ryerson, C., Watkinson A., and Weatherly, J., 2006. Waterborne transport, ports and waterways: A review of climate change drivers, impacts, responses and mitigation. *EnviCom- Task Group 3: Climate Change and Navigation-(PIANC)*

Hyman, R., Potter, J., Savonis, M., Burkett, V., and Tump, J., (2006): Why Study Climate Change Impacts on Transportation? *Gulf Coast Study, Phase I*

Intergovernmental Panel on Climate Change, 2007a. Climate change 2007: impacts, adaptation and vulnerability. Contribution of Working Group II to the Fourth Assessment Report of the Intergovernmental Panel on Climate Change. *Cambridge University Press, Cambridge.*

Intergovernmental Panel on Climate Change, 2007b. Climate change 2007: mitigation of climate change. Contribution of Working Group III to the Fourth Assessment Report of the Intergovernmental Panel on Climate Change. *Cambridge University Press, Cambridge.*

Intergovernmental Panel on Climate Change, 2007c. Climate change 2007: the physical science basis. Contribution of Working Group I to the Fourth Assessment Report of the Intergovernmental Panel on Climate Change. *Cambridge University Press, Cambridge.*

IPSL (2005). The new IPSL climate system model: IPSL-CM4. Institute Pierre Simon Laplace des Sciences de l'Environment Global, Paris, France. Jha, M., Z. Pan, E. S. Takle, and R. Gu (2004), Impacts of climate change on streamflow in the

Upper Mississippi River Basin: A regional climate model perspective, J. Geophys. *Res., 109, D09105, doi:10.1029/2003JD003686*.

Jungclaus J.H., M. Botzet, H. Haak, N. Keenlyside, J-J Luo, M. Latif, J. Marotzke, U. Mikolajewicz, and E. Roeckner (2006) Ocean circulation and tropical variability in the AOGCM ECHAM5/MPI-OM. J Climate 19:3952-3972.

K-1 model developers (2004) K-1 coupled model (MIROC) description, K-1 technical report, 1. In: Hasumi H, Emori S (eds) Center for Climate System Research, University of Tokyo, 34 pp.

Kling G.W., Hayhoe K., Johnson .B., Magnuson J.J., Polasky S., Robinson S.K., Shuter B.J., Wander M.M., Wuebbles D.J., Zak D.R., Lindroth R.L., Moser S.C. and Wilson M.L. (2003). Confronting climate change in the Great Lakes Region: Impacts on our communities and ecosystems. *Union of Concerned Scientists, Cambridge, Massachusetts, and the Ecological Society of America, Washington, D.C.*

Koetse M., Rietveld, P., 2009. The impact of climate change and weather on transport: An overview of empirical findings. *Transportation Research Part D*

Legutke, S. and R. Voss (1999) The Hamburg Atmosphere-Ocean Coupled Circulation Model ECHO-G. Technical report, No. 18, German Climate Computer Centre (DKRZ), Hamburg, 62 pp.

Lenart, M., 2008, Downscaling techniques. *The University of Arizona (Southwest Clomate Change Network)*

Liu, L., Xu, Z., , Huang, J., 2009, Impact of Climate Change on Streamflow in the Xitiaoxi Catchment, Taihu Basin. *Wuhan University Journal of Sciences Vol.14 No.6, 525-531*

Maurer, E.P. and Hidalgo, H.G., 2007. Utility of daily vs. monthly large-scale climate data: An intercomparison of two statistical downscaling methods. *Hydrology and Earth Systems Sciences Discussions* 12: 551-563.

Maurer, E. P., L. Brekke, T. Pruitt, and P. B. Duffy (2007), 'Fine-resolution climate projections enhance regional climate change impact studies', *Eos Trans. AGU, 88*(47), 504.

Meehl, G.A., Covey, C., Taylor, K.E., Delworth, T., Stouffer, R.J. (more), 2007: The WCRP CMIP3 Multimodel Dataset: A new era in climate change research. *Bulletin of the American Meteorological Society*, 88, 1383-1394.

Moreda, F. (1999), Conceptual rainfall - runoff models for different time steps with special consideration for semi-arid and arid catchments. *Laboratory of Hydrology, Faculty of Applied Sciences, VUB Pleinlaan 2, 1050 Brussels, Belgium*

Obeysekera, J., Irizarry, M., Park, J., Barnes, J., Dessalegne, T., 2007: Climate change and its implications for water resources management in south Florida. H*ydrologic & Environmental Systems Modeling Department, South Florida Water Management District, 3301 Gun Club Road, West Palm Beach, FL 33406, USA*

Russell G.L., J.R. Miller, D. Rind, R.A. Ruedy, G.A. Schmidt, and S. Sheth (2000) Comparison of model and observed regional temperature changes during the past 40 years. *J Geophys Res 105:14891-14898.*

Salas-Mélia D., F. Chauvin, M. Déqué, H. Douville, J.F. Gueremy, P. Marquet, S. Planton, J.F. Royer, and S. Tyteca(2005) Description and validation of the CNRM-CM3 global coupled model. *Clim Dyn (in review)*

Sankarasubramanian, A & Vogel, Richard M. (2002). Annual Hydroclimatology of the US*, Water Resources Research*, 38 (6), 1083.

Singh, R., Maheshwari, B., Malano, H.M., (2009), Developing a conceptual model for water accounting in peri-urban catchments. *18th World IMACS / MODSIM Congress, Cairns, Australia 13-17 July 2009*

Thomas, H.A., C.M. Marin, M.J. Brown, and M. B Fiering, 1983. Methodology for Water Resource Assessment Report to U.S. Geological Survey. *Rep. NTIS 84-124163, National Technical Information Service, Springfield, Virginia.*

USACOE, 1997. Black Creek Basin Comprehensive Floodplain Management Study Phase II- *Special Publication SJ98-SP10, Prepared by U.S. Army Corps of Engineers, Jacksonville District.*

Washington W.M., J.W. Weatherly, G.A. Meehl, A.J. Semtner, T.W. Bettge, A.P. Craig, W.G. Strand, J. Arblaster, V.B. Wayland, R. James, Y. Zhang (2000) Parallel climate model (PCM) control and transient simulations. *Clim Dyn 16:755-774.*

Yukimoto S., A. Noda, A. Kitoh, M. Sugi, Y. Kitamura, M. Hosaka, K. Shibata, S. Maeda, and T. Uchiyama (2001) The new Meteorological Research Institute coupled GCM (MRI-CGCM2) -- *model climate and variability. Pap Meteorol Geophys 51:47-88.*